

CAMS Service Evolution



D3.1 Report on TROPOMI SO₂, O₃, CO, and HCHO total columns data assimilation

Due date of deliverable	31/10/2025
Submission date	19/11/2025
File Name	CAMEO-D3.1-V1.0
Work Package /Task	3.1 and 3.2
Organisation Responsible of Deliverable	INERIS
Author name(s)	Gaël Descombes, Alexandre Siméon, Anthony Ung (INERIS) Zhuyun Ye (AU) Ann Lange (FZJ) Lennart Robertson, Ana Carvalho (SMHI) Joanna Struzewska, Jacek W. Kaminski, Karol Przewdzicki (IOS-PIB) Mihaela Mircea, Andrea Bolignano Gino Briganti, Felicita Russo (ENEA) Uppstu Andreas (FMI)
Revision number	V1
Status	Issued
Dissemination Level	Public



Funded by the
European Union

The CAMEO project (grant agreement No 101082125) is funded by the European Union.

Views and opinions expressed are however those of the author(s) only and do not necessarily reflect those of the European Union or the Commission. Neither the European Union nor the granting authority can be held responsible for them.

1 Executive Summary

This report describes the research performed within task 3.1 and task 3.2 “Enhancement of Satellite Data assimilation regional CAMS models”. The goal of the seven teams, contributing to task 3.1, is to assimilate TROPOMI SO₂ total vertical columns density (VCD), which have a low signal to noise ratio. The SO₂-COBRA dataset is selected in this study, and the **CAMS Satellite Operator (CSO)** is used and implemented in the data assimilation systems of six teams. The assimilation involves various techniques such as variational (3D-VAR for DEHM, EURAD-IM, MATCH and Sasaki for GEM-AQ), Optimal Interpolation (MINNI), and Ensemble Kalman Filter Methods (CHIMERE, MINNI and SILAM). Vertical resolution of the model operational configuration is increased to allow simulation of total columns above 200 hPa.

In task 3.1, the same data assimilation experiment is performed by the teams and a common postprocessing is applied to evaluate the results. It provides results hourly, daily and on average over the period of August 2023, in Europe, as well as at hotspot locations. First, each partner presents their experiment as well as some additional work. Second, an intercomparison of the assimilation of SO₂ VCD is made and shows a general reduction of the VCD bias for all models, which however varies from slight to large bias changes. The VCD RMSE largely decreases for GEM-AQ and MINNI-OI and it slightly decreases for CHIMERE, EURAD-IM and SILAM (neutral for DEHM). Correlation in VCD SO₂ are largely increased for GEM-AQ and MINNI-OI and also improved for CHIMERE and SILAM. The analysis increments in SO₂ concentration varies according to the systems and models used. DEHM-3D-VAR and MINNI-OI have likely larger increment in the highest layer of atmosphere, while larger SO₂ concentration analysis increments are found within the planetary boundary layer for the other DA-systems, close to hotspot emission point sources. Definition of the background error covariance error of the different system plays a key role to spread out the concentration increment and this is also highlighted by results of GEM-AQ (variational Sasaki approach), MATCH (3D-VAR), CHIMERE (Ensemble Adjustment Kalman Filter), and SILAM (Ensemble Kalman Filter) when adding the elevated volcanic SO₂ of ETNA.

The seven air quality models are finally evaluated against SO₂ surface concentrations (EEA). Benefits are small but bias is reduced for SO₂ surface concentrations for CHIMERE, EURAD-IM and GEM-AQ. CHIMERE and SILAM have a decrease of RMSE.

In task 3.2, CHIMERE, DEHM, GEM-AQ, MINNI and SILAM that volunteered, present data assimilation results of their experiments on TROPOMI total columns of HCHO, CO, and O₃. Teams have processed their own results on their own experiment. HCHO VCD DA is performed by all the teams of this task and improves spatial consistency with column patterns for all the models by reducing their bias. The evaluation of CHIMERE and SILAM results on ozone against surface stations (EEA) does not show improvements and may degrade slightly the performance. GEM-AQ assimilates data assimilation of S5P/CO leads to moderate analysis. No comparison is made with surface observations.

An overall summary and outlook are left in the last section. It remains a challenge for regional models to improve hourly or daily concentrations results at the surface, assimilating only S5P products. Some additional work done on the DA systems should help to go further. The issue of the observation bias correction at regional scale should be addressed and the forthcoming availability of hourly data provided by Sentinel 4 will also allow further investigation. Regional models have demonstrated the capacity to assimilate total columns of several chemical species, but effort should continue to improve air quality forecast results.

Table of Contents

1	Executive Summary	2
2	Introduction	4
2.1	Background.....	4
2.2	Scope of this deliverable	4
2.2.1	Objectives of this deliverable	4
2.2.2	Work performed in this deliverable.....	5
2.2.3	Deviations and counter measures.....	5
2.2.4	CAMEO Project Partners involved in this deliverable:.....	5
3	Data assimilation systems.....	6
3.1	Introduction	6
3.2	CHIMERE Ensemble Adjustment Kalman Filter (EAKF)	7
3.3	DEHM 3D-VAR.....	7
3.4	EURAD-IM 3D-VAR.....	7
3.5	GEM-AQ.....	8
3.6	MATCH 3D-VAR.....	8
3.7	MINNI OI and EAKF.....	9
3.8	SILAM Ensemble Kalman Filter	9
4	Data Assimilation of SO ₂	10
4.1	Introduction	10
4.2	Sentinel 5P SO ₂ selected Data	10
4.2.1	Choosing the Sentinel 5P SO ₂ retrieval.....	10
4.2.2	Quality control and processing of the Sentinel 5P observations for data assimilation.....	13
4.3	Evaluation over the period of August 2023.....	14
4.3.1	Presentation of SO ₂ results by Model.....	14
4.3.2	Intercomparison of SO ₂ data assimilation	42
4.3.3	Evaluation of data assimilation impact on surface SO ₂ concentration	44
4.4	Conclusions	50
5	Data Assimilation of other Sentinel 5P L2 products.....	51
5.1	Introduction	51
5.2	Assimilation of HCHO in CHIMERE	51
5.3	Assimilation of HCHO and CO in GEM-AQ	54
5.4	Assimilation of HCHO in DEHM	62
5.5	Assimilation of HCHO, CO and O ₃ in MINNI-OI.....	64
5.6	Assimilation of HCHO in SILAM.....	66
5.7	Conclusions	67
6	Conclusion.....	68
7	References	69

2 Introduction

2.1 Background

Monitoring the composition of the atmosphere is a key objective of the European Union's flagship earth observation programme Copernicus, with the Copernicus Atmosphere Monitoring Service (CAMS) providing free and continuous data and information on atmospheric composition.

The CAMS Evolution (CAMEO) project enhances the quality and efficiency of the CAMS service and help CAMS to better respond to policy needs such as air pollution and greenhouse gases monitoring, the fulfilment of sustainable development goals, and sustainable and clean energy.

CAMEO helps prepare CAMS for the uptake of forthcoming satellite data, including Sentinel-4, -5 and 3MI, and advance the aerosol and trace gas data assimilation methods and inversion capacity of the global and regional CAMS production systems.

CAMEO develops methods to provide uncertainty information about CAMS products, in particular for emissions, policy, solar radiation and deposition products in response to prominent requests from current CAMS users.

CAMEO contributes to the medium- to long-term evolution of the CAMS production systems and products as described in Colette et al 2025. Forecast and analysis are performed by an ensemble of eleven models over Europe.

The transfer of developments from CAMEO into subsequent improvements of CAMS operational service elements is a main driver for the project and is the main pathway to impact.

The CAMEO consortium, led by ECMWF, the entity entrusted to operate CAMS, includes several CAMS partners thus allowing CAMEO developments to be carried out directly within the CAMS production systems and facilitating the transition of CAMEO results to future upgrades of the CAMS service.

This will maximise the impact and outcomes of CAMEO as it can make full use of the existing CAMS infrastructure for data sharing, data delivery and communication, thus supporting policymakers, business and citizens with enhanced atmospheric environmental information.

2.2 Scope of this deliverable

2.2.1 Objectives of this deliverable

This deliverable presents effort to assimilate Sentinel 5 Precursor (S5P) products to improve air quality modelling at the regional scale by:

- Increasing the capabilities for high resolution satellite S5P data assimilation in regional models,
- Comparing impact of data assimilation for different models and data assimilation systems,
- Evaluating data assimilation to improve air quality forecast at the surface in concentration,
- Providing conclusions and perspectives.

2.2.2 Work performed in this deliverable

This deliverable presents the work planned in the Description of Action (DoA, WP3 T3.1).

Task 3.1.1: Assimilation of TROPOMI (Tropospheric Monitoring Instrument) SO₂ (sulfur dioxide) in CAMS2_40 Regional Models by all seven teams contributing to task 3.1. The assessment includes a sensitivity to the choice of the selected retrieval. Developments are performed by the seven teams to increase the ability of the different regional models and systems to assimilate SO₂ total columns. Results presented are strongly dependent of the models and assimilation techniques used. The coordination focuses on designing consistent numerical plans in the selection of retrieval products and evaluation procedure to demonstrate the added value for the air quality system as a whole.

Task 3.1.2: Assimilation of TROPOMI CO (carbon monoxide), O₃ (ozone), HCHO (formaldehyde) in CAMS2_40 Regional Models. Selected teams assess the feasibility and benefit of assimilating additional gaseous species.

2.2.3 Deviations and counter measures

No deviations have been encountered.

2.2.4 CAMEO Project Partners involved in this deliverable:

SMHI	SVERIGES METEOROLOGISKA OCH HYDROLOGISKA INSTITUT
FMI	ILMATIETEEN LAITOS
INERIS	INSTITUT NATIONAL DE L'ENVIRONNEMENT INDUSTRIEL ET DES RISQUES - INERIS
IOS-PIB	INSTYTUT OCHRONY SRODOWISKA - PANSTWOWY INSTYTUT BADAWCZY
FZJ	FORSCHUNGSZENTRUM JÜLICH GMBH
AU	AARHUS UNIVERSITET
ENEA	AGENZIA NAZIONALE PER LE NUOVE TECNOLOGIE, L'ENERGIA E LO SVILUPPO ECONOMICO SOSTENIBILE

3 Data assimilation systems

3.1 Introduction

Seven of the 11 teams contributing to the CAMS regional systems and their related data assimilation systems are first presented in Table 1 and discussed in more details, hereafter from section 3.2 to 3.8. DEHM, EURAD-IM, MATCH and GEM-AQ use variational methods, CHIMERE and SILAM use ensemble methods, MINNI uses OI (optimal interpolation) and an ensemble method.

Model	Da-system	Background error covariance	DA Time window
CHIMERE	Ensemble Adjustment Kalman Filter (EAKF)	Perturbation on emissions, BCs and Meteorology (20 members)	Cycling, closest hour of orbit time (+/- 30 min)
DEHM	3D-VARiational	B diagonal, NMC variance	Cycling, closest hour of orbit time (+/- 30 min)
EURAD-IM	3D-VARiational	Diffusion approach	No cycling, closest hour of orbit time (+/- 30 min)
GEM-AQ	Sasaki variational DA	B diagonal, NMC variance	Cycling (DA window 12H +/- 3h)
MATCH	3D-VARiational	B diagonal, NMC variance	Merging orbits for the current hour
MINNI	Optimal Interpolation (OI)	NMC variance of log C	Cycling, closest model timestep of orbit time
	Ensemble Adjustment Kalman Filter (EAKF)	Perturbation on emissions and BCs (20 members)	Cycling, closest hour of orbit time (+/- 30 min)
SILAM	ENsemble Kalman Filter (ENKF)	Perturbation on emissions, BCs and Meteorology (20 members)	Cycling, closest hour of orbit time (+/- 30 min)

Table 1: Description of the data assimilation systems used

All models include a model top above 200 hPa, as shown in Table 2. DEHM, EURAD-IM, GEM-AQ and MATCH use their operational vertical grid while CHIMERE, MINNI-OI and SILAM increase the resolution of their vertical grid. CHIMERE vertical model levels grow from 9 levels with a model top to 500 hPa to 20 levels with a model top to 200 hPa. MINNI-OI vertical model levels grow from 10 levels with a model top to 7 km to 14 levels with a model top of 12 km. And SILAM vertical model levels grow from 10 levels with a model top to 8700 m to 18 with a model top to 120 hPa. DEHM, EURAD-IM, GEM-AQ, MINNI have the highest horizontal resolution, about 0.1 degree, while the resolution of MATCH and CHIMERE is 0.2 degree and 0.3 degree for SILAM. All the models use the CAMS-REG-AP v6.1.1 or CAMS-REG-AP v7.0 inventories which do not includes SO₂ volcanic emissions. GEM-AQ, SILAM, CHIMERE and MATCH did some sensitivity tests to consider natural volcanic emissions by performing inversion or based on emission estimation such as coming from CAMS monthly estimate (following Fioletov et al., 2011 and Carn et al., 2017).

CAMEO

Model	Horizontal resolution	Vertical resolution [# levels]	Top level	Emissions
CHIMERE	0.2 Deg	20	200 hPa	CAMS-REG-AP v6.1.1
DEHM	0.1 Deg	29	100 hPa	CAMS-REG-AP v6.1.1
EURAD-IM	0.1 Deg (9 km x 9 km)	23	100 hPa	CAMS-REG-AP V7.0
GEM-AQ	0.1 Deg	28	10 hPa	CAMS-REG-AP v6.1.1
MATCH	0.2 Deg	39	100 hPa	CAMS-REG-AP V7.0
MINNI	0.1/0.15 Deg	17	12000 m	CAMS-REG-AP v6.1.1
SILAM	0.3 Deg	18	120 hPa	CAMS-REG-AP v6.1.1

Table 2: Description the model configurations

3.2 CHIMERE Ensemble Adjustment Kalman Filter (EAKF)

The CHIMERE model is run at a horizontal resolution of 0.2 degree. Twenty vertical model levels are used with a top of the domain at 200 hPa, as shown in Table 2.

The CHIMERE model is coupled with the *Data Assimilation Research Testbed* system (DART from NCAR, the U.S. *National Centre for Atmospheric Research*). The Ensemble Adjustment Kalman Filter (EAKF, J.L. Anderson 2001) is running with 20 members. Main perturbations are applied to anthropogenic, biogenic emissions. Perturbations on boundary conditions are also applied. Some targeted model processes, such as deposition and vertical diffusion are also perturbed. Gaspari and Cohn (1999) localization is used to reduce the impact of long-distance correlations as well as adaptive inflation (to preserve the CHIMERE ensemble spread).

The CAMS Satellite Operator (CSO) forward operator has been implemented within the CHIMERE-DART-EAKF framework.

3.3 DEHM 3D-VAR

The DEHM model is run at the horizontal resolution of 0.1 degree as used in CAMS, and 29 vertical model levels using terrain-following σ -coordinates from the surface up to 100 hPa (see Table 2).

The DEHM model is coupled with the three-dimensional variational (3D-VAR) method as described in Silver et al. (2016). The NMC method (Kahnert, 2008) was implemented to calculate the background error covariance matrix. The calculations are based on the differences between two simulations that use different meteorology.

The CAMS CSO has been used to download, pre-process, and superobbing the observations for assimilation in DEHM. The observational errors are from the satellite products and processed with the CAMS CSO. The observation operator interpolates the modelled concentrations from model vertical levels into the vertical levels of averaging kernel from satellite products using pressure and converts to modelled total column density equivalent to the observed ones.

3.4 EURAD-IM 3D-VAR

The EURAD-IM model is run with a one-step nesting sequence. The first domain has a horizontal resolution of 45 km x 45 km using a Lambert conformal projection, while the nested domain has a horizontal resolution of 9 km x 9 km. The modelling results are finally projected onto a 0.1-degree CAMS common grid. The vertical resolution is described by 23 terrain-following levels up to a domain top at 100 hPa (see Table 2).

CAMEO

The EURAD-IM assimilation technique applied here is the 3D-VAR method (Elbern et al., 2007). The cost function is described using an incremental formulation, whereby the background error covariances are calculated using the diffusion approach of Weaver and Courtier (2001).

The CAMS CSO has been used to download and pre-process the observations in preparation for their assimilation in EURAD-IM. The observation operator interpolates and integrates the modelled pollutant concentrations from all tropospheric model levels into the averaging kernel grid, converting the column value into the observed quantity and thus calculating the model equivalent.

3.5 GEM-AQ

The GEM-AQ model is run at the horizontal resolution of 0.1 degree and 28 hybrid vertical levels with the model top at 10hPa (see Table 2).

The GEM-AQ assimilation technique is a variational method based on Sasaki (1969). The cost function is a weighted sum of the squares of the background error and the analysis increment in the state space (model grid). The weighting factors express the estimation of the accuracy of measurements and model results, in relative terms. Minimization of the functional is accomplished under a dynamical constraint of linear advection (Burgers equation). The solution of this problem leads to an elliptic (non-homogeneous Helmholtz-type) equation, which is solved by an iterative relaxation method.

3.6 MATCH 3D-VAR

In the CAMEO project, MATCH (Robertson et al., 1999) model was used over the CAMS Regional domain, as described in Colette et al. (2025). From that setup, we also took the description of its data assimilation scheme. The scheme is a variational spectral method (Kahnert, 2008). In this method, background covariance matrices are then built in spectral space. The spectral approach implies that horizontal covariances are assumed isotropic and homogeneous. A benefit is that the background error covariance matrix becomes diagonal and represents the spectral response of a Gaussian distribution. The vertical correlations are handled separately by a covariance matrix for each wave number. The variational solution is then evaluated in spectral eigen-spaces.

The background error covariance matrices are derived by the so called NMC method (Parrish and Derber, 1992) using analysed and forecasted weather data to derive uncertainties. Intermittent data assimilation is applied having observations assimilated by the end of each hour. Satellite measurements over the current hour are regrided before injection (Table 1). The setup allows for merging satellite measurements over a larger time window but that is not activated here. For full chemistry the analysed components propagate through chemistry and transport into unobserved components.

The model is applied with a horizontal resolution of $0.2^\circ \times 0.2^\circ$, with 39 vertical levels up to 100hPa (Table 2). Anthropogenic emissions are based on CAMS-REG-V7.0 version while volcanic emissions are of quite old origin. The latter has also been switched off in one run as well.

Processing satellite measurements have been inspired by the CSO tool while the elements in satellite data used are stored in GRIB. Regridding of the satellite data is made into 0.2×0.2 degrees grid, where superobbing is based on weighting pixels by the geometric mean having the quality flag (qa) as weights.

A variational bias correction was also implemented with the state vector extended with the bias elements. In the current setting only the bias itself is considered and not dependencies

CAMEO

on other bias driving elements in the satellite data. With the spectral representation employed the wave numbers are distributed in east–west bands over the processes, and each process holds its own bias giving a south-north distributed bias.

3.7 MINNI OI and EAKF

The MINNI modelling system was run at the horizontal resolution of 0.1/0.15 degree and with seventeen vertical model levels up to ca. 12 km, as shown in Table 2. The two assimilation techniques implemented in MINNI are: Optimal Interpolation (OI) and Ensemble Adjustment Kalman Filter (EAKF) (Anderson, 2001) which was coupled using the Data Assimilation Research Testbed (DART) tool (<http://doi.org/10.5065/D6WQ0202>). Both techniques are using the CSO (CAMS Satellite Operator) (cams.ci.tno.nl/cso) developed to facilitate the assimilation of satellite data in regional air quality model. OI scheme developed for satellite data assimilation is based on Adani and Uboldi (2023) and considers the spatial and temporal error structures of the background field through the background error covariance matrix (B). This matrix, for simplicity, was assumed diagonal considering thus that the retrievals at different points do not influence each other. Besides, model data were corrected only where the observations were available. EAKF scheme runs a 20-member ensemble over an hourly assimilation window. The model perturbations are achieved by varying anthropogenic emissions and boundary conditions to estimate model uncertainties. Vertical localization was performed using the 5th-order Gaspari-Cohn (GC) rational function (Gaspari and Cohn, 1999), while prior inflation was applied to minimize filter divergence due to insufficient variance. The Quantile Conserving Ensemble Filter Framework Method (Anderson, 2022) was applied to preserve the positivity of the trace gas concentrations. The performances of both assimilation techniques were evaluated against the same reference simulation which does not include Etna volcano emissions in the regional emission inventory (Table 2). More details on MINNI setup and input data for this simulation may be found in Colette et al. (2025).

3.8 SILAM Ensemble Kalman Filter

In SILAM, TROPOMI COBRA (processor version 2.0.0) SO₂ retrievals were assimilated using the Ensemble Kalman Filter. The ensemble, consisting of 40 members, was formed by perturbing the emissions and the boundary condition of all species, as well as by perturbing the time of the meteorological data. The emission perturbation was performed by applying a random linear emission scaling factor to each emission species. The random correction factor was based on a 2D normal distribution with a standard deviation of 0.5 and a spatial correlation distance of 300 km. The boundary condition perturbation was also based on a 2D normal distribution, so that each column along the sides of the domain is assigned a constant perturbation factor. The relative standard deviation was set to 0.1 (0.02 for ozone) and the spatial correlation distance was set to 600 km. A Gaspari-Cohn type localization distance of 300 km was applied to reduce the impact of spurious correlations. In situ data from air quality measurement stations was not assimilated. The resolution of the simulation was 0.3° x 0.3° and the model vertical consisted of 18 layers extending to about 120 hPa.

The TROPOMI retrievals were based on the “sulfurdioxide_total_vertical_column” variable of the input files, and the retrieval standard deviation was set to equal the “sulfurdioxide_total_vertical_column_precision”. The data were then spatially averaged into the resolution of the simulation. Retrievals having a QA value of less than 0.75 were ignored. Also, negative average retrievals were assimilated, but the output of the assimilation was forced to be at least zero. In the assimilation, the model state vector was formed by the 3D in-air concentration of the observed species. Assimilation was performed at hourly intervals, but so that the difference between the model and observation was stored for the exact time of the observation. The non-instant assimilation may cause slight additional errors but allows for simultaneous assimilation of multiple types of observations with low additional computational cost (although in these simulations no additional observations were assimilated).

4 Data Assimilation of SO₂

4.1 Introduction

SO₂ impacts air quality at local scale and global scale. The part of anthropogenic emissions represents around 70 % and mainly comes from coal burning, oil and gas industry, and smelting activities. The additional 30 % natural sources of SO₂ emissions are largely coming from volcanoes. An eruption can impact SO₂ concentrations in the upper troposphere and lower stratosphere and large SO₂ plumes, combined with volcanic ash, can also cause severe problems and damage to aviation. Large amounts of SO₂ are mainly locally emitted by point sources. In Europe, Icelandic volcanoes, such as the large 2010 Eyjafjallajökull eruption or eruptions from the Etna volcano in Sicily are the main natural sources, while the coal-fired power plants in Eastern Europe are the main anthropogenic emission sources.

The decade-long study investigating OMI (Ozone Monitoring Instrument) VCDs (vertical column densities) by Krotkov et al. (2016) has shown the ability to retrieve trends in annual and overall average emission inventories. In addition, high consistency in retrieving SO₂ emission annual means is found when applying the method of Fioletov et al. (2017) at located hotspots. However, the assimilation of SO₂ columns remains challenging due to the low signal-to-noise ratio of single swath data. Standard deviation values are more likely to be higher in summer than in winter due to the weaker signal (Fioletov et al., 2020). This problem remains despite the higher pixel resolution of TROPOMI with about 3.5 km by 5 km, compared to OMI that has a horizontal resolution of about 13 km by 24 km at nadir. Fioletov et al., 2020 shows that spatially averaging the retrieval reduces the uncertainty by more than a factor of 2.5 compared to the emission estimates. In addition, the algorithms used to retrieve VCDs continue to improve, and this should further reduce the uncertainties.

For these reasons, strict selection criteria evaluating the retrieval quality and detectability are applied to select the most useful SO₂ dataset as explained in section 4.2. Then, each partner performs data assimilation of SO₂ VCDs for the selected period of August 2023 and analysed their results in section 4.3.1. Finally, intercomparisons of the different model results are presented in sections 4.3.2 and 4.3.3, where the focus is placed on quantifying the impact on the representation of SO₂ surface concentrations.

4.2 Sentinel 5P SO₂ selected Data

4.2.1 Choosing the Sentinel 5P SO₂ retrieval

This section aims to select one of the two SO₂ total column datasets available along the CAMEO project. The operational SO₂ retrieval was first performed by using the DOAS algorithm. Since November 2024, the SO₂-COBRA (Theys et al., 2021) is used to deliver the SO₂ operational total column (product release, version 02.00.00).

Preliminary comparisons by Theys et al. (2021) show consistent results for both methods. However, considering a SCD (slant column density) as done by Theys et al. (2021) obtains a noise reduction in the mid latitudes. Thus, the COBRA algorithm detects more anthropogenic point sources with an estimated detection limit of about 8 kt.yr⁻¹ SO₂ emissions.

In the following comparisons, data are screened following the Quality Control (QC) guidance from Theys et al. (2021) and the *Product User Guide, The ATBD (Algorithm Theoretical Basis Document)*:

- Solar zenith angles larger than 60°,
- Radiometric cloud fraction lower than 30 %,
- TROPOMI rows 26-424 (removing row far from nadir),
- qa_value flag above 0.5.

CAMEO

Figure 1 presents the mean on the left for SO₂-DOAS (on top) and SO₂-COBRA (in the middle) total columns (VCDs) and their corresponding probability density functions (PDFs) (at the bottom). SO₂-COBRA dataset exhibits slightly lower mean values ($7.4 \times 10^{-7} \text{ mol.m}^{-2}$) in comparison with the SO₂-DOAS product ($4.3 \times 10^{-5} \text{ mol.m}^{-2}$) but shows reduced spatial noise and smoother regional structures on average over August 2023. PDFs indicate many negative values representing around 54 % of the data in the SO₂-DOAS dataset and 49 % in the SO₂-COBRA dataset.

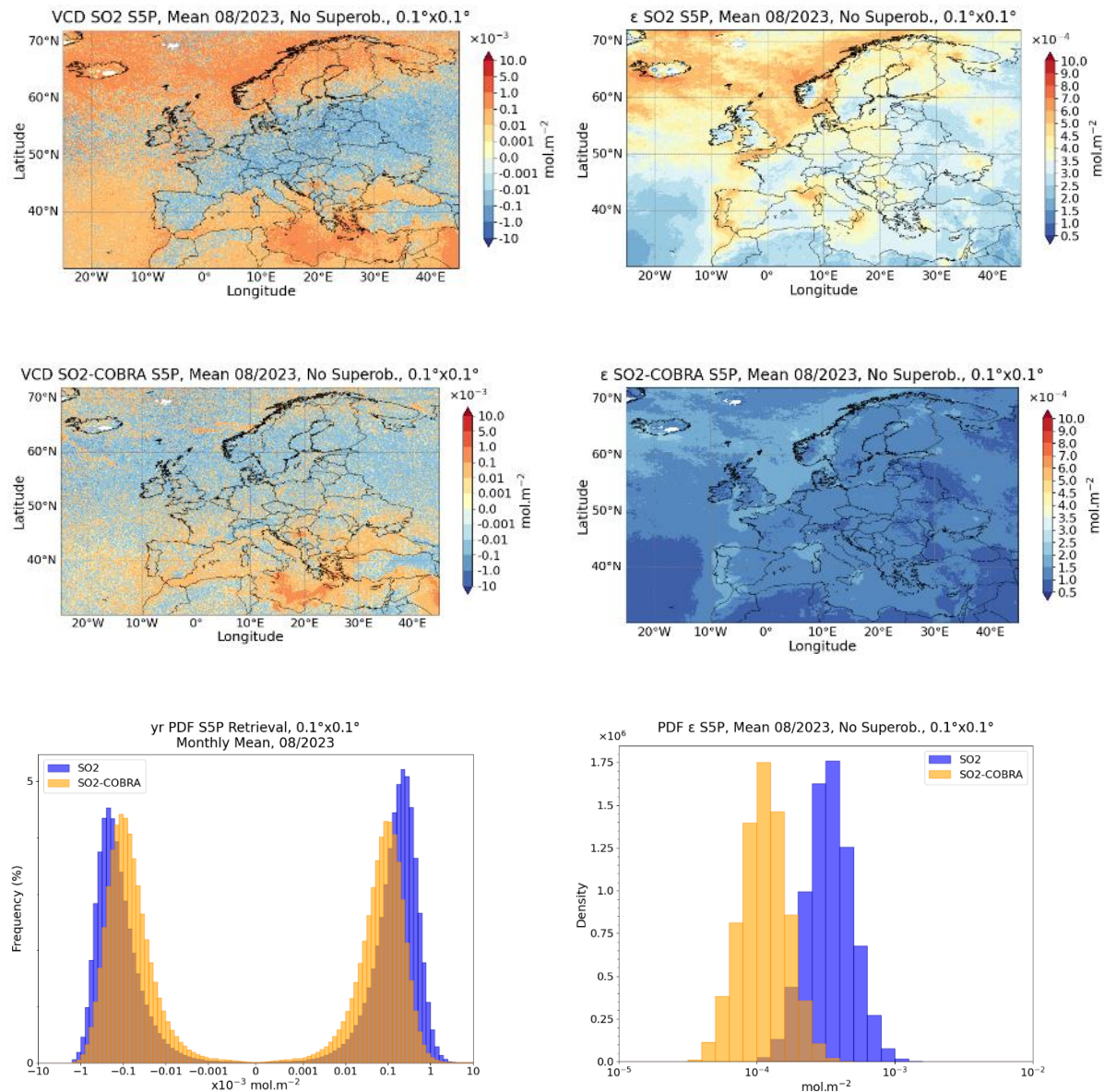


Figure 1: The left column represents the SO₂ VCDs and the right column the SO₂ VCDs errors. The top row represents the DOAS-SO₂ VCDs on the left and their related errors on the right. The middle row represents the COBRA-SO₂ VCDs on the left and their related errors on the right. The bottom row represents PDFs of SO₂-DOAS and SO₂-COBRA VCDs on the left and their related errors on the right. (No super-observation is applied; horizontal resolution is at $0.1^\circ \times 0.1^\circ$ on CAMS domain for August 2023).

CAMEO

The spatial mean distribution of the retrieval error (ϵ) for both datasets on the right in Figure 1, show that the SO₂-COBRA errors (1.21×10^{-4} mol.m⁻²) are smaller than those of the original SO₂-DOAS dataset (3.61×10^{-4} mol.m⁻²) on average. In addition, the SO₂-DOAS dataset has slightly higher mean and error values than the SO₂-COBRA dataset. Thus, the signal-to-noise ratio (SNR) is computed as the absolute value of ratio between the retrieved total column (VCD) and its associated error (ϵ):

$$\text{SNR} = \frac{|\text{VCD}|}{\epsilon}$$

Figure 2 shows the PDFs of SNR values for both datasets under three conditions: (left) all VCDs, (middle) only positive VCDs, and (right) high SO₂ scenes (VCD > 0.5 × 10⁻³ mol.m⁻²). The SO₂-COBRA dataset exhibits higher SNR values than the standard SO₂ product. On average, the SNR increases when VCD is higher respectively from 0.65 (SO₂-DOAS) to 1.00 (SO₂-COBRA) for all VCDs, from 0.80 to 1.15 for VCD > 0 mol.m⁻² and from 2.52 to 5.18 for VCD > 0.5 × 10⁻³ mol.m⁻². Overall, the SO₂-COBRA dataset has a higher SNR and is selected for the experiment of this report.

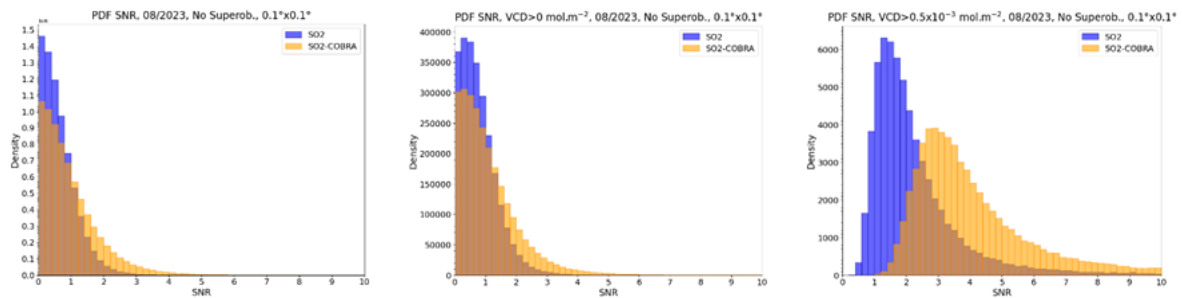


Figure 2 : Probability density functions (PDFs) of the signal-to-noise ratios (SNR) for the SO₂ (blue) and SO₂-COBRA (orange) datasets, without superobbing, at 0.1° x 0.1° horizontal resolution, over the CAMS domain for August 2023. Panels show SNR PDFs for (left) all total column values (VCDs), (middle) only positive VCDs, and (right) VCDs greater than 0.5 × 10⁻³ mol.m⁻².

4.2.2 Quality control and processing of the Sentinel 5P observations for data assimilation

The *Product User Guide*, the *ATBD (Algorithm Theoretical Basis Document)* and Theys et al. (2021), provide guidance to apply Quality Control (QC) to S5p/SO₂ observations. The generic observation operator CAMS Satellite Operator (CSO, available via a TNO GitLab server <https://ci.tno.nl/gitlab/cams/cso>) has been used and implemented in the data assimilation system by 6 partners. Table 3 summarizes the data processing and QC applied. Super-observation is applied to all model studies except for MINNI. Only positive values are kept for DA, except for SILAM which assimilates all values. None of the partners have applied thinning.

Model	Super-observation	Error observation	Data processing and QC
CHIMERE	Yes	Default Averaged	qa_value > 0.75 SZA < 60 Only row 26-424 Superobbing at model resolution 0.2 degree, DA with obs > 0. Cloud fraction < 0.3
DEHM	Yes	Default Averaged	qa_value > 0.8 SZA < 60 degree Cloud fraction < 0.3 Superobbing at model resolution 0.1 degree, DA with obs > 0.
EURAD-IM	Yes	Default Averaged	qa_value > 0.5 Only row 50-400 Superobbing at model resolution of 9 km, DA with obs > 0.
GEM-AQ	Yes	Default Averaged	qa_value > 0.75
MATCH	Yes	Default Averaged	qa_value > 0.5 Superobbing at model resolution, DA with obs > 0.
MINNI	No	Default	qa_value > 0.75
SILAM	Yes	Default Averaged	qa_value > 0.75

Table 3: Description of the Quality Control (QC) processing of the Sentinel 5P SO₂-COBRA data.

Values of the SO₂ total column observations that are assimilated varies for each team considering the Quality Control, super-observation and model resolution, as shown in table 4. EURAD-IM and DEHM use super-observation, and QC is slightly different as EURA-IM is not keeping pixels row far from nadir and a lower qa_value flag. The SO₂ VCD mean of EURA-IM is roughly 30% smaller than DEHM. CHIMERE and EURAD-IM use similar QC but super-observation is applied in EURAD-IM at the resolution around 0.1°, while super-observation is applied to 0.2° in CHIMERE. This process led to a VCD mean value of around 20% larger than for EURAD-IM. In addition, both models, MINNI and GEM-AQ applied similar quality control but MINNI-OI, which is not using super-observation, has a SO₂ VCD mean about 40% larger than GEM-AQ. Finally, CHIMERE and SILAM, which apply super-observation respectively at 0.2° and 0.3° of resolution and different QC, have less than 20% of difference in VCD even if SILAM is keeping negative values.

CAMEO

Those differences also explained differences for observations in the time series presented later in the document 4.3.1.

Units (mol.m ⁻²)	CHIMERE	DEHM	EURAD-IM	GEM-AQ	MATCH	MINNI-OI	SILAM
OBS	8.86×10 ⁻⁵	1.48×10 ⁻⁴	1.07×10 ⁻⁴	1.69×10 ⁻⁴	6.19×10 ⁻⁵	2.74×10 ⁻⁴	1.01×10 ⁻⁴

Table 4: Total column observation mean values after quality control over the CAMS regional domain and August 2023.

4.3 Evaluation over the period of August 2023

INERIS has defined and performed a common postprocessing to analyse the SO₂ VCDs data assimilation results of all teams and their impact on SO₂ concentration.

Results of data assimilation of SO₂-COBRA VCDs over the CAMS European domain are presented by each team in section 4.3.1. Results are analysed on average over the full month of August 2023 but also at defined hotspot locations. The industrial hotspot of Sabac in Serbia and the Etna volcano in Italy are selected because of their highest total columns on a daily and monthly average basis as shown in Figure 3. The Etna volcano hotspot assimilation allows evaluating the capacity to assimilate a natural hotspot source with emission modulation in time. A larger eruption started 13 August 2023 at night and lasted a few days before slowing down until the end of the period.

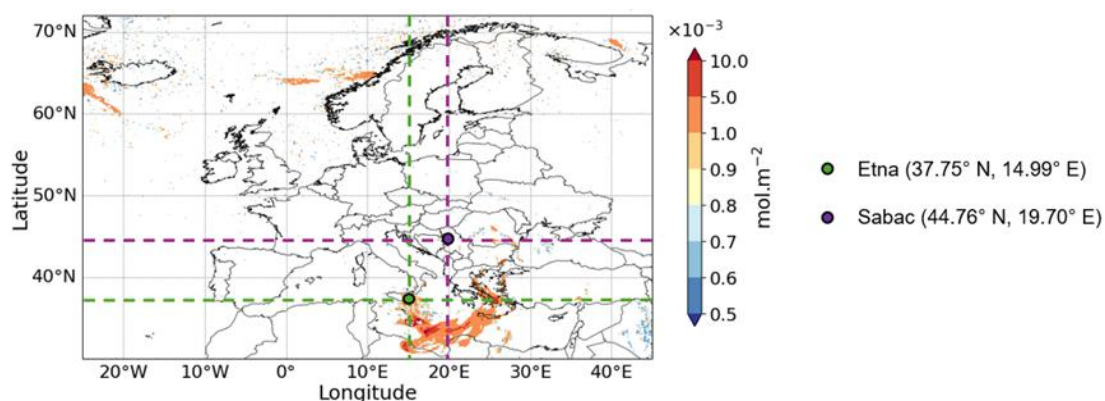


Figure 3: Hotspots selection according to S5P SO₂-COBRA VCD above 0.5×10⁻³ mol.m⁻² on average over August 2023 in Europe.

Intercomparisons are then performed to gather the main conclusions according to different models and systems used. Section 4.3.2 focuses on VCDs impact while section 4.3.3 highlights result on surface concentrations. Additional contributions to VCDs data assimilation/inversion also contribute to the common conclusions, recommendations and perspectives of this study.

4.3.1 Presentation of SO₂ results by Model

4.3.1.1 CHIMERE results

First, data assimilation experiment of SO₂ VCDs of SENTINEL 5P impact is shown on average over the period of August 2023 in Figure 4. The large underestimation in the CHIMERE background (run with no assimilation) is reduced over the domain. The difference in SO₂ total column, between the runs with no assimilation and with assimilation, is globally positive, showing larger values around higher emission point sources. However, this difference is

CAMEO

negative in the northwest part of the domain around Iceland and in the southeast in Syria and Iraq.

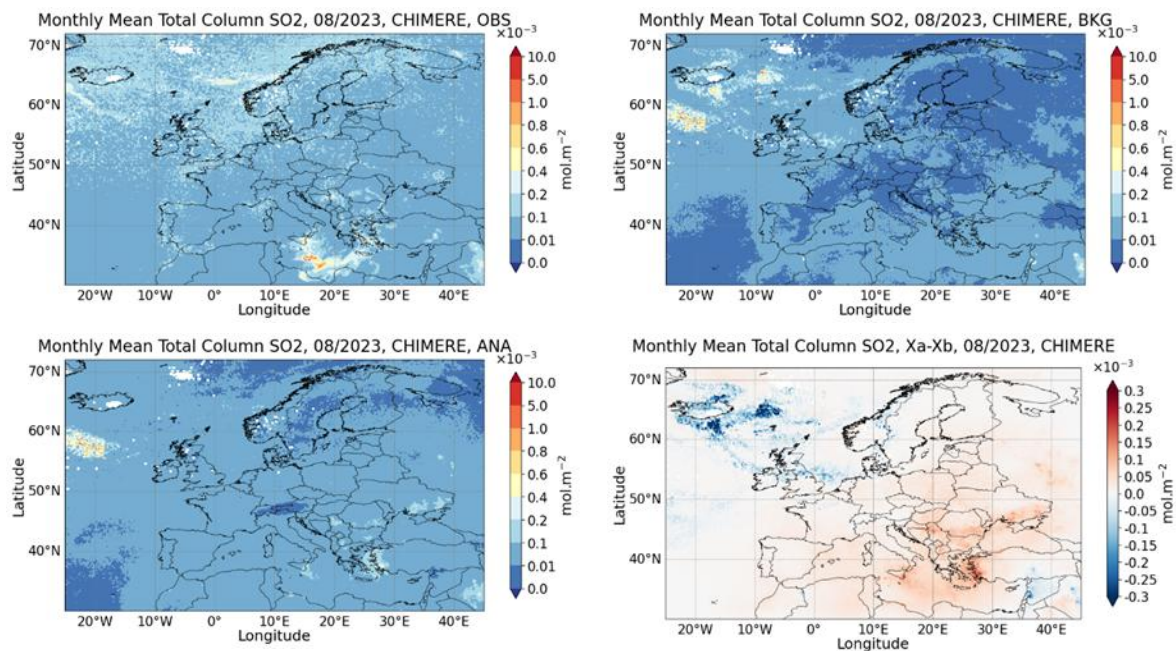


Figure 4: SO₂ total columns mean over August 2023 of the S5P-COBRA satellite observations on the top left, of CHIMERE simulated VCD mean on the top right (no assimilation), CHIMERE simulated VCD mean with assimilation on the bottom left and the difference CHIMERE mean assimilation-no assimilation on the bottom right.

The evolution of SO₂ VCD spatially averaged at orbit time presented in Figure 5 shows a positive global increment. However, a large decrease of VCD around Iceland occurs after August 29th as the large amount of SO₂ coming from the boundary conditions above 600 hPa is strongly reduced by the assimilation and leads to an overall negative bias. Large positive increments are found from August 17th to August 19th according to the large advection of the SO₂ plume over the Mediterranean Sea that occurred after the eruption during the night of August 13th.

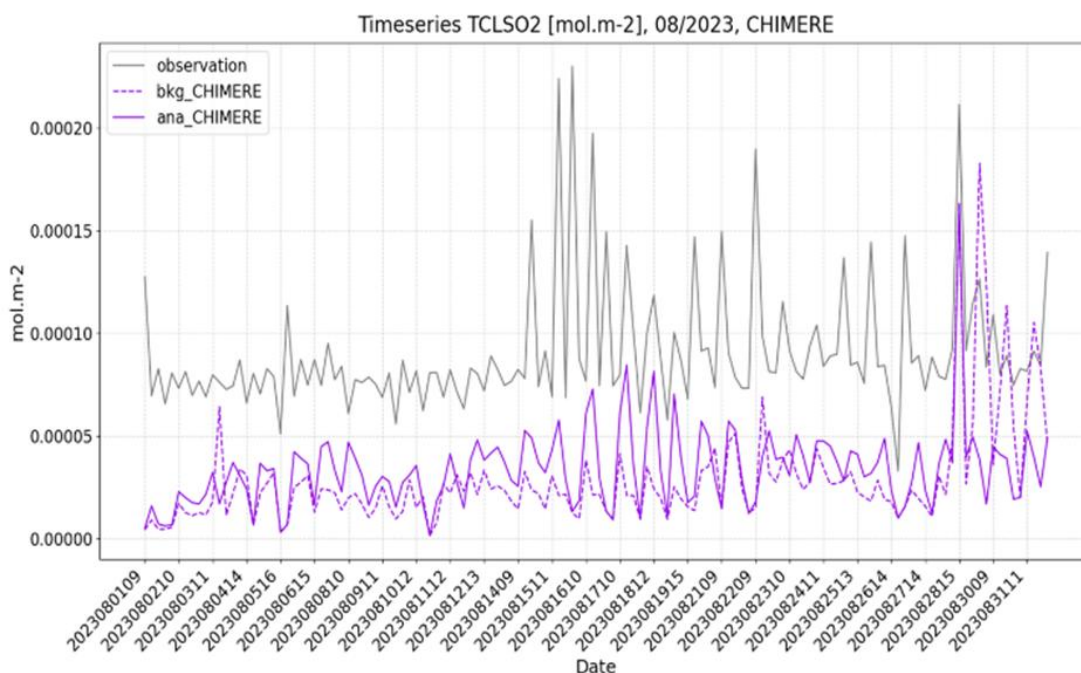


Figure 5: Time series of SO₂ total columns over the CAMS domain for August 2023.

The probability of distribution functions (PDFs), presented in Figure 6 shows that assimilation move the distribution toward higher concentrations, decreasing both the percentage of low values and increasing the number of high values. This leads to a reduction of bias as well as a slight reduction of RMSE.

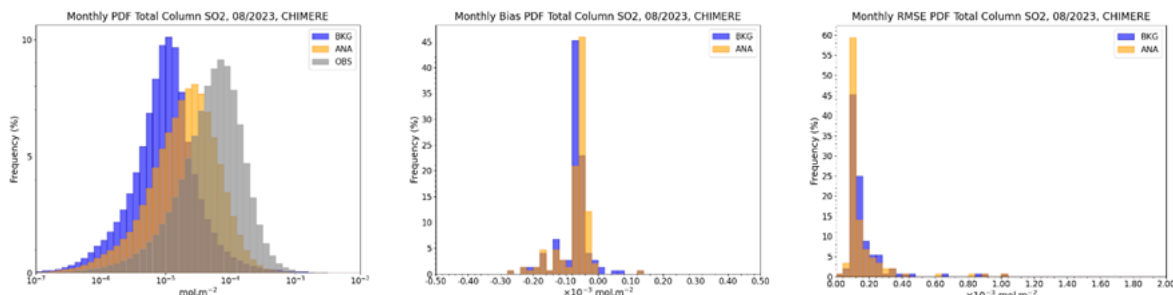


Figure 6: Probability Density Function (PDF) of S5P VCD observations and CHIMERE simulated VCD on the left, bias scores PDF in the middle, and Root Mean Square Error (RMSE) over the CAMS domain for August 2023

The positive SO₂ VCD increment leads to a positive SO₂ concentration analysis increment at the surface, shown in Figure 7, except in Syria and Iraq. The largest increments are around emission sources and along shipping routes in the Mediterranean Sea. One part of the larger increment is due to the assimilation of S5P VCD related to Etna volcano eruption SO₂ plume because the covariance error of the ensemble does not represent this event.

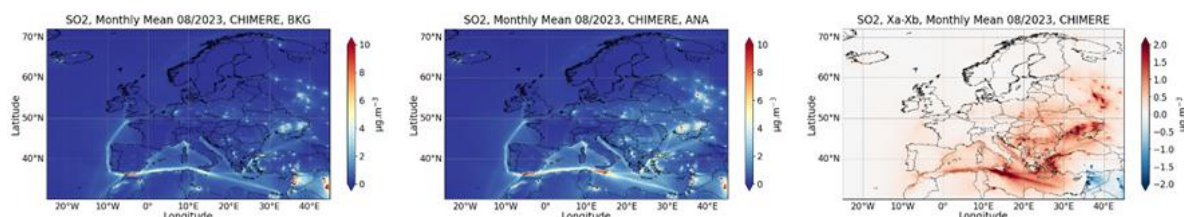


Figure 7 : SO₂ surface concentration in Europe for August 2023: CHIMERE without assimilation (left), CHIMERE with assimilation (middle), and the difference between CHIMERE with and without assimilation (right).

Hereafter, a focus is made for the two selected hotspots for having large VCD, Etna in Italy and Sabac in Serbia. The time series evolution of SO₂ VCD in Figure 8 shows that run with assimilation (ana) is more aligned with S5P observations which allows reducing one part of the large underestimation in the run with no assimilation (bkg).

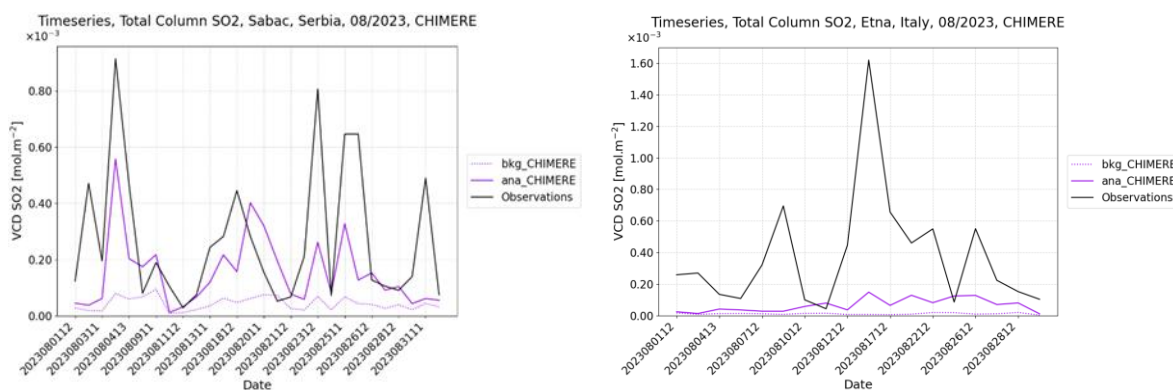


Figure 8: CHIMERE Times series of SO₂ total columns over August 2023 at Sabac location on the left and at Etna location on the right.

The vertical profiles of SO₂ concentration on average over August 2023 in Figure 9, show large impacts at Sabac hotspot location. The SO₂ concentration is largely increased within the boundary layer close to anthropogenic sources relying on the background error covariances error definition of the ensemble. Moreover at Mt. Etna, where SO₂ is likely emitted high in altitude, the impact on surface concentrations remains small.

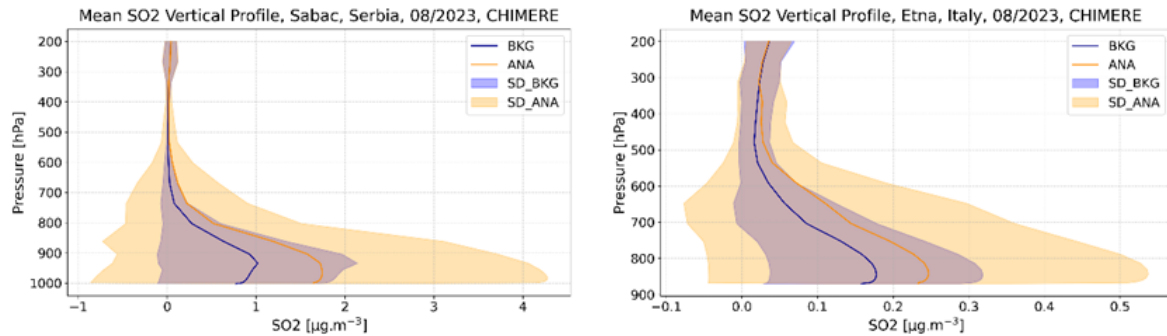
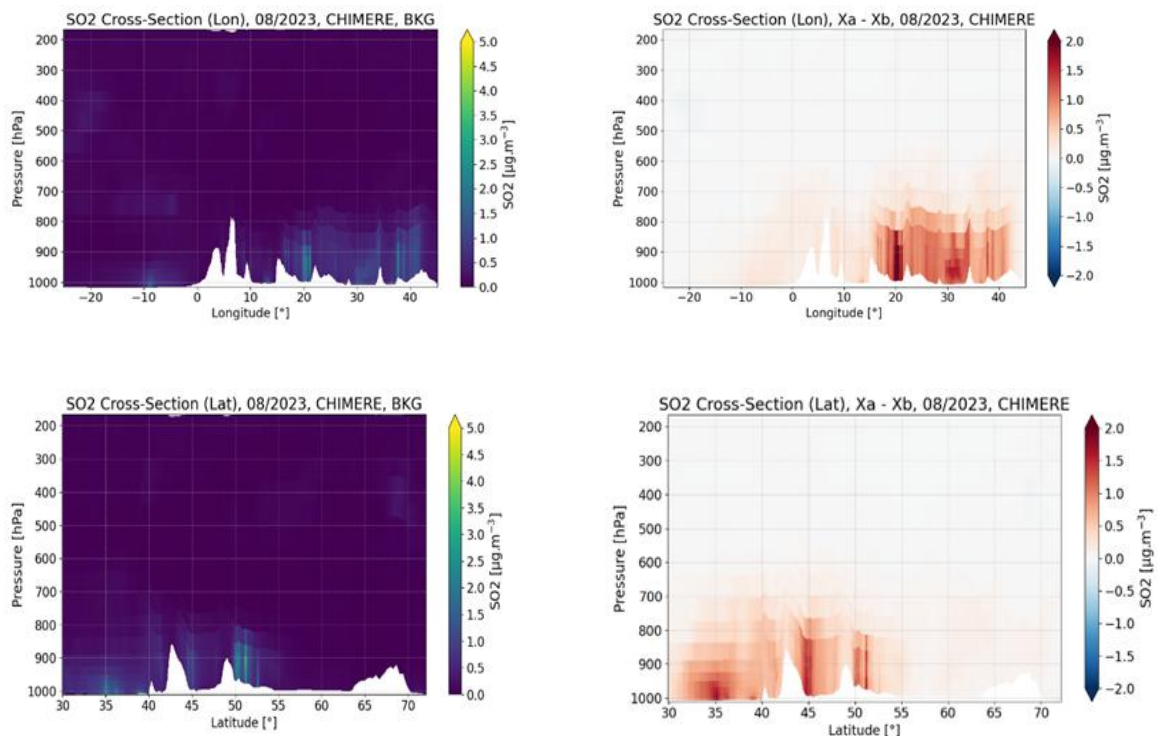


Figure 9: CHIMERE vertical mean profiles of SO₂ concentration over August 2023 at Sabac location on the left and at Etna location on the right (the legend SD means Standard Deviation)

The vertical cross sections in Figure 10, for Sabac and Mt. Etna show additional information on how analysis increments are spread out over the domain. The model results remain larger within the boundary layer close to anthropogenic emission sources as volcano emissions are not considered here in the emission inventory, neither in the ensemble members.



CAMEO

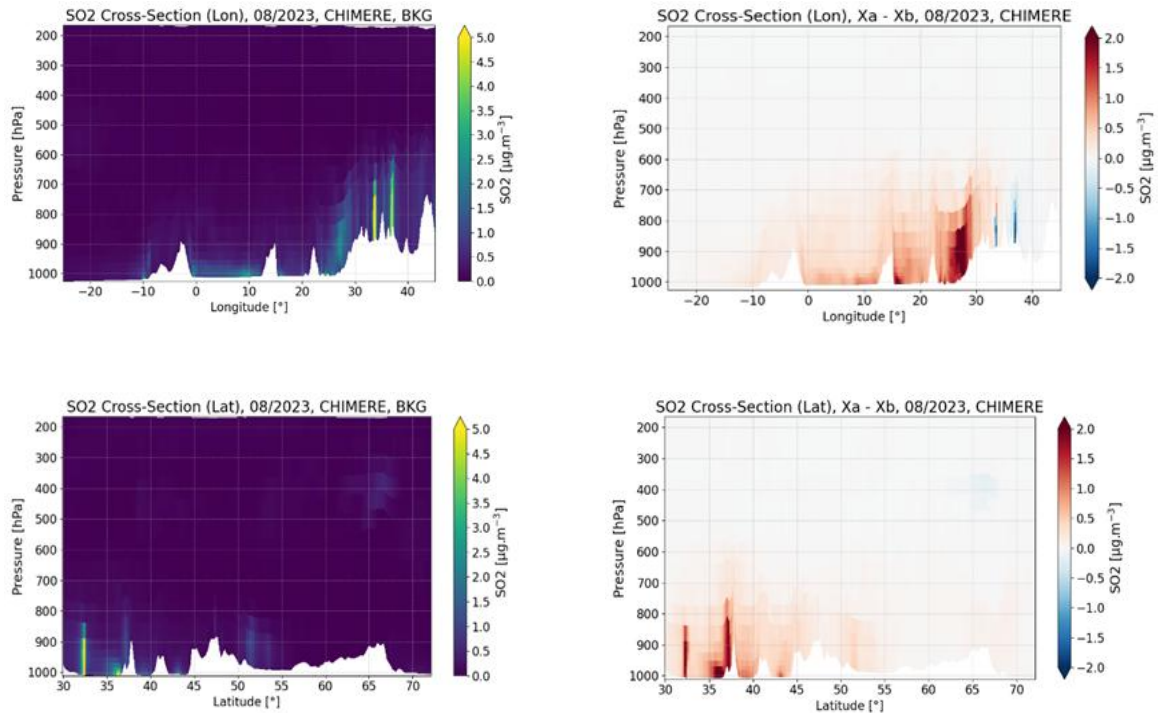


Figure 10: Vertical cross sections of SO₂ concentration means over August 2023. CHIMERE mean of the run no assimilation is on the left and on the right, its difference with the run with assimilation (positive means analysis is higher). Top row is the longitude cross section at Sabac location (44.76°N 19.7° E). The second row is for the latitude cross section at Sabac location. The third row is the longitude cross section at Etna location (37.75°N 14.99° E). Bottom row is for the latitude cross section at Etna location.

In order to improve results, volcano perturbation emissions are implemented in CHIMERE. Figure 11 shows a positive increment in SO₂ total column over the mediterranean sea where the SO₂ plume is located. In the meantime, the analysis increment for concentrations at the surface is slightly reduced close to Mt Etna and along the shipping routes in comparison with the increment shown in Figure 7.

While concentrations were increased close to the surface without the volcano emissions in CHIMERE, the maximum analysis increment is around 500 hPa when volcano emissions are included as shown by the averaged monthly vertical profile in Figure 12 and in Figure 13. The time series on the total column shows that the analysis is within the same range of values as observations.

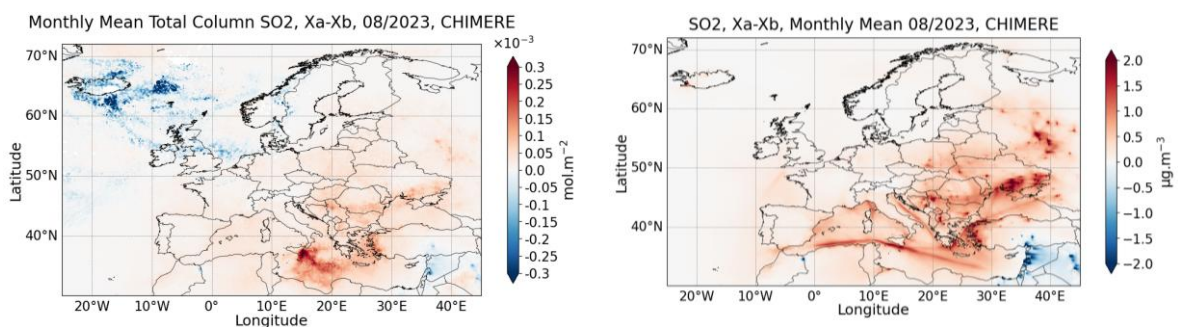


Figure 11: Difference between CHIMERE with assimilation (Etna volcano emissions included) and without assimilation for SO₂ total column in mol.m⁻² on the left and in SO₂ concentration in µg.m⁻³ on the right

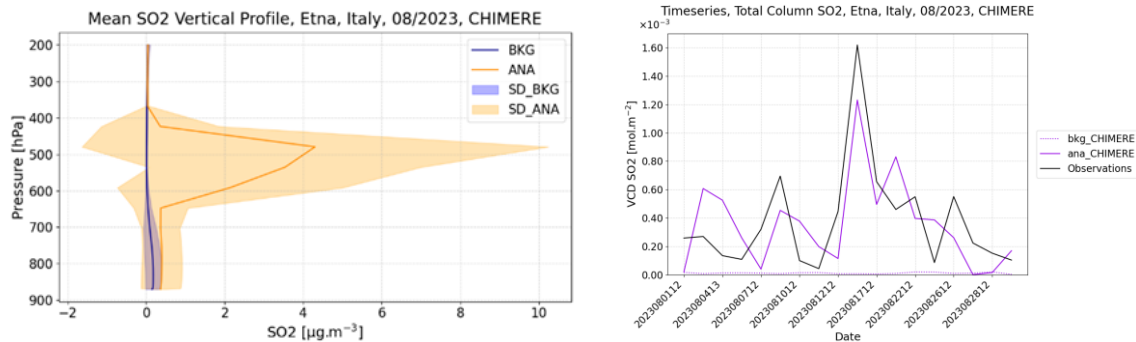


Figure 12: CHIMERE mean vertical profiles of SO₂ concentration over August 2023 on the left and time series of SO₂ total columns on the right (Mt Etna).

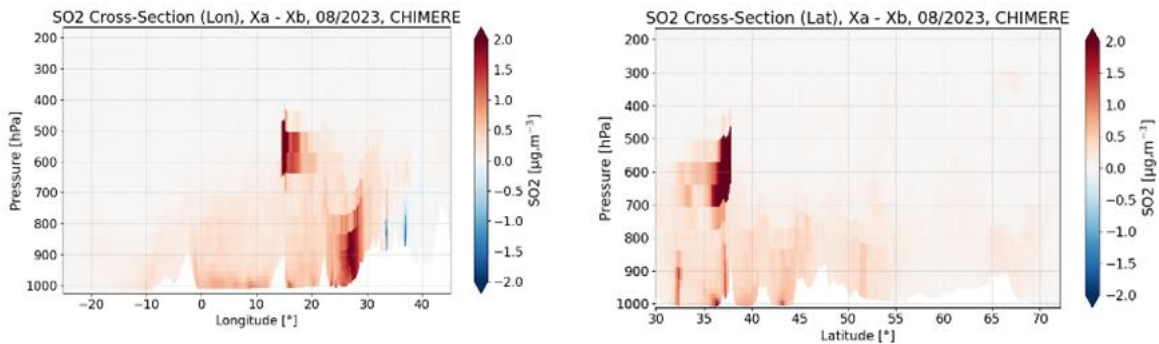


Figure 13: Difference between CHIMERE with assimilation (Etna volcano included) and without assimilation for SO₂ total column

4.3.1.2 DEHM results

Figure 14 presents the spatial distribution of SO₂ total column density over August 2023, comparing S5P-COBRA satellite products with DEHM model results. The satellite data reveals elevated SO₂ total column density over southern Italy, likely capturing volcanic emissions from Mt. Etna, along with other isolated anthropogenic hotspots across Europe. The DEHM prior without assimilation (top right) shows a more uniform distribution with lower concentrations, missing the volcanic signal. This is because volcano emissions are not included in the DEHM model runs. The posterior with assimilation (bottom left) shows enhanced SO₂ values over Mediterranean region and along the shipping routes, but decreased SO₂ over Iceland the North Sea region.

CAMEO

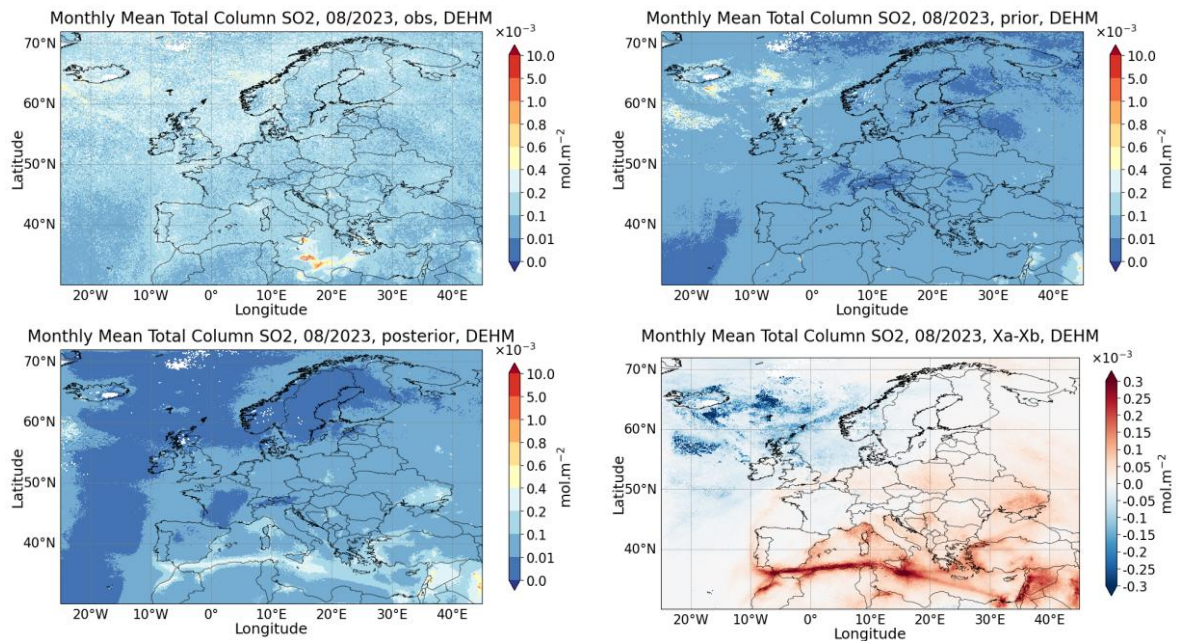


Figure 14: SO₂ total columns mean over August 2023 of the S5P-COBRA satellites observations on the top left, of DEHM mean on the top right (no assimilation), of DEHM mean with assimilation on the bottom left and the difference DEHM mean assimilation-no assimilation on the bottom right

The PDFs of SO₂ total column density (Figure 15 left) shows that the DEHM prior (BKG, blue) centers at lower concentrations than the observations (OBS, grey), and the analysis (ANA, orange) presents a broader distribution with peak extends toward higher values. The PDFs of bias (right) also show that the background presents a systematic underestimation with all negative bias, and the bias after assimilation narrows and shifts slightly closer to zero, but still negative.

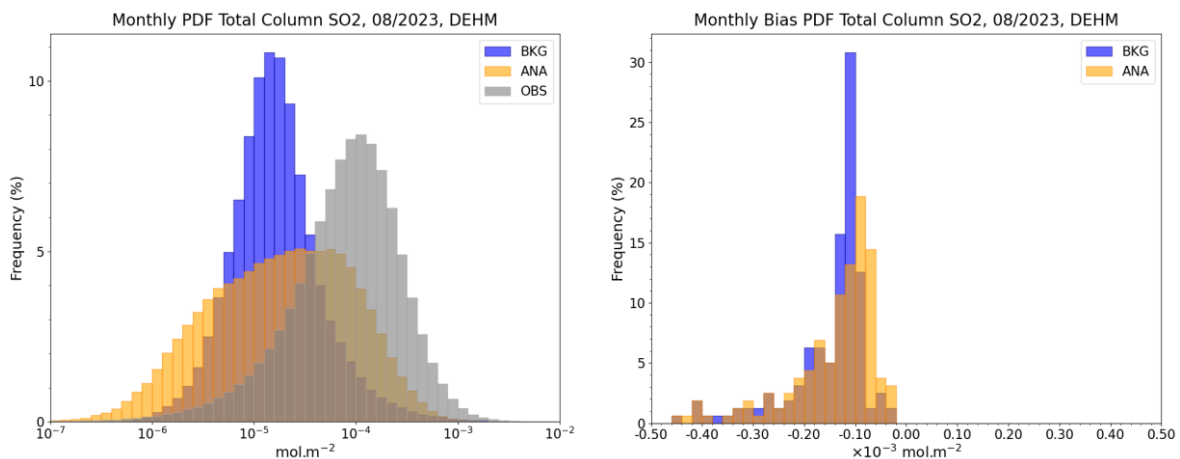


Figure 15: PDFs of the total column SO₂ on the left and the bias of DEHM simulations compared with S5p-COBRA on the right

The DEHM simulations of surface SO₂ concentrations show only small changes (<0.2 ug.m⁻³) after data assimilation for most of the domain (see Figure 16). Assimilation presents positive increments over southern Europe and northern Africa region, and negative increments over central Europe and southeastern part of the domain.

CAMEO

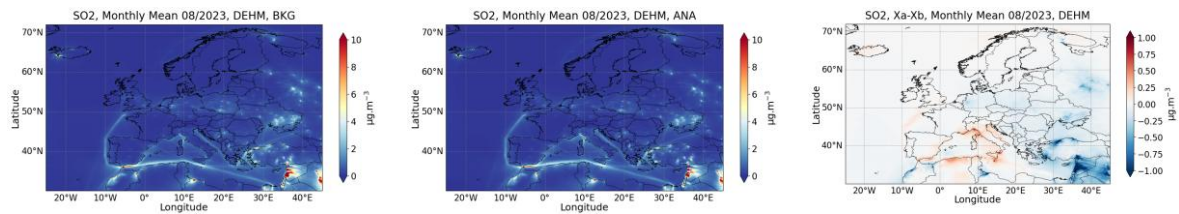


Figure 16: SO₂ surface concentration over August 2023 with DEHM no assimilation on the left, with DEHM assimilation in the middle and the difference between DEHM assimilation and no assimilation on the right

At two hotspot locations, Sabac and Etna, more significant increases of total SO₂ column density are seen after data assimilation (Figure 17). At Sabac (left), observations exhibit high variability, but background DEHM shows relatively low and stable values. The analysis captures most of the observed peaks, especially the one on August 26. At Mt. Etna (right), the background DEHM shows near-zero concentrations, and completely missed all the peaks. The values are overall increased in the analysis, but it is still challenging to capture the variability in observations.

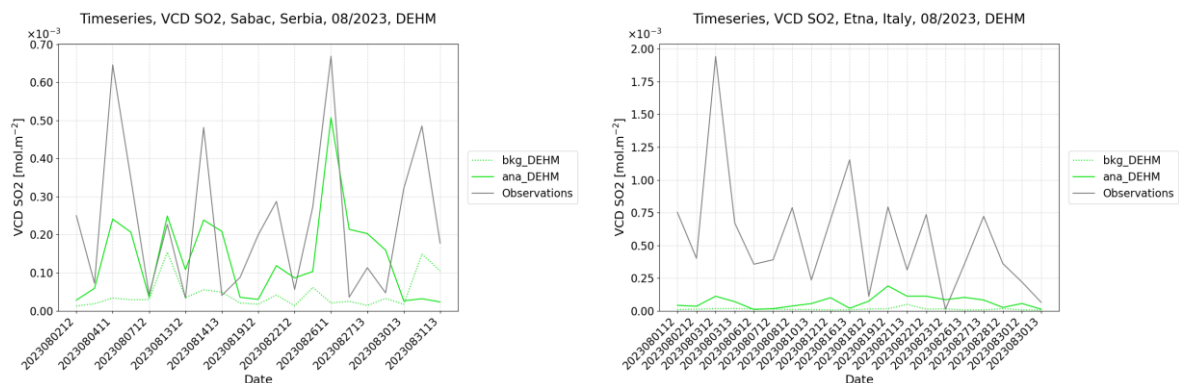


Figure 17: Times series of SO₂ total columns over August 2023 at Sabac location on the left and at Etna location on the right for DEHM simulations

The vertical profiles show different assimilation effects at the two locations (Figure 18). At Sabac (left), enhancements occur mostly at the upper troposphere from 800hPa to 100 hPa, with slight decreases in the boundary layer. However, at Mt. Etna (right), analysis shows increased SO₂ concentrations at all model levels. This is highlighted also by the vertical cross sections in Figure 19.

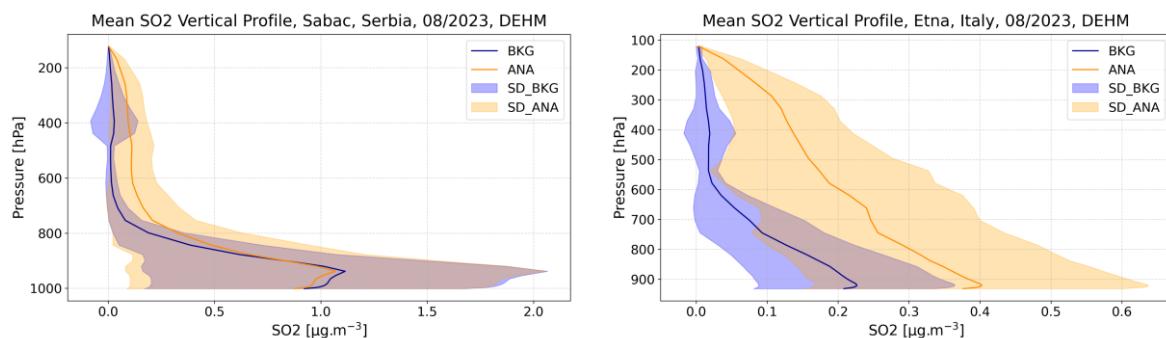
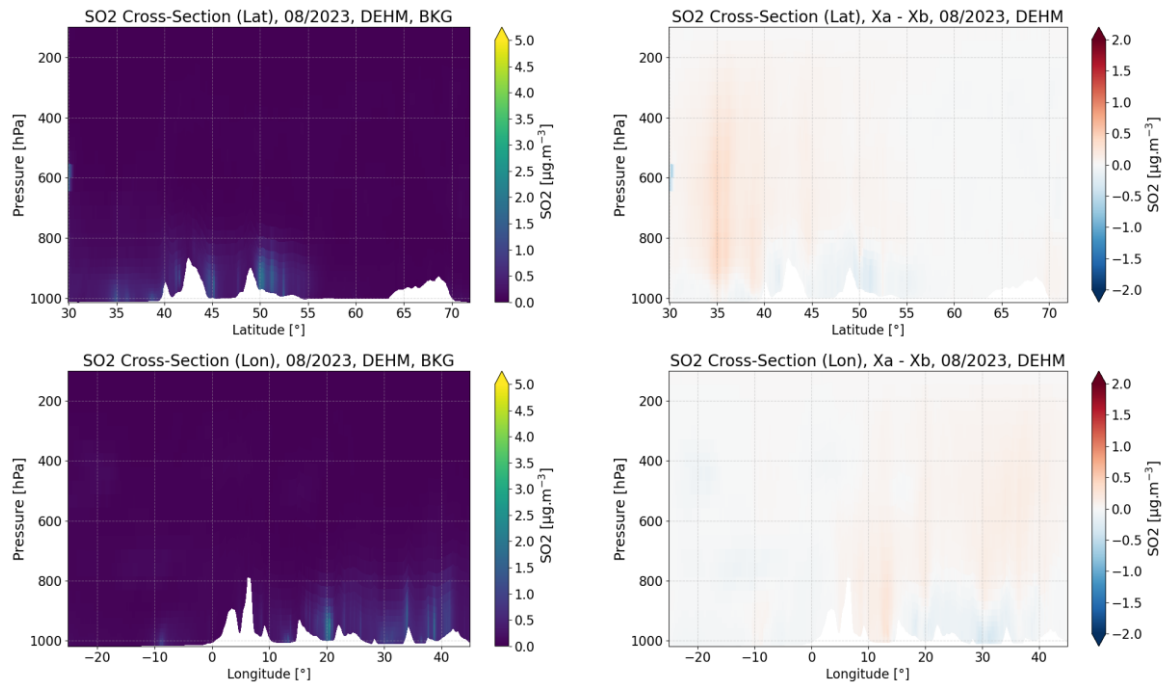


Figure 18: Vertical mean profiles of SO₂ concentration over August 2023 at Sabac location on the left and at Etna location on the right for DEHM simulations

Sabac:



Etna:

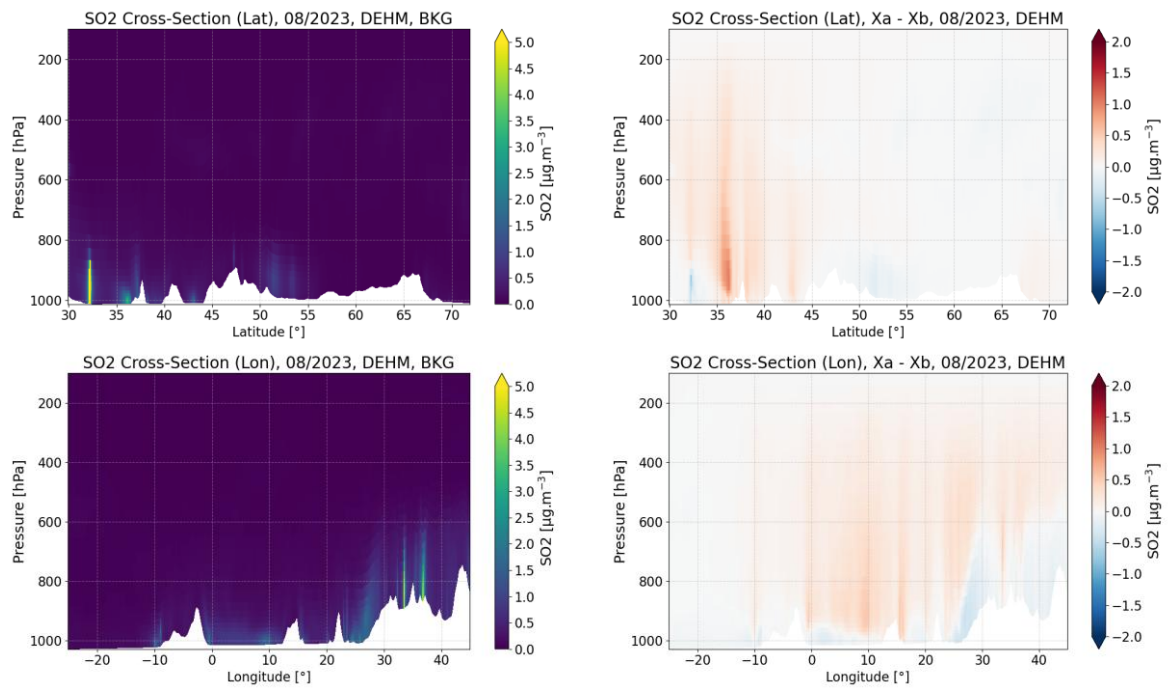


Figure 19: Vertical cross sections of SO₂ concentration mean over August 2023. The figures are the DEHM mean at Sabac (top panel) and Etna (bottom panel) location with no assimilation (prior) on the left and the differences between posterior and prior on the right.

4.3.1.3 EURAD-IM results

The EURAD-IM simulations only include SO₂ emissions from anthropogenic sources. Volcanic emissions are not considered, neither as diffusive degassing nor as major emissions during eruptive phases. Comparing the monthly mean total SO₂ columns over Europe from TROPOMI satellite observations with EURAD-IM simulations without assimilation (Figure 20) reveals that the satellite often observes higher values, particularly over northern and western Europe. The highest SO₂ column densities are detected at Mt. Etna and to the south of the volcano, as well as over the Greek Aegean Islands, where there are some active volcanos. In contrast, EURAD-IM prior simulations feature major SO₂ hotspots in Turkey and south-east Ukraine. Assimilating the S5P-COBRA data leads to slight increases in SO₂ column values across most of Europe. Decreases in SO₂ column values are analysed over south-east Ukraine, over the Crimean Peninsula, in Turkey, Syria and Lebanon. The analysis also depicts very small decreases in SO₂ total columns over eastern Poland and in smaller areas of western Russia. Furthermore, the analysis increment reveals that the satellite-observed high total SO₂ column values from the Mt. Etna volcano does not have a major impact in the EURAD-IM posterior.

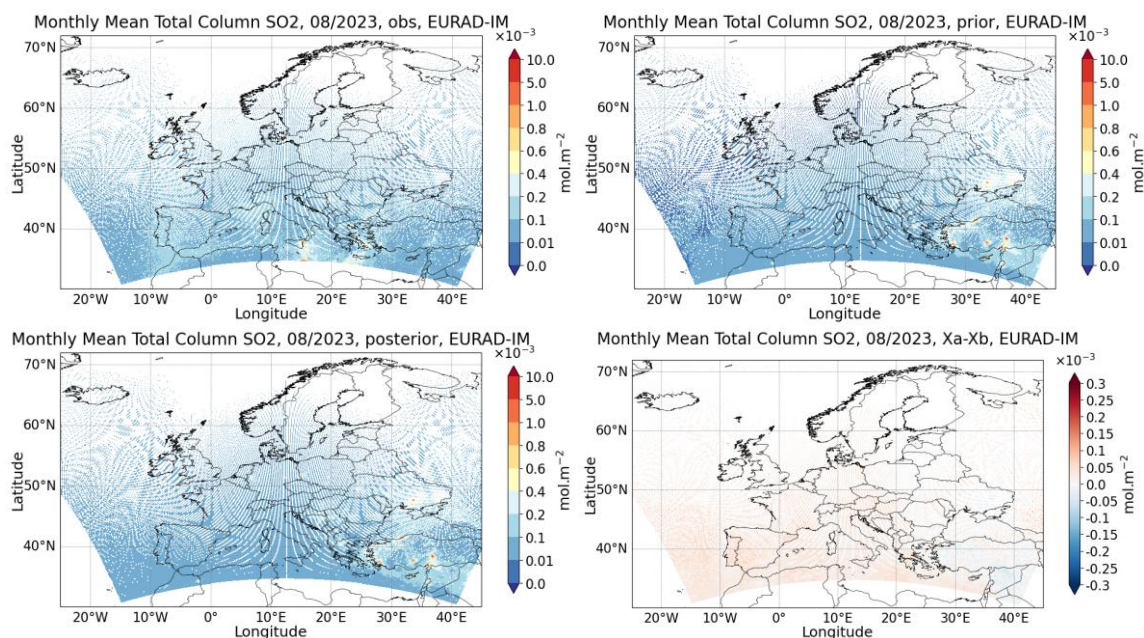


Figure 20: SO₂ total columns as a mean over August 2023 of the S5P-COBRA satellites observations on the top left, of EURAD-IM on the top right (no assimilation), of EURAD-IM with assimilation on the bottom left and the difference EURAD-IM assimilation-no assimilation on the bottom right

The successful assimilation of total SO₂ columns from TROPOMI in EURAD-IM is illustrated in Figure 21. It depicts the comparison of the probability density functions (PDF) of the model prior, the model posterior, and the observations. While the prior PDF is centred around lower column values (around $3e^{-5}$ mol m⁻²) with a larger variance, the observations tend towards SO₂ columns around $1e^{-4}$ mol m⁻² with higher frequency. The resulting posterior PDF is optimally positioned between the prior and observation PDFs, exhibiting the highest probability and smallest variance. The EURAD-IM prior and posterior have the same maximum in their bias PDFs at around -0.07 mol m⁻², pointing towards a general underestimation. The posterior PDF, however, shifts closer to less bias.

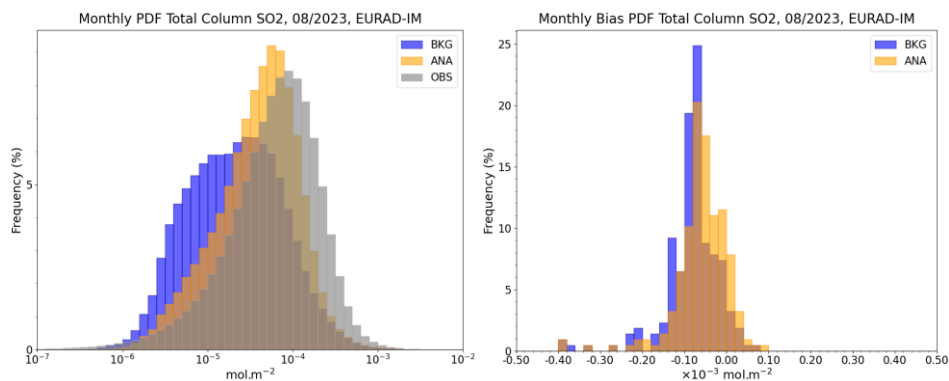


Figure 21: Comparison of the total SO₂ column PDFs of EURAD-IM model results and the assimilated TROPOMI-COBRA data (left) and the corresponding EURAD-IM bias PDFs (right).

Figure 22 shows the mean surface concentrations of SO₂ in August for EURAD-IM prior and posterior, as well as the difference between them. The model's prior and posterior surface concentrations depict strong SO₂ hotspots in industrial areas, particularly in Russia, Ukraine, the Baltic countries, Turkey and Syria, as well as in northern African countries. However, assimilation of TROPOMI SO₂ columns does not reveal any significant corrections at these hotspots. Rather, the analysis increment shows a smooth correction towards higher SO₂ concentrations across Europe, except in the south-east corner of the domain.

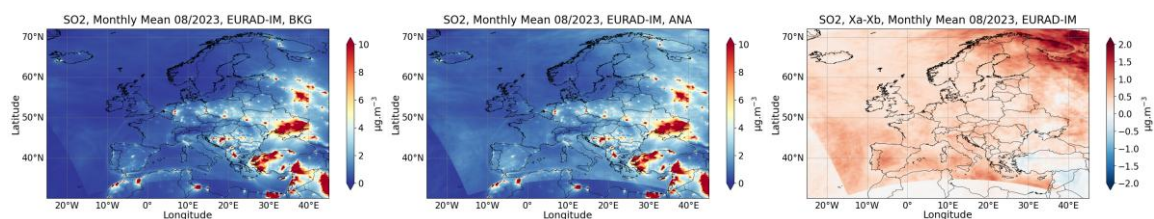


Figure 22: SO₂ surface concentration over August 2023 with EURAD-IM applying no assimilation on the left, with EURAD-IM including assimilation in the middle and the difference between EURAD-IM assimilation and no assimilation on the right.

Examining the temporal evolution of SO₂ columns over Sabac and Mt. Etna in August 2023 (Figure 23) reveals that EURAD-IM is ineffective at extracting information from pronouncedly high observed column values. This is particularly evident in Sabac on 4, 23 and 26 August, and at Mt. Etna on 8, 13–16 and 21–24 August. Apparently, the observations are too far from the model prior, which probably prevents any corrections. While at Mt. Etna, all increments move towards the observations, at Sabac there are a few occasions when the analysis deviates from the observations (on 13, 24 and 20 August).

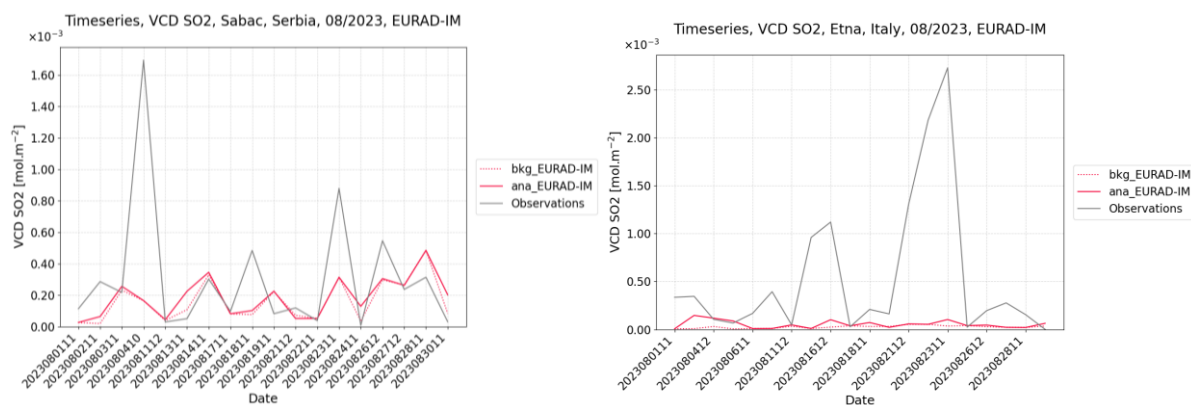


Figure 23: Times series of SO₂ total columns over August 2023 at Sabac location on the left and at Etna location on the right.

Figure 24 shows mean vertical SO₂ profiles extracted from the EURAD-IM prior and posterior at Sabac and Mt. Etna. At Sabac, the modelled profiles are almost identical, showing near surface concentrations of around 5 μg m⁻³, an increase to approximately 7 μg m⁻³ at 950 hPa with altitude, and then a continuous decrease to zero SO₂ at altitudes above 400 hPa. This indicates the presence of a slightly elevated SO₂ plume that is detached from the ground. The standard deviations of both profiles predominantly coincide. At Mt. Etna, the modelled profiles are also identical above an altitude of 700 hPa. At ground level, however, the prior profile depicts concentrations of around 0.7 μg m⁻³, whereas the posterior profile shows 1.1 μg m⁻³. This indicates that the assimilation of volcanic SO₂ loaded TROPOMI columns resulted in increased SO₂ concentrations in EURAD-IM. However, EURAD-IM’s prior SO₂ concentrations are extremely low here (see also Figure 22), which apparently suppressed stronger corrections in the assimilation process. Furthermore, this figure clearly shows that the current configuration of the EURAD-IM assimilation system only allows for corrections at altitudes of highest concentrations in the prior. This consequently confirms that volcanic emissions must be considered in the prior in order to assimilate SO₂ column values efficiently.

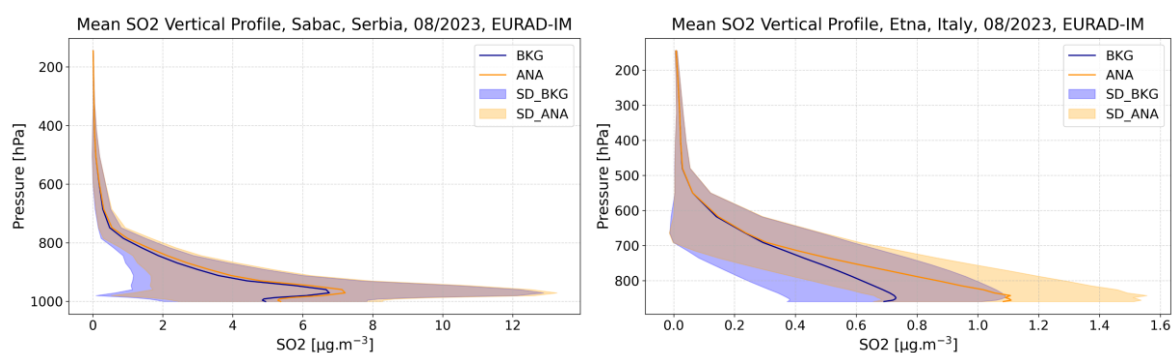


Figure 24: Vertical mean profiles of EURAD-IM SO₂ concentrations in August 2023 at Sabac location on the left and at Etna location on the right.

Figure 25 confirms these findings by showing the SO₂ vertical cross-sections at Sabac (latitudinal) and Mt. Etna (longitudinal) for the EURAD-IM prior and analysis increments. concentrations at Sabac (44° 45' 20" N) remain relatively stable, with the strongest SO₂ increments occurring within the lowest levels (>900 hPa) at the lowest and highest latitudes in the cross section. Increments here only point towards increased concentrations. The longitudinal cross section crossing Mt. Etna (37° 48' 55" E) shows small positive increments to the west of 25° E and slight SO₂ decreases to the east. No elevated increment related to the volcanic eruption is obtained.

CAMEO

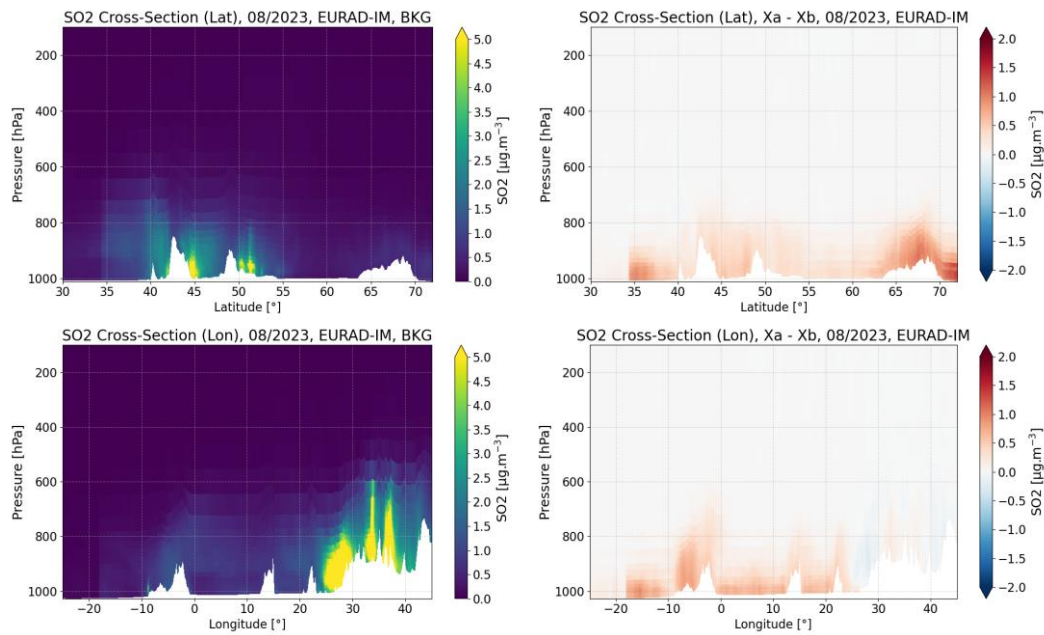
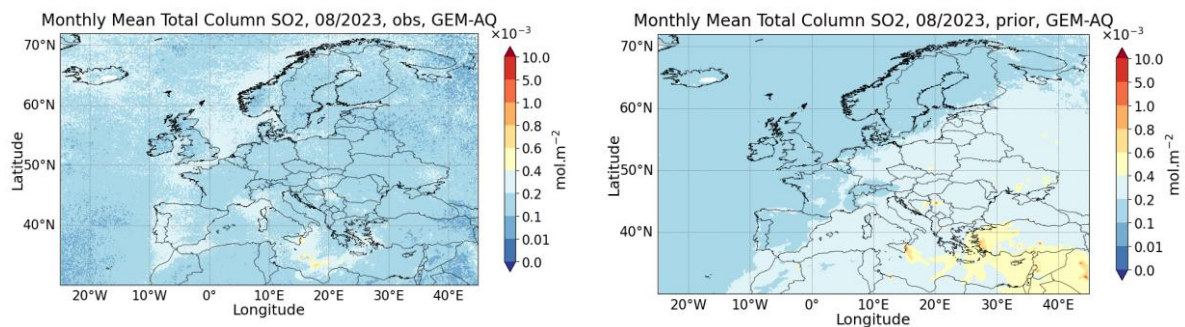


Figure 25: Vertical cross sections of SO₂ concentration mean over August 2023. The top figures are the latitudinal EURAD-IM means at Sabac location with no assimilation on the left and the assimilation increment on the right. The bottom figures are the longitudinal EURAD-IM means at Etna location with no assimilation on the left and the assimilation increment on the right

4.3.1.4 GEM-AQ results

The GEM-AQ model exhibited a systematic overestimation of SO₂ concentrations compared with satellite observations, particularly across the Eastern Mediterranean and the Middle East. Data assimilation effectively reduced these regional biases, aligning model outputs more closely with observed values while preserving important localized features such as the persistent emissions from Mt. Etna and the hotspot near the Serbian city of Sabac. Over inland Europe, where GEM-AQ tends to simulate elevated background concentrations, the assimilation process partially corrected the overestimation without suppressing meaningful local variability (Figure 26).



CAMEO

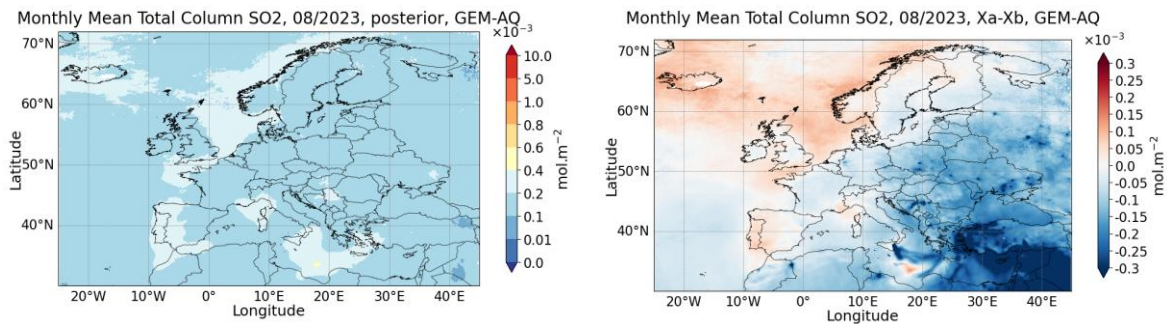


Figure 26: SO₂ tropospheric columns averaged for August 2023 of the S5P-COBRA satellites observations on the top left, of GEM-AQ mean on the top right (no assimilation), of GEM-AQ mean with assimilation on the bottom left and the difference GEM-AQ mean assimilation-no assimilation on the bottom right.

At the domain scale, the Probability Density Functions (PDFs) show that both the background (BKG) and assimilated (ANA) SO₂ column distributions are narrower than the observed (OBS) distribution. The assimilation (ANA) shifts the model distribution closer to the observations and reduces the overall bias spread (Figure 27), demonstrating improved model performance.

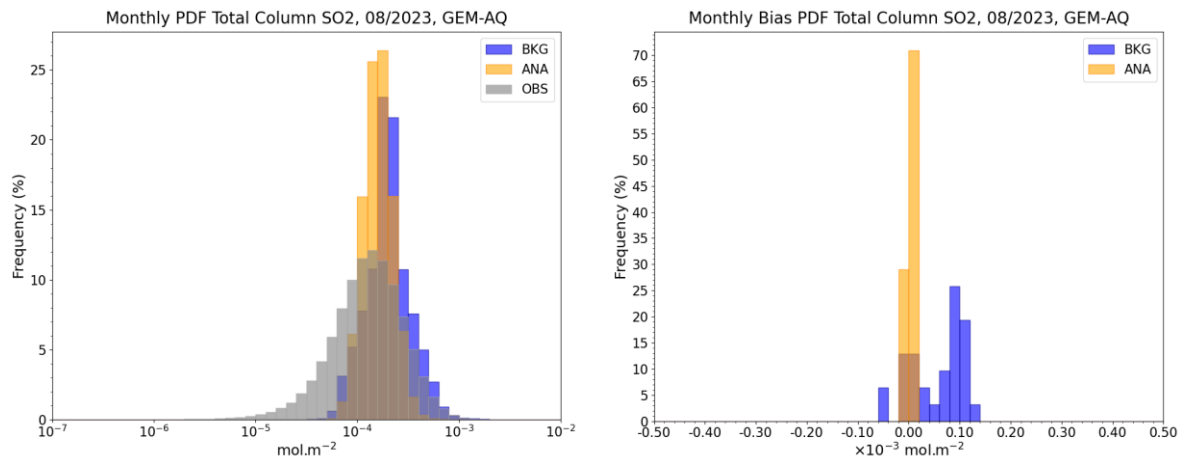


Figure 27: Comparison of the total SO₂ column PDFs of GEM-AQ model results and the assimilated TROPOMI-COBRA data (left) and the corresponding GEM-AQ bias PDFs (right).

At the surface level, assimilation reduces SO₂ concentrations in regions where the background model overestimated SO₂ column values. All source regions show reductions after assimilation. The difference map showed positive anomalies over the Atlantic Ocean and Western Europe and negative anomalies over south-eastern Europe and the Middle East (Figure 28).

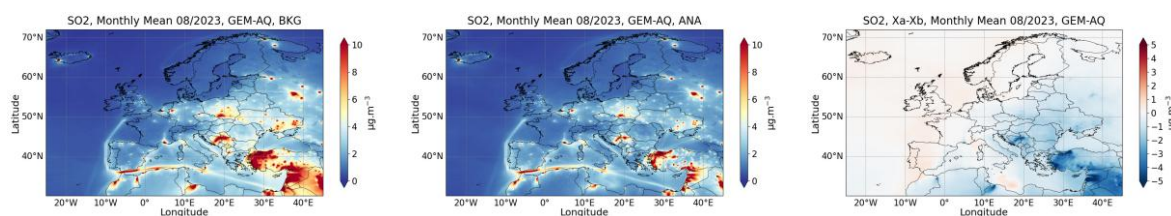


Figure 28: SO₂ surface concentration averaged for August 2023 with GEM-AQ no assimilation on the left, with GEM-AQ assimilation in the middle and the difference between GEM-AQ assimilation and no assimilation on the right

CAMEO

Time series of tropospheric SO₂ columns at selected locations further illustrate the benefits of assimilation. At Sabac, assimilation more accurately captures both the persistent local hotspot and daily variability compared to the background simulation. Similarly, at Mt. Etna, assimilation reduces the overestimation of volcanic emissions while retaining the temporal signature of degassing events (Figure 29).

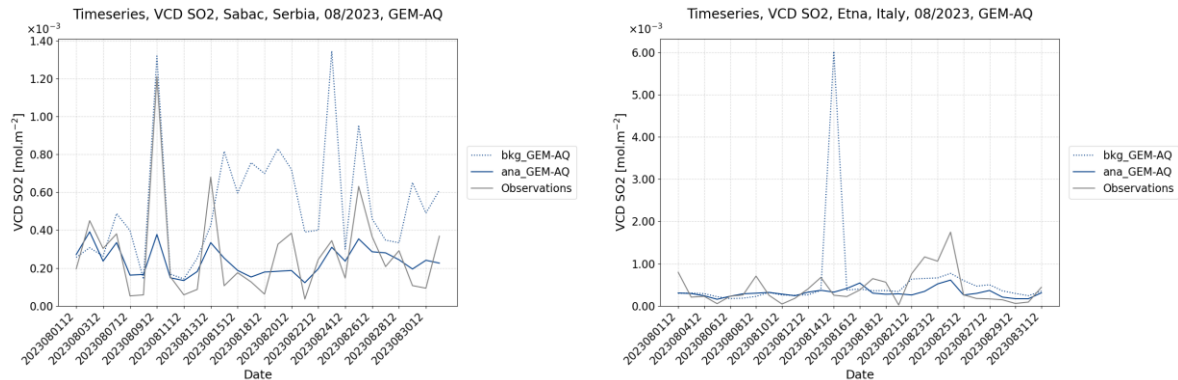


Figure 29: Times series of SO₂ tropospheric columns averaged for August 2023 at Sabac on the left and at Mt. Etna on the right

Vertical mean profiles of SO₂ concentrations at Sabac and Mt. Etna show clear differences between the background (BKG) and assimilated (ANA) fields (Figure 30). At Sabac, higher SO₂ concentrations in the boundary layer are significantly reduced after assimilation, while at Mt. Etna, the assimilation lowers the pronounced maximum near 600 hPa.

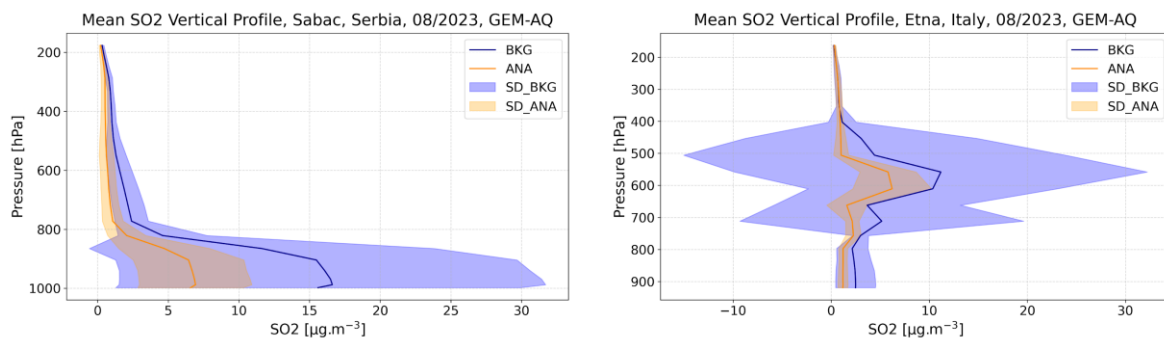


Figure 30: Vertical mean profiles of SO₂ concentration averaged for August 2023 at Sabac on the left and at Mt. Etna on the right

Vertical cross sections at Sabac and Mt. Etna complement the profile analysis by illustrating the spatial distribution of SO₂ with height and horizontal distance. Assimilation reduces background values and constrains the vertical redistribution of SO₂, indicating that the impact of strong local sources such as industrial activity at Sabac and volcanic emissions at Mt. Etna — is overrepresented in the GEM-AQ background simulation (Figure 31).

CAMEO

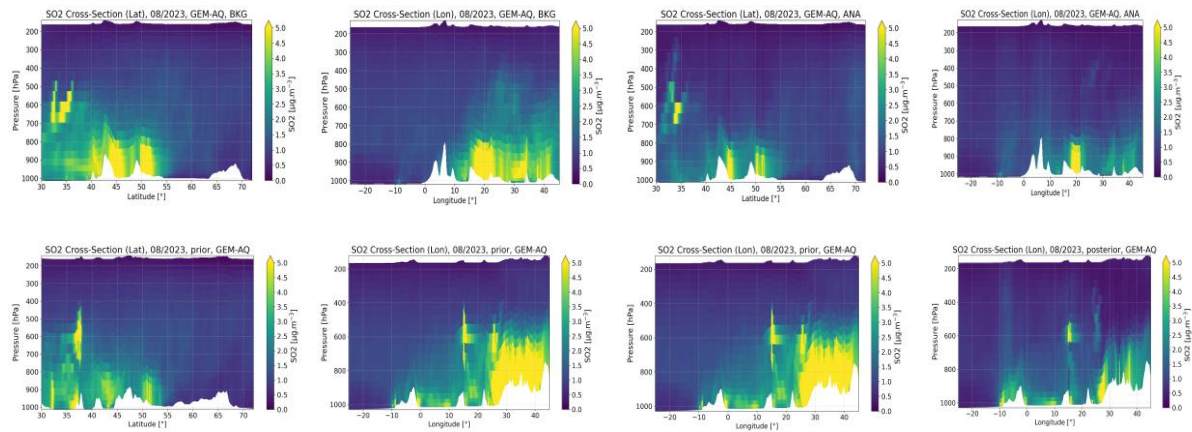


Figure 31: Vertical cross sections of SO₂ concentration averaged for August 2023. The top figures are the GEM-AQ mean at Sabac with no assimilation on the left and with assimilation on the right. The bottom figures are the GEM-AQ mean at Mt. Etna with no assimilation on the left and with assimilation on the right

4.3.1.5 MATCH results

The MATCH results comparable to the ones produced by the models implicated in the exercise of assimilating SO₂ sentinel 5p (COBRA algorithm) are presented from Figure 32 to Figure 37.

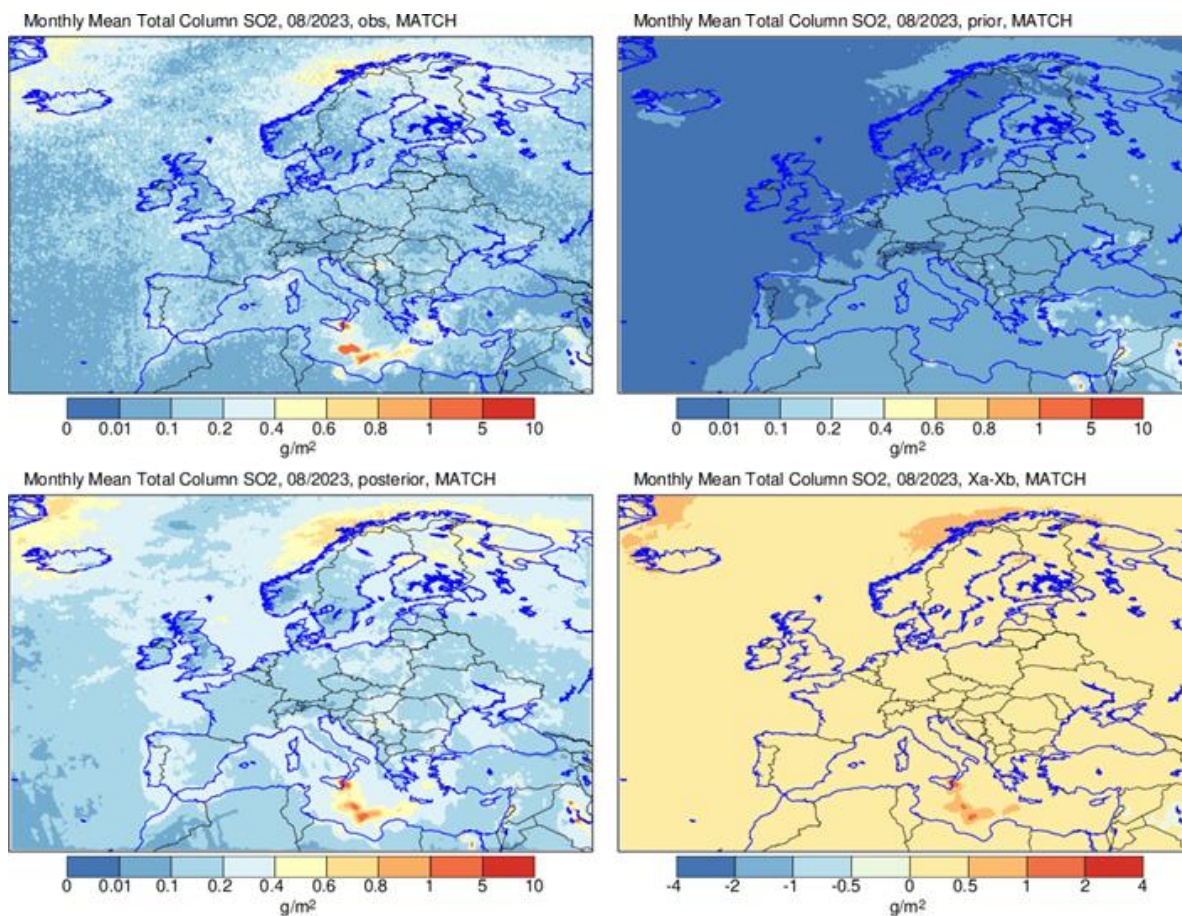


Figure 32: SO₂ total columns mean over August 2023 of the S5P-COBRA satellites observations on the top left, of MATCH mean on the top right (no assimilation), of MATCH mean with assimilation on the bottom left and the difference MATCH mean assimilation-no assimilation on the bottom right

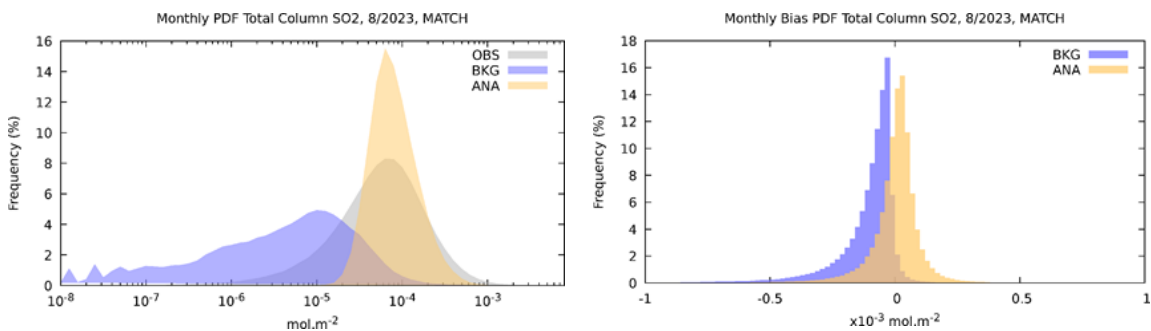


Figure 33: Comparison of the total SO₂ column PDFs MATCH model results and the assimilated TROPOMI-COBRA data (left) and the corresponding MATCH bias PDFs (right).

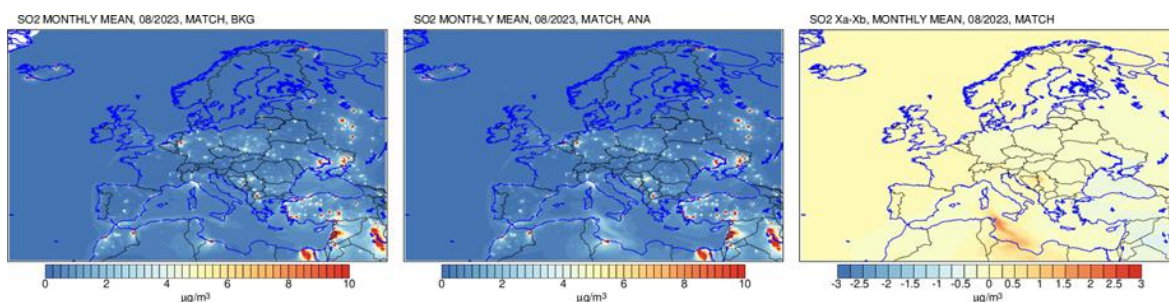


Figure 34: SO₂ surface concentration over August 2023 with MATCH no assimilation on the left, with MATCH assimilation in the middle and the difference between chimere assimilation and no assimilation on the right.

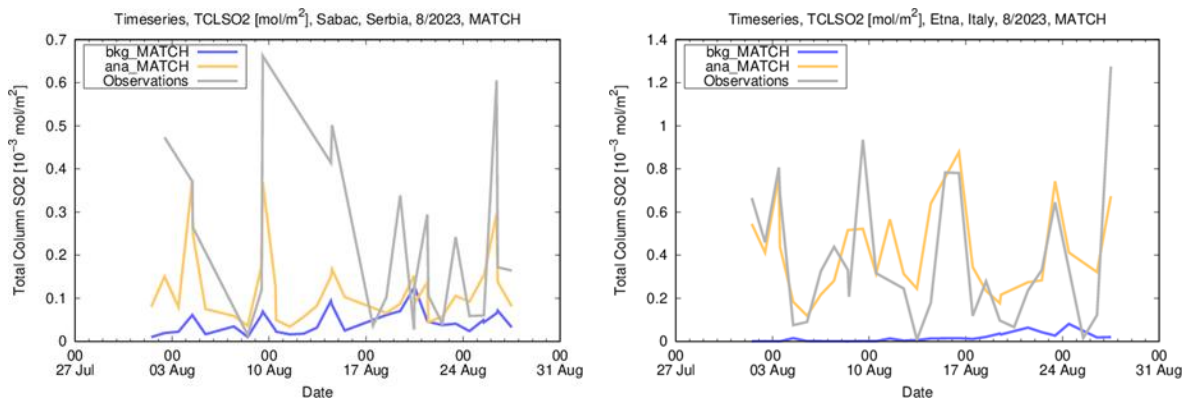


Figure 35: MATCH times series of SO₂ total columns over August 2023 at Sabac location on the left and at Etna location on the right.

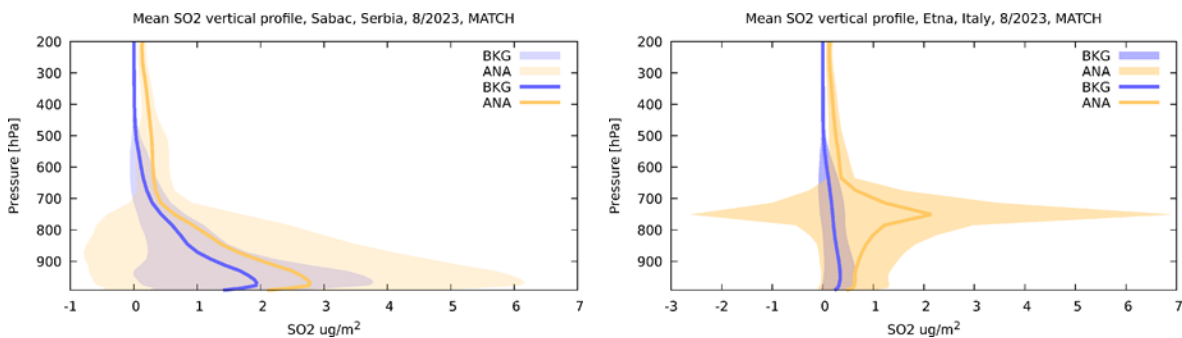


Figure 36: MATCH times series of SO₂ total columns over August 2023 at Sabac location on the left and at Etna location on the right.

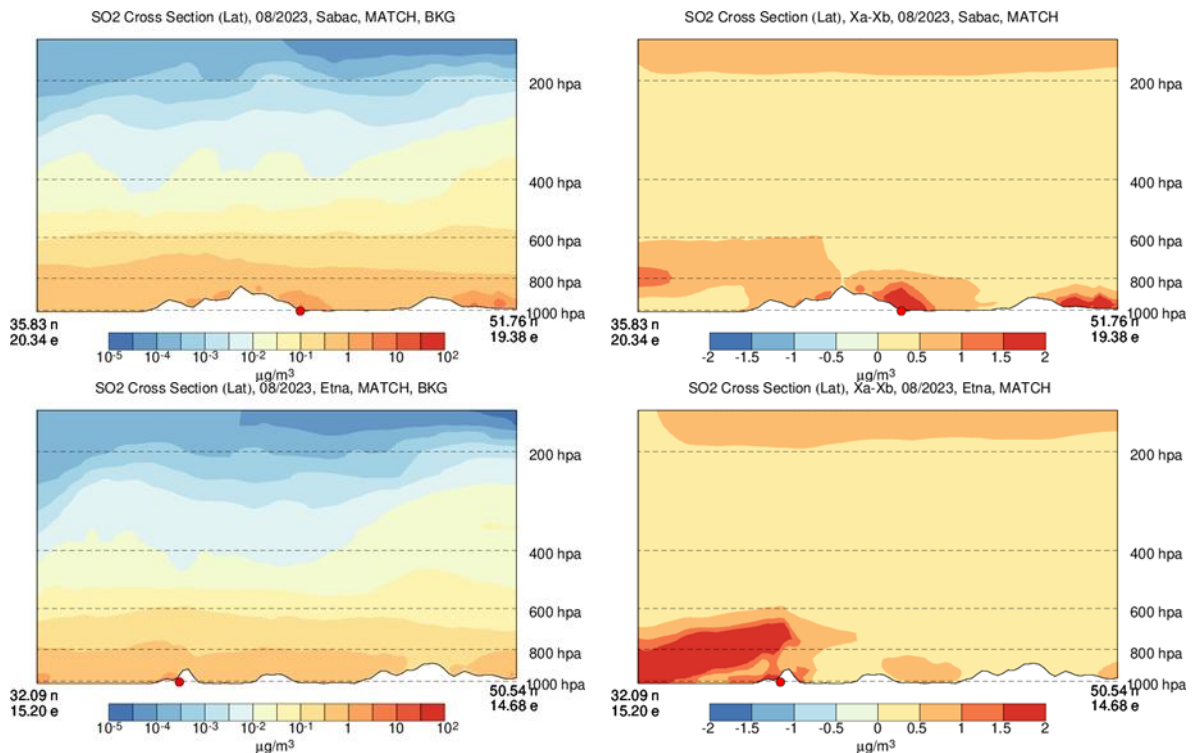


Figure 37: Vertical cross sections of SO₂ concentration mean over August 2023. The top figures are the MATCH mean at Sabac location with no assimilation on the left and with assimilation on the right. The bottom figures are the MATCH mean at Etna location with no assimilation on the left and with assimilation on the right.

The former experience on assimilating S5P NO₂ in the MATH 3d-var analysis system has shown a strong degradation when using the product given column precision, which is not noticeable when assimilating S5P SO₂.

The adopted constant obs-error is in general smaller than the column precision which leads to a stronger fit to the observations than when the column precision is used.

4.3.1.6 MINNI results

In this section, MINNI includes data assimilation results using Optimal Interpolation (OI) and Ensemble Adjustment Kalman Filter (EAKF).

MINNI-OI

Figure 38 shows that the MINNI-OI assimilation of SO₂ satellite retrievals makes “visible” Etna volcano emissions and its plume over the central Mediterranean Sea, up to Greece and Turkey. In these areas, the assimilation increases the monthly mean simulated total column SO₂ with more than $0.3e^{-3} \text{ mol.m}^{-2}$.

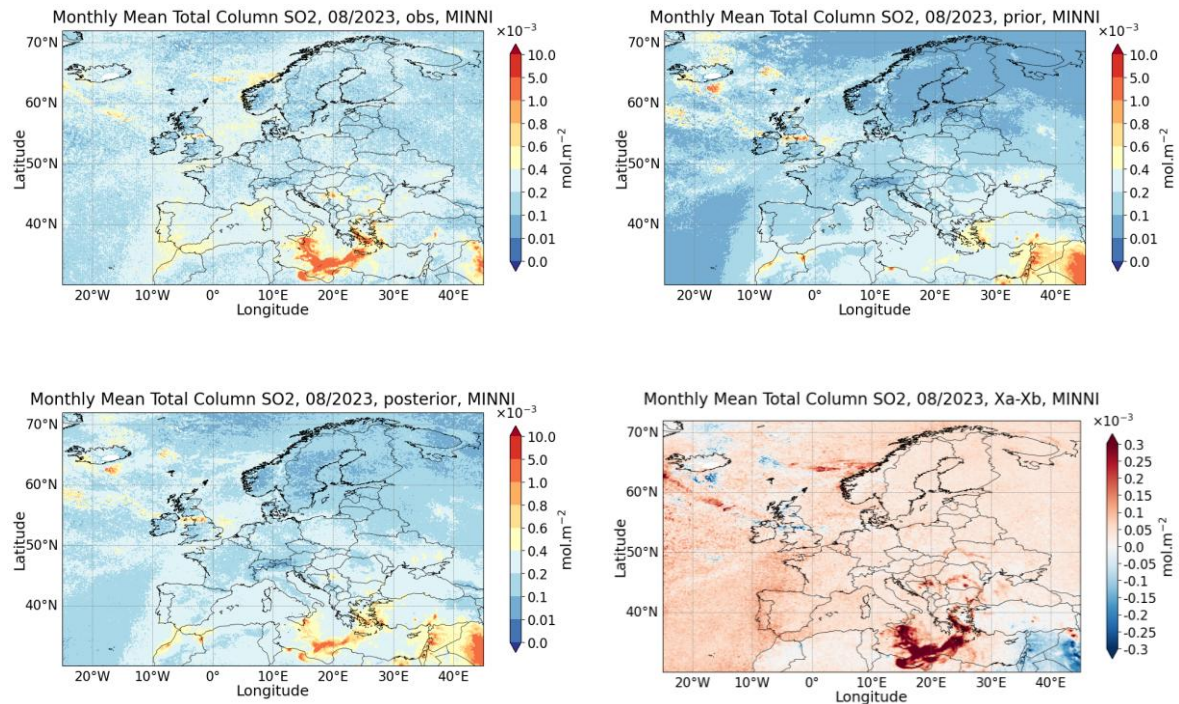


Figure 38: SO₂ total column mean over August 2023 of the S5P-COBRA satellites observations on the top left, of MINNI-OI mean on the top right (no assimilation), of MINNI-OI mean with assimilation on the bottom left and the difference MINNI-OI mean assimilation-no assimilation on the bottom right.

Figure 39 (left graph) confirm that MINNI-OI assimilation led to an increase of simulated SO₂ total column, this time in correspondence of the orbit time: the distribution after assimilation (ANA) is shifted to higher values on both axis with respect to the simulation without assimilation (BKG). The same behaviour is also visible in the bias distribution (right graph) showing that most of the orbit time biases for ANA are ranging between $\pm 0.1e^{-3} \text{ mol/m}^{-2}$.

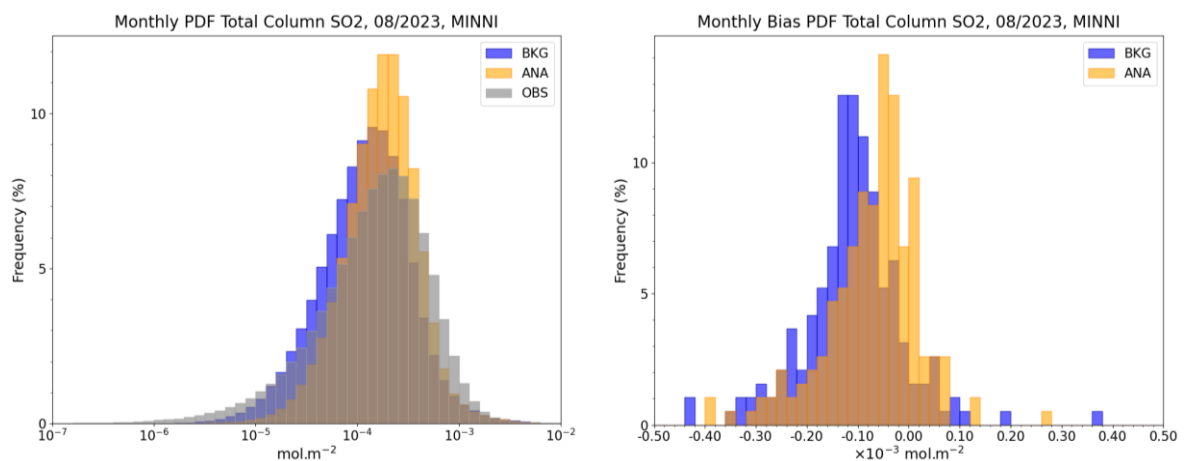


Figure 39: MINNI-OI PDFs scores: total column(left) and bias model-observation (right)

CAMEO

The MINNI-OI assimilation impact on surface SO₂ concentrations is in the range $\pm 0.1 \mu\text{g m}^{-3}$ (Figure 40, right graph). The assimilation of satellite retrievals leads to a decrease of SO₂ concentration in the southern (North Africa) and eastern parts of the domain, and to an increase over central and northern parts of Europe.

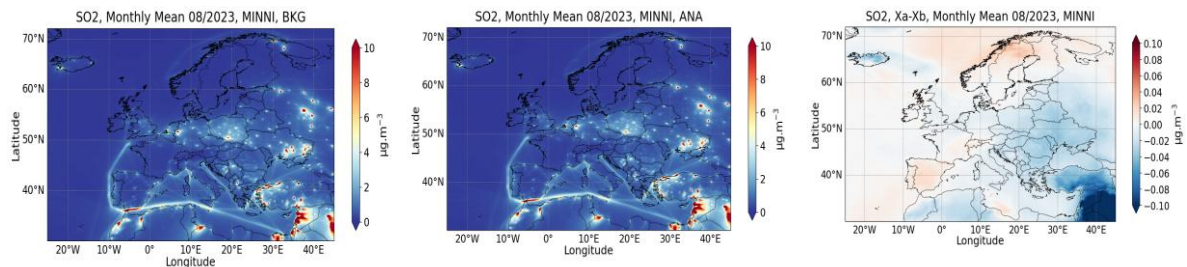


Figure 40: SO₂ surface concentration over August 2023 with MINNI-OI no assimilation on the left, with MINNI-OI assimilation in the middle and the difference between MINNI-OI assimilation and no assimilation on the right

Figure 41 shows that MINNI-OI assimilation increases the simulated SO₂ total column (ana) with respect to simulation without assimilation (bkg) for all time orbits both at Sabac and Etna. The increase is proportional with the observed SO₂ total column. Thus, it is less at Sabac where satellite retrievals have values up to $3e^{-3} \text{ mol/m}^{-2}$ than at Etna where the values are up to $8e^{-3} \text{ mol/m}^{-2}$. This is particularly important for air quality assessments as the latter is a natural and significant source of SO₂ which is not included in emissions input data.

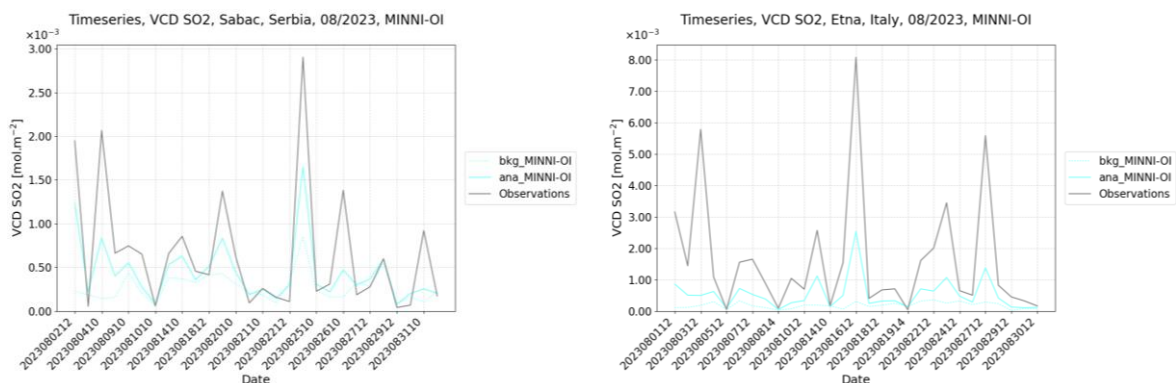


Figure 41: Times series of SO₂ total column with MINNI-OI over August 2023 at Sabac location on the left and at Etna location on the right

Figure 42 shows that, at both locations, the assimilation scheme leads to an increase of SO₂ concentration in the upper layers, above 700 and 600 hPa at Sabac and Etna, respectively. In the first layers above the surface, no difference between ANA and BKG simulations is observed at Sabac, while very little difference is observed over Etna. The changes observed over Sabac at high altitudes may be induced by SO₂ transported from Etna area where the satellite retrievals have the highest values (Figure 38 and Figure 41).

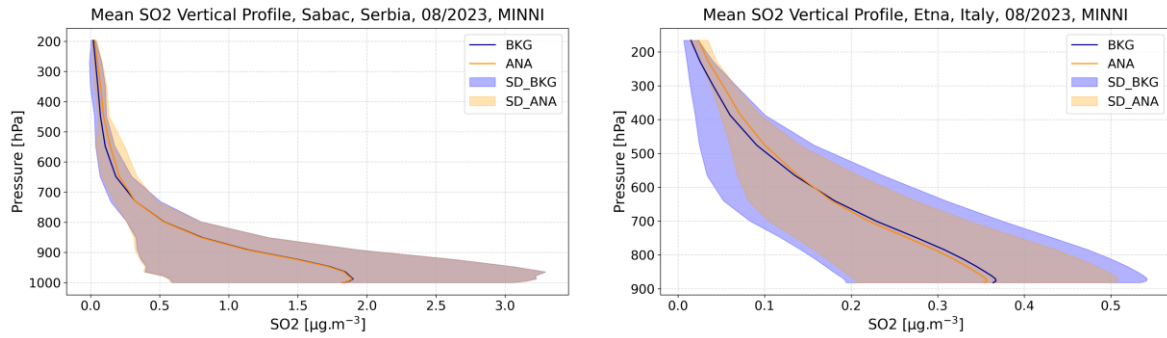
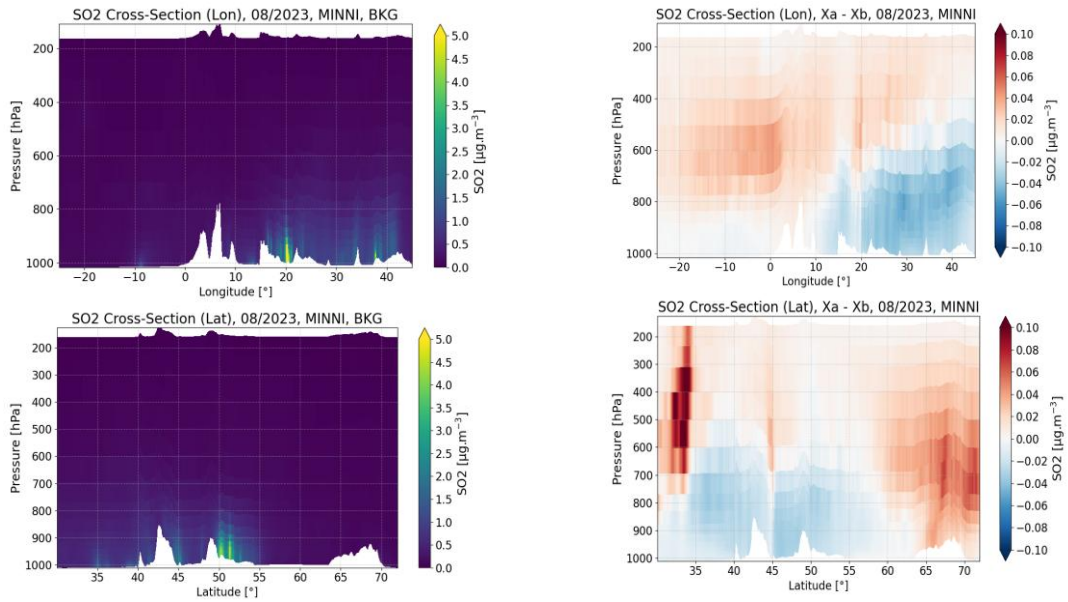


Figure 42: Vertical mean profiles of SO₂ concentration over August 2023 with MINNI-OI at Sabac location on the left and at Etna location on the right

Figure 43 (right graphs) shows that the patterns of vertical cross section of SO₂ concentration differences at Sabac and Etna produced by MINNI-OI assimilation are similar for longitudinal sections (lon) and, also for latitudinal (lat) ones. Lon graphs show an increase of concentrations in the western part of the domain at high altitudes and a decrease in the eastern part at low altitudes. Lat graphs show a decrease of SO₂ concentrations in the middle of the domain at low altitudes and an increase in other parts of the domain. As for time series shown in Figure 41, the concentration differences are higher for Etna cross sections than for Sabac. However, they are all in the range $\pm 0.1 \mu\text{g m}^{-3}$ as Figure 42.

Sabac



Etna

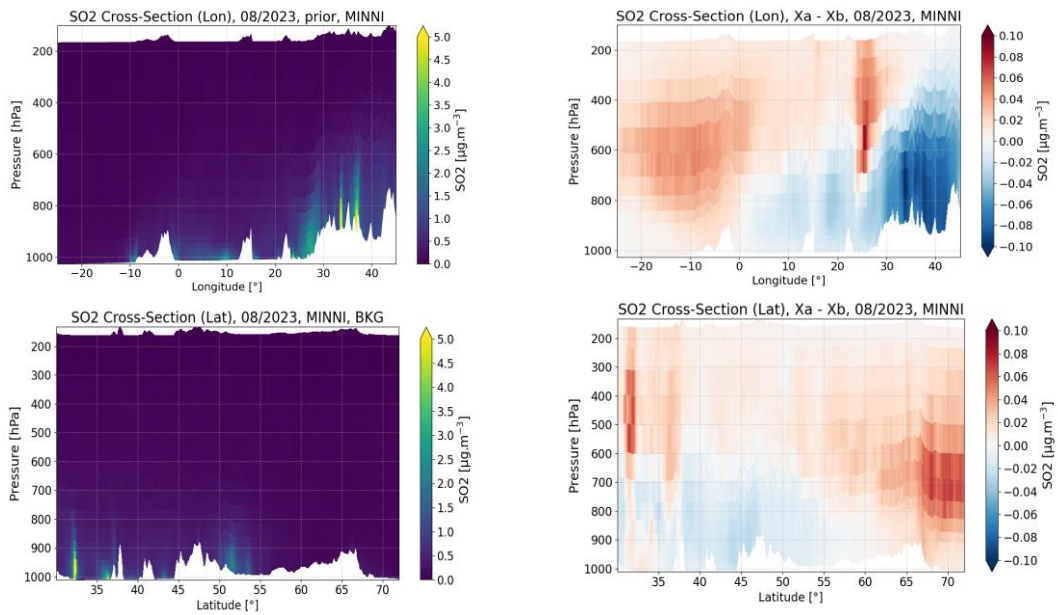


Figure 43: Vertical cross sections of SO₂ concentration mean over August 2023 at Sabac and Etna locations for MINNI-OI: no assimilation (prior) (left graphs) and differences between assimilation (posterior) and no assimilation (prior) (right graphs).

MINNI-EAKF

Figure 44 shows that the MINNI-EAKF assimilation of SO₂ satellite retrievals also capture the contributions of Etna volcano and its plume over the central Mediterranean Sea, but the increases of the monthly mean simulated total column SO₂ are by a factor of two lower than MINNI-OI (up to ca. $0.15e^{-3}$ mol/m²). This may be explained by the conceptual differences in the two approaches: one is dynamic while the other is static, and by the differences in assimilation time: one is hourly while the other is at orbit time.

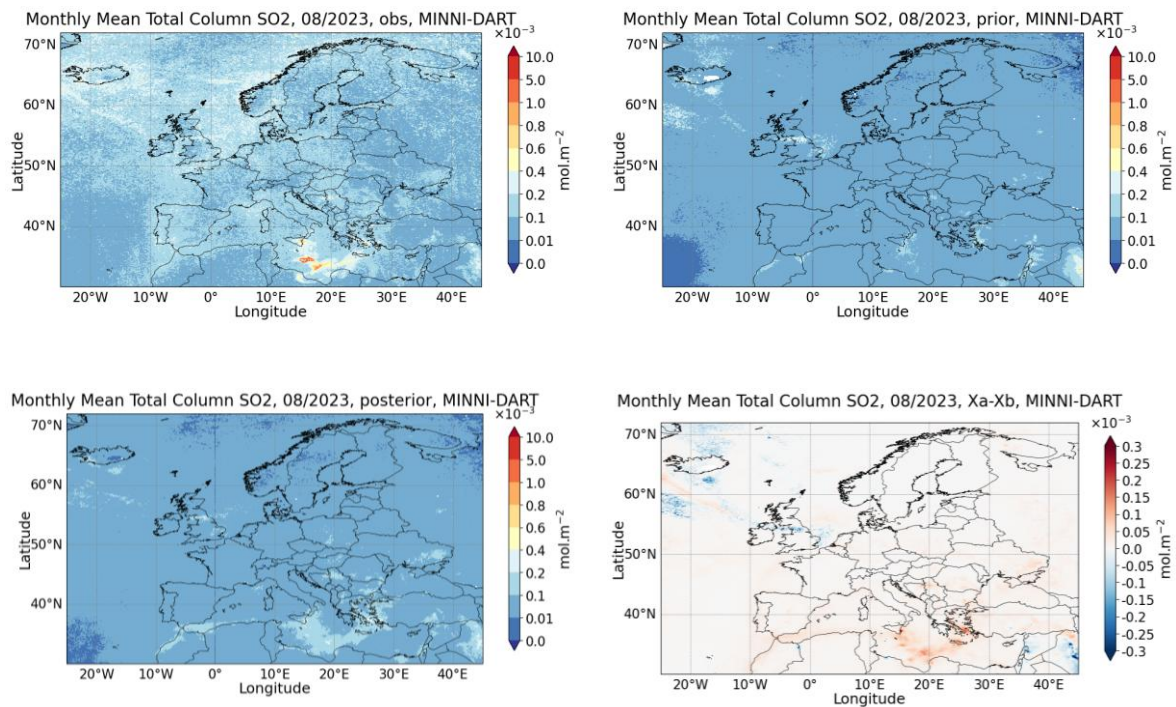


Figure 44: SO₂ total columns mean over August 2023 of the S5P-COBRA satellites observations on the top left, of MINNI-EAKF mean on the top right (no assimilation), of MINNI-EAKF mean with assimilation on the bottom left and the difference MINNI-EAKF mean assimilation-no assimilation on the bottom right

As Figure 44, Figure 45 (left graph) confirms that MINNI-EAKF assimilation led to an increase of hourly simulated SO₂ total column: the distribution after assimilation (ANA) is shifted to higher values on y-axis with respect to the simulation without assimilation (BKG). The shift of bias distribution for ANA and BKG (right graph) is similar, and all biases are negative.

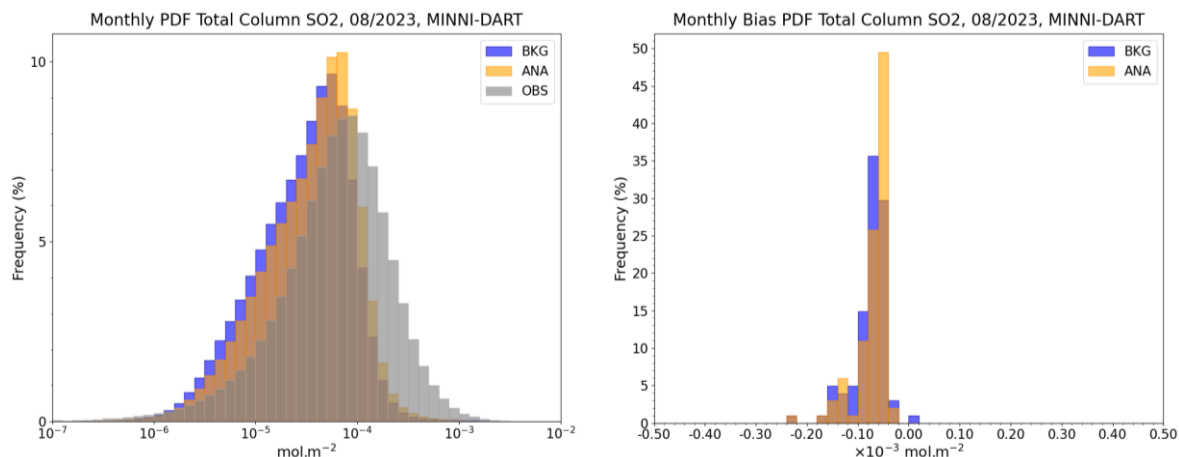


Figure 45: MINNI-EAKF PDFs scores: total column and bias model-observation

The MINNI-EAKF assimilation impact on surface SO₂ concentrations is higher than MINNI-OI: up to 5 µg m⁻³ increase along ship routes with respect to 0.1 µg m⁻³ (Figure 46, right graph). The assimilation of satellite retrievals leads to a decrease of SO₂ concentration in the south-eastern part of the domain, and to increases next to SO₂ sources.

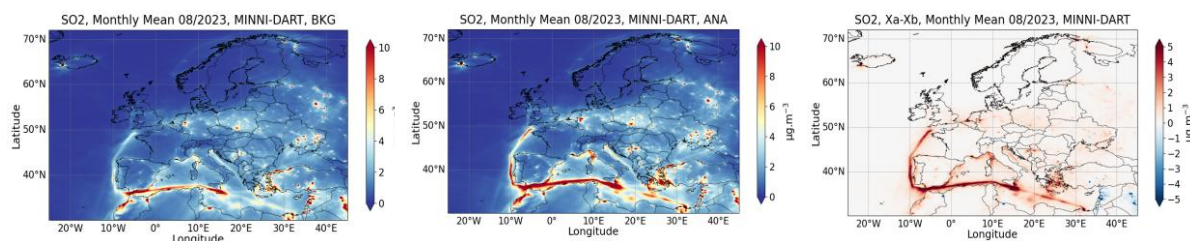


Figure 46: SO₂ surface concentration over August 2023 with MINNI-EAKF no assimilation on the left, with MINNI-EAKF assimilation in the middle and the difference between MINNI-EAKF assimilation and no assimilation on the right

4.3.1.7 SILAM results

Full 2023 was assimilated using three different emission setups: (1) basic emissions, (2) a constant volcanic degassing source added, (3) both the volcanic source and an oceanic dimethyl sulfide source (with the DMS directly mapped into SO₂ at a 50 % yield) added. Setup (3) is presented in the August model comparison, although setups (2) and (3) yielded nearly identical scores against surface stations.

Average total columns for August 2023 are shown in Figure 47. The impact on the degassing source of Etna is clear in the background simulation and there is also a contribution from Icelandic volcanoes. The degassing term is too strong on most days when compared against the TROPOMI retrievals, and the assimilation thus reduced the SO₂ columns near Etna. The eruption that started on August 13 was observed by TROPOMI only on August 14, when the plume had already dispersed south of the volcano. The eruption resulted in a stronger plume of SO₂ than the degassing source in SILAM, and the assimilation adjusted this by creating a separate puff of SO₂ south of the volcano, which is clearly visible in the difference between the analysis and the prior.

CAMEO

Interestingly, the assimilation did also enhance modelled SO₂ plumes above the northern Atlantic Ocean and the Barents Sea. These plumes originate from the boundary condition, and due to its perturbation, the assimilation is quite sensitive to the retrievals in the regions. However, the boundary condition perturbation does not perturb the location of a plume, only its strength (and although the time of the driving meteorological data is perturbed, it does not likely shift the locations of the plumes by sufficient amounts). Additionally, the retrievals in the northern latitudes may also exhibit measurement issues, such as high solar and satellite zenith angles. Due to high cloud coverage and the QA requirement, the TROPOMI retrievals typically form just small patches over northern latitudes, often corresponding to SO₂ column values that are clearly higher than those simulated by the model. Assimilation of a small patch may often greatly increase the strength of a nearby plume in model due to the covariance of the ensemble. Compared to variational data assimilation, the EnKF is likely more sensitive to this effect due to not being limited by a fixed background covariance. Overall, the enhancement of the northern latitude SO₂ plumes is likely an artefact due to retrieval errors, a too low model background, or a suboptimal boundary condition perturbation. However, as actual plumes are often co-located with water clouds, and as SO₂ columns are not retrieved for cloudy pixels, it cannot be ruled out that the assimilation could also be beneficial in some cases, despite that the monthly average retrieval does not show such strong plumes.

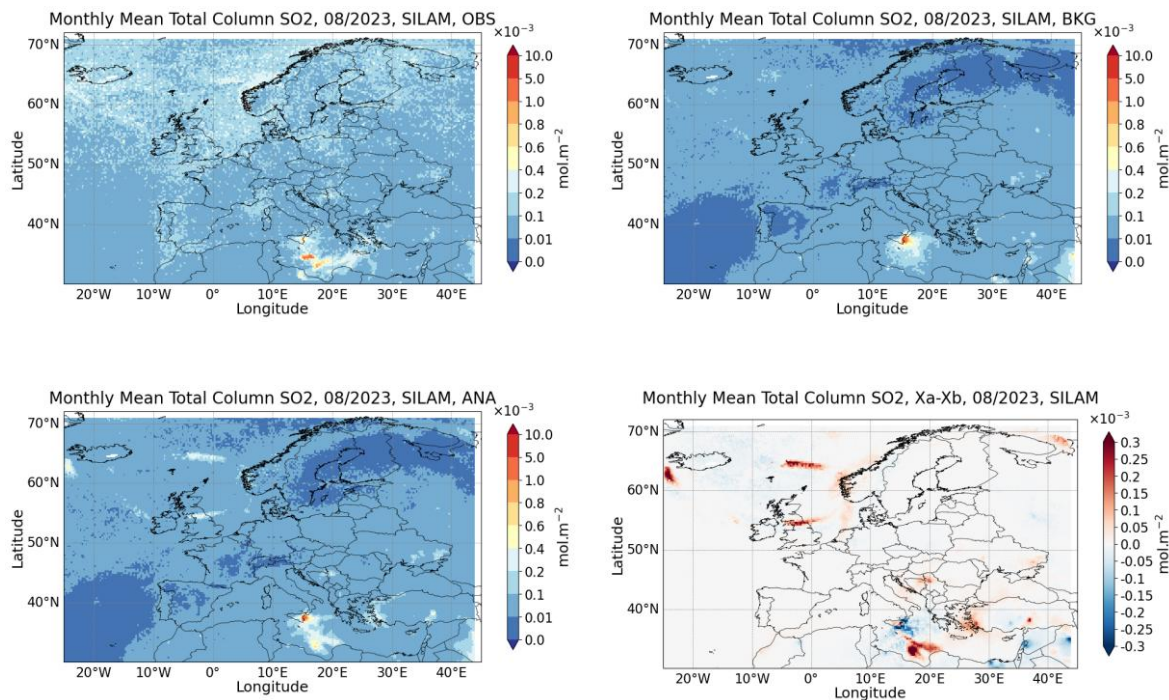


Figure 47: SO₂ total column mean over August 2023 of the S5P-COBRA positive valued retrievals on the top left, of SILAM mean on the top right (no assimilation), of SILAM mean with assimilation on the bottom left and the difference SILAM mean assimilation-no assimilation on the bottom right. Note that SILAM did also assimilate negative retrievals, which account for about half of the total retrievals

Figure 47 also shows the average of the positive valued retrievals over the domain. It is important to note that the SILAM assimilation setup differs significantly from the setups of the other models in the study, as also negative pixel-averaged retrievals are assimilated. This is highlighted in Figure 48, which shows histograms of the SILAM background and analysis total columns against the retrievals. When comparing the analysis against only positive valued retrievals (on a logarithmic scale), it would appear that the assimilation is causing the model to diverge from the observations, whereas the subfigure on a linear scale presents the full

CAMEO

distribution of the assimilated retrievals, showing that it is not straightforward to assess how reasonable the impact of the assimilation is on the PDF.

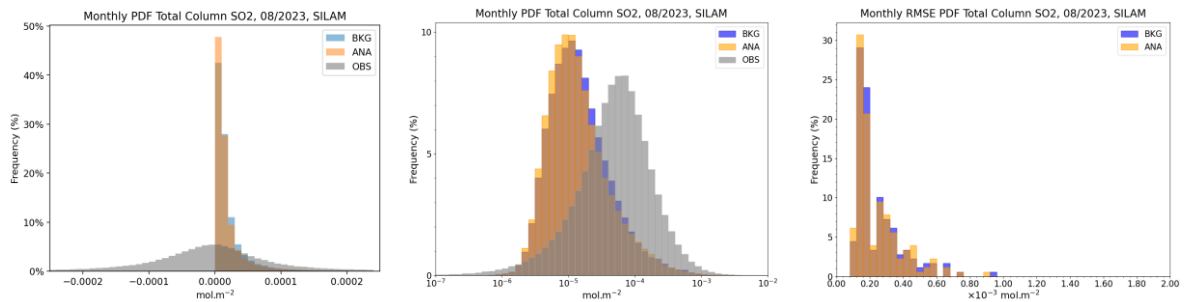


Figure 48: SILAM PDFs scores. Left: total columns on linear scale including all assimilated retrievals. Middle: total columns on logarithmic scale including only positive retrievals. Right: RMSE model-observation

Time series Figure 49 of the SILAM background and analysis compared against retrievals at Sabac and at Etna. While the assimilation generally improves the comparison, there are also discrepancies, such as the massive peak in the analysis at Sabac. A contributing factor to this may be that the comparison is not strictly apples to apples, as the SILAM values refer to full hour averages. Specifically, the analysis is the model average for the full hour after the assimilation is also impacted by advection (and to a lesser extent chemistry). Thus, the SILAM analysis that is presented in this report (such in section 4.3.2) likely compares somewhat worse to the observations than what the actual instant analysis would do.

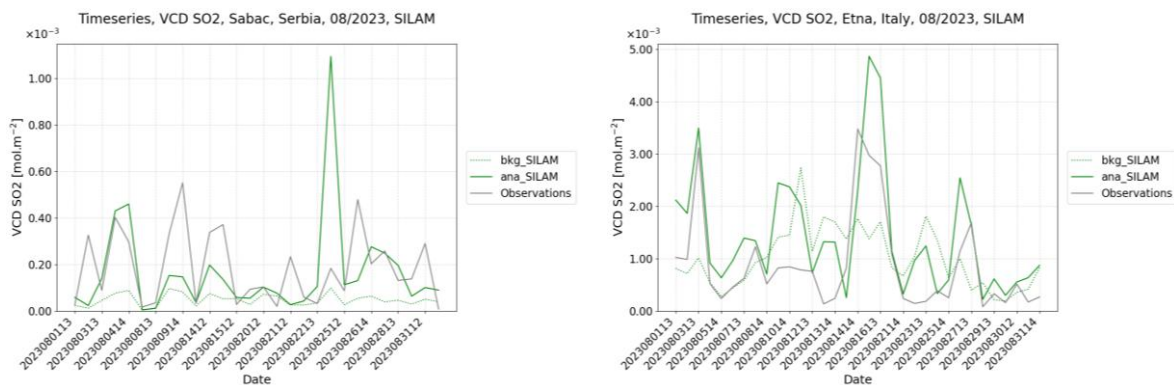


Figure 49: Times series of SO2 total columns over August 2023 at Sabac location on the left and at Etna location on the right.

One of the goals of the SILAM assimilation was to test the impact of SO₂ column assimilation on model scores against air quality measurement stations. Unfortunately, the quality of the in situ data is generally very poor, and due to this it is very difficult to assess the impact of the assimilation (the measurements have significant issues concerning calibration and drift which render even assessment of model bias almost impossible). Thus, scores against surface PM_{2.5} measurements are presented, as these have a much higher quality than SO₂ measurements (the downside is of course that most of the full PM_{2.5} signal does not originate from sulphur-containing species). While Section 4.3.3 focuses on model intercomparison for the month of August, Table 4 summarizes SILAM scores for SO₂ and PM_{2.5} for simulation

CAMEO

cases (1) and (2) described above as well as a control run for full year 2023. The differences of the annual average assimilated surface SO₂ concentrations with respect to the control run are shown in Figure 50 for both assimilation setups (setup (3) exhibited scores that were almost identical to setup (2)).

	control	setup (1)	setup (2)
SO2 bias (all stations)	-2.649	-2.672	-2.616
SO2 corr (all stations)	0.108	0.111	0.120
SO2 RMSE (all stations)	9.576	9.580	9.555
SO2 bias (opstations)	-1.050	-1.114	-1.056
SO2 corr (opstations)	0.256	0.260	0.267
SO2 RMSE (opstations)	4.209	4.212	4.205
PM2.5 bias (all stations)	-0.670	-0.905	-0.925
PM2.5 corr (all stations)	0.582	0.584	0.584
PM2.5 RMSE (all stations)	8.795	8.713	8.686
PM2.5 bias (opstations)	1.229	0.996	1.005
PM2.5 corr (opstations)	0.622	0.622	0.620
PM2.5 RMSE (opstations)	6.376	6.237	6.258

Table 4: Scores for full 2023 for a control run and two assimilation runs, without (“setup (1)”) and with (“setup (2)”) volcanic emissions. Scores for all stations and operational evaluation stations are presented separately. The unit for bias and RMSE is ug/m3.

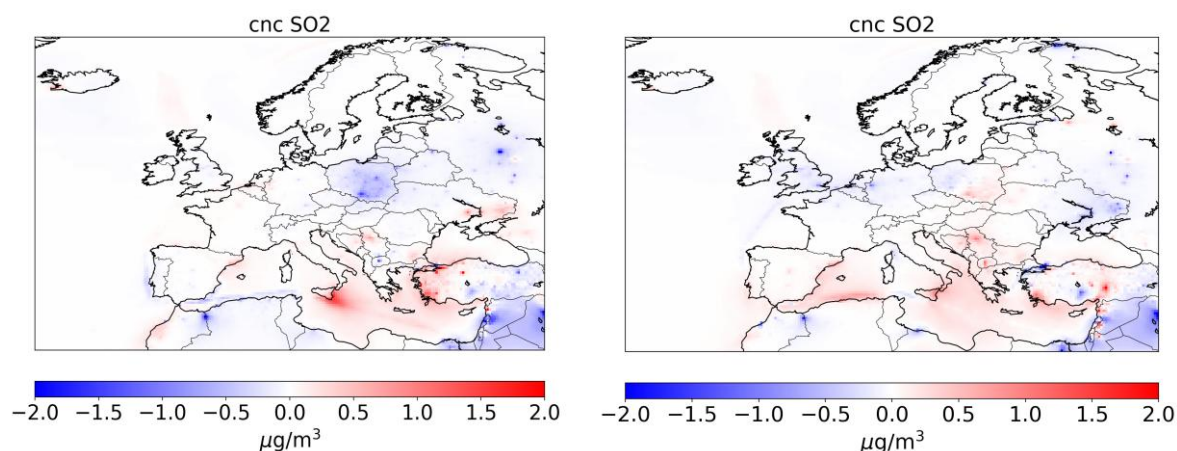


Figure 50: Annual average surface SO₂ concentration difference with respect to the control run for setup (1), which did not include volcanic emissions (left), and setup (2), which did include volcanic degassing emissions (right).

SILAM SO₂ emission assimilation

For testing the impact of SO₂ emission assimilation, the full year 2023 was assimilated. The state vector was formed by the perturbed scaling factor to the emissions of SO₂. The model perturbations were the same as in the assimilation of in-air concentrations, but the distribution of the emission scaling factors was set to tend towards the distribution defined by the initial parameters of the perturbation within a correlation time of 10 days. The assimilation window was increased to 48 hours. A control run was performed with the assimilated emissions and compared against a run with the a priori emissions.

CAMEO

The resulting assimilation-adjusted emissions are compared against the a priori emissions in Figure 51. The coarse resolution of the a priori volcanic emissions is clearly visible in the figures, and it is noteworthy that the assimilation can concentrate a large part of the emission on the exact location of Etna. The assimilation also adjusts the emissions around Sabac to be higher than in the prior and also makes both upwards and downwards adjustments especially in Turkey and in the Middle East. Especially for the month of August there is a notable upwards adjustment of emissions in the region of the Aegean Sea. This is possibly a result of suboptimal SO₂ chemistry in SILAM, as the simplified chemical mechanism does not take into account saturation effects that occur in dense plumes. Thus, SO₂ in volcanic plumes is converted too quickly into sulphates, which the assimilation then compensates for by adjusting the unrelated SO₂ emissions farther away from the volcano.

When compared against all measurement stations of surface SO₂ (validated, yet low-quality EEA observations) for full 2023, the average modelled SO₂ value increased from 1.8 ug/m³ to 2.0 ug/m³, the hourly correlation improved from 0.070 to 0.102 and the hourly RMSE increased from 13.0 ug/m³ to 13.1 ug/m³. For all stations of PM_{2.5}, the average hourly correlation increased from 0.516 to 0.522, the RMSE decreased from 10.42 ug/m³ to 10.39 ug/m³, with average model value staying roughly constant. The model setup was slightly different than in the case with assimilation of in-air concentrations, thus the scores are not completely comparable. Thus, in the light of these scores, the assimilation of emission does not bring any clear improvement, although the evaluation is hampered by the lack of high-quality measurement data close to the main emission sites.

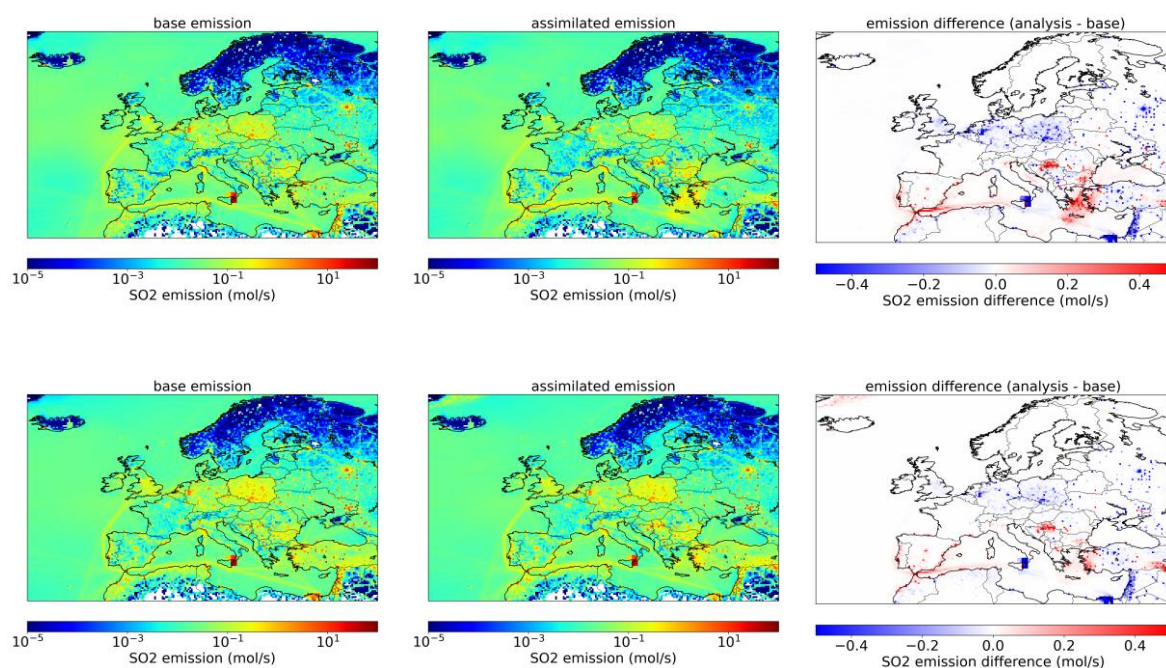


Figure 51: Top panel: Average a priori emissions for August 2023 (left), average assimilated emissions for August 2023 (middle), and their difference (right) Bottom panel: The corresponding figures for full 2023

4.3.2 Intercomparison of SO₂ data assimilation

The analysis of VCD is a statistical optimal solution which is weighted by the observation, the simulated VCD, the observation error and the data assimilation algorithm which includes the model background error covariance. This section shows DA results in VCD for teams that are using different models and different DA systems. Results in surface concentration are evaluated later in section 4.3.3.

The values of simulated VCD depend on simulated concentrations by the models and other parameters such as their horizontal and vertical mesh grid resolution. In addition, statistical results for all models are calculated from the observation used by each model which may vary according to their pre-processing (Quality Control and super-observation), as shown in section 4.2.2.

The range of simulated VCD over the period of August 2023, shown in Figure 52, is large (MATCH is not included in this section because of problem of delivery for the last run). The statistics are performed by day to compare results in Europe from teams that have different DA time windows. Table 5: Intercomparison of statistical results in SO₂ total columns with and without assimilation over August 2023 in Europe. Table 5 summarized the results of bias, RMSE, correlation over August 2023.

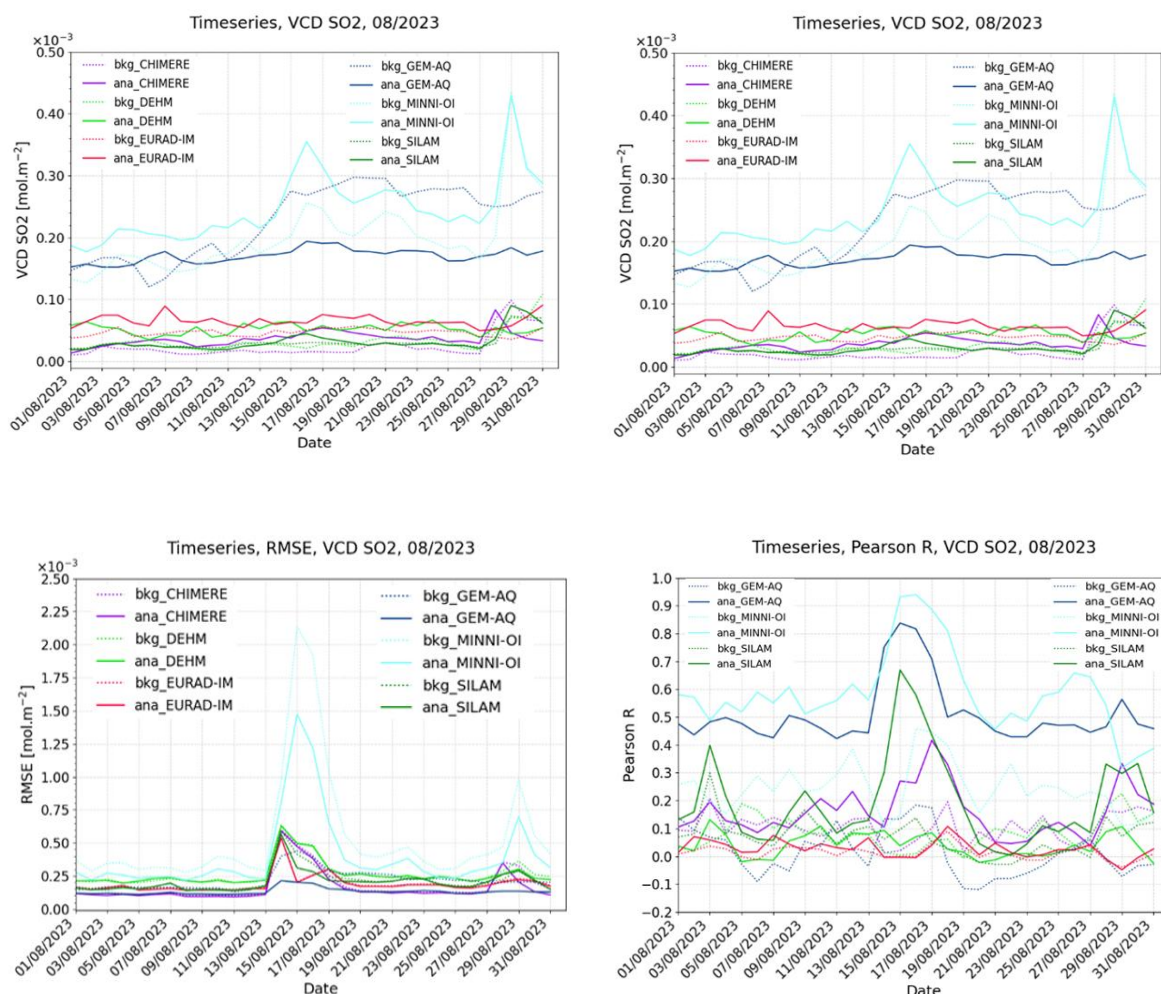


Figure 52: Time series of daily SO₂ VCD for the mean on the top left, the bias on the top right, the RMSE on the bottom left and the correlation on the bottom right.

GEM-AQ and MINNI-OI have close VCDs on average. MINNI-OI has a negative bias most of the time while GEM-AQ remains close to observation before introducing volcano emission. Since August 14th GEM-AQ remains positive while MINNI-OI has a negative bias. EURAD-IM has low VCD. SILAM, DEHM and CHIMERE simulate the lowest VCDs. The three models have a negative bias over the period. Data assimilation allows reducing the bias for all models and GEM-AQ does not have bias after analysis.

MINNI-OI has the largest RMSEs in the run with no assimilation. MINNI-OI does not apply super-observation which may partly explain this result. There is more chance that the observation is not fully representative of the VCD modelled within the mesh grid. RMSEs are strongly reduced in the run with assimilation. Models such as SILAM, DEHM and CHIMERE with the lowest simulated observation columns in the run with no assimilation, have small or no improvements for RMSE over the full period.

All the models have poor VCD correlation in the run with no assimilation, lower correlation than 0.1, except for MINNI-OI which has VCD correlation around 0.22. After assimilation, MINNI-OI and GEM-AQ have the largest correlations, respectively 0.62 and 0.73. The optimal interpolation in MINNI allows large changes locally and the highest atmospheric layers of its domain, which is prone to increase the correlation with VCD SO₂-COBRA observations. Sasaki variational approach applied to the GEM-AQ SO₂ background concentration strongly improves correlation in SO₂ VCD. While 3D-VAR method using a background covariance error based on the NMC method do not increase significantly correlation of DEHM and EURAD-IM, which remains lower than 0.1. CHIMERE and SILAM use ensemble Kalman approach, and the correlation is improved to reach respectively 0.21 and 0.32.

Overall, GEM-AQ (variational Sasaki) and MINNI-OI are the models that fit the most the observations after data assimilation with lower bias, RMSE and higher correlation on average over the domain.

	VCD (mol.m ⁻²)	BIAS (mol.m ⁻²)	RMSE (mol.m ⁻²)	R
CHIMERE				
No assimilation	0.2270×10^{-4}	-6.590×10^{-5}	2.186×10^{-4}	0.058
Assimilation	0.3520×10^{-4}	-5.336×10^{-5}	2.055×10^{-4}	0.207
DEHM				
No assimilation	0.3246×10^{-4}	-11.670×10^{-5}	2.848×10^{-4}	0.070
Assimilation	0.5240×10^{-4}	-9.672×10^{-5}	2.814×10^{-4}	0.043
EURAD-IM				
No assimilation	0.4653×10^{-4}	-6.036×10^{-5}	2.076×10^{-4}	0.012
Assimilation	0.6534×10^{-4}	-4.156×10^{-5}	2.025×10^{-4}	0.021
GEM-AQ				
No assimilation	2.301×10^{-4}	6.127×10^{-5}	2.349×10^{-4}	0.061
Assimilation	1.707×10^{-4}	0.1905×10^{-5}	1.359×10^{-4}	0.624
MINNI-OI				
No assimilation	1.997×10^{-4}	-7.472×10^{-5}	6.972×10^{-4}	0.215
Assimilation	2.464×10^{-4}	-2.804×10^{-5}	4.890×10^{-4}	0.731
SILAM				
No assimilation	0.310×10^{-4}	-6.949×10^{-5}	2.350×10^{-4}	0.070
Assimilation	0.319×10^{-4}	-6.856×10^{-5}	2.219×10^{-4}	0.316

Table 5: Intercomparison of statistical results in SO₂ total columns with and without assimilation over August 2023 in Europe.

CAMEO

In addition, results are presented at hotspot locations in Table 6. Due to the variability of the results, the choice is made to present only mean columns, normalized bias and RMSE according to the mean observation total column, as summarized in Table 7.

	Sabac (VCD in mol.m ⁻²)		Etna (VCD in mol.m ⁻²)	
	nBIAS	nRMSE	nBIAS	nRMSE
	CHIMERE			
No assimilation	-0.903	1.358	-0.971	1.373
Assimilation	-0.434	0.968	-0.827	1.238
	DEHM			
No assimilation	-0.809	1.151	-0.977	1.249
Assimilation	-0.405	0.844	-0.879	1.162
	EURAD-IM			
No assimilation	-0.476	1.339	-0.951	1.655
Assimilation	-0.398	1.345	-0.900	1.622
	GEM-AQ			
No assimilation	0.944	1.377	0.362	2.674
Assimilation	-0.142	0.735	-0.262	0.834
	MINNI-OI			
No assimilation	-0.584	1.124	-0.900	1.449
Assimilation	-0.320	0.690	-0.672	1.130
	SILAM			
No assimilation	-0.743	1.071	0.141	1.061
Assimilation	-0.114	1.242	0.640	0.996

Table 6: Intercomparison of statistical results in SO₂ total columns with and without assimilation over August 2023 at Etna in Italy and Sabac in Serbia.

OBS (mol.m ⁻²)	CHIMERE	DEHM	EURAD-IM	GEM-AQ	MATCH	MINNI-OI	SILAM
Etna	3.762×10 ⁻⁴	5.535×10 ⁻⁴	5.405×10 ⁻⁴	4.176×10 ⁻⁴	4.356×10 ⁻⁴	1.626×10 ⁻³	8.750×10 ⁻⁴
Sabac	2.293×10 ⁻⁴	2.398×10 ⁻⁴	3.063×10 ⁻⁴	2.729×10 ⁻⁴	1.763×10 ⁻⁴	6.521×10 ⁻⁴	1.837×10 ⁻⁴

Table 7: SO₂ total column mean observations at Etna in Italy and Sabac in Serbia.

At Sabac in Serbia, data assimilation allows reducing the normalized bias (nBias) for all models and allows decreasing the normalized RMSE (nRMSE), except for EURAD-IM and SILAM. The period is too short to evaluate a consistent correlation but the time series of models in section 3.2, show high sensitivity for some models.

At Etna in Italy, GEM-AQ, which includes Etna SO₂ emissions around 500 hPa, has an improvement by assimilating the VCD and having an analysis increment in SO₂ concentration above the planetary boundary layer. A better estimation of Etna emissions would be beneficial. Slight improvements are found for the other models by having a small analysis increment located near the surface. The increment is smaller and not located at the right height according to the background error covariance definition in the data system.

4.3.3 Evaluation of data assimilation impact on surface SO₂ concentration

The European regional air quality ensemble usually performs analysis including observations at the surface. Here, the results of the different partners are evaluated for runs with no assimilation and runs that assimilate only S5P SO₂ total columns. In the process of data

CAMEO

assimilation of SO₂ total columns, the statistical optimum total column assimilated is converted to concentration. The range of SO₂ surface concentration of the teams varies according to the SO₂ apriori background model, the background error covariance definition and the DA systems.

4.3.3.1 Selection of the surface observations dataset

The Air Quality e-Reporting surface stations (EEA Data Service <https://www.eea.europa.eu/data-and-maps/data/aqereporting-9/aq-ereporting-products>) selected come from the validated dataset in April 2025 (ETC-HE Report 2025/2, Jaume Targa et al. April 2025). Only the surface stations which pass the following quality control are finally used:

- The quality flag is equal to 1;
- Hourly availability rate above 75% for each surface station;
- Turkish stations are excluded because of less confidence in the dataset: all the model results are poorly correlated to the observations (in comparison to other areas) and may screw the statistical results.

Finally, 531 out of 788 surface stations, as shown in Figure 53, are selected for the comparison with the models.

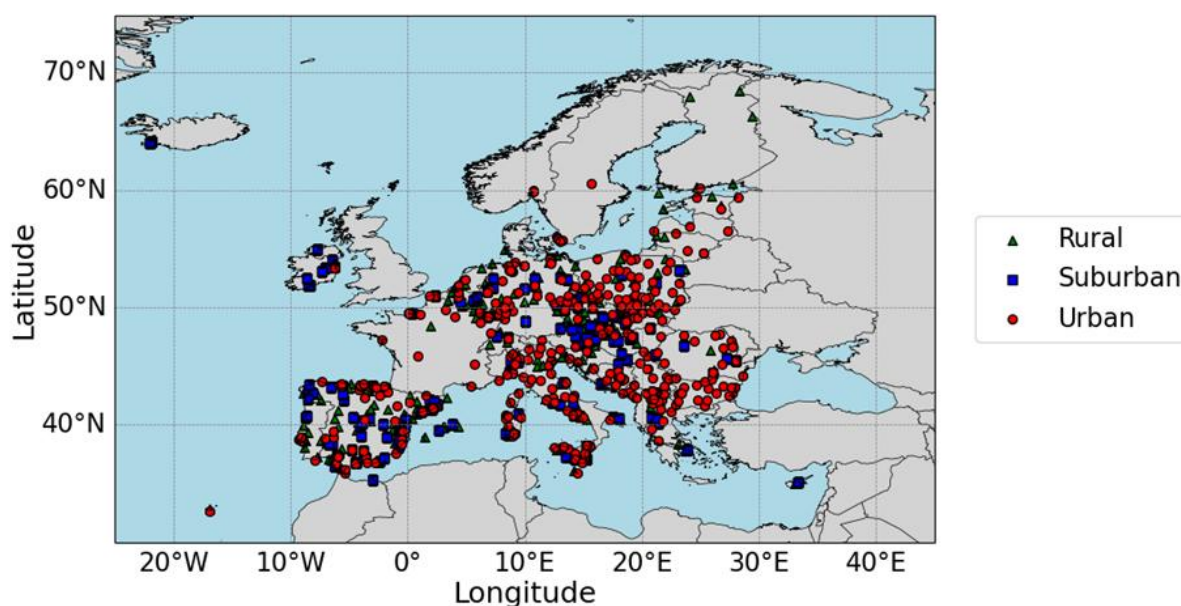


Figure 53: SO₂ Air Quality e-Reporting surface stations from EEA Data Service in Europe (788 surface stations, excluding Türkiye).

QC sensitivity tests have been performed on the selected SO₂ surface over August 2023 to ensure as little variability as possible in the statistical results presented next. It was found that for hourly data:

- 5 stations are over 500 µg.m⁻³, no station is over 1000 µg.m⁻³, by applying the QC described above.
- 205 stations are over 500 µg.m⁻³, 121 stations are over 1000 µg.m⁻³, when the quality flag is not considered.

4.3.3.2 Results at surface observations

The range of the SO₂ mean surface concentrations at the observation location is quite large, as shown in Table 8, which summarizes the comparison of the mean calculated according to the QC applied. Observations and model means remain in a close range of values on average and provide more confidence about outliers and the effect of applying a quality flag equal to 1.

Quality Control	OBS $\mu\text{g.m}^{-3}$	CHIMERE	DEHM	EURAD	GEM-AQ	MATCH	MINNI-OI	SILAM
Obs < 500	3.351	1.286	0.759	2.537	4.035	1.276	1.648	1.799
QaFlag = 1	3.669	1.303	0.782	2.515	4.076	1.246	1.650	1.887

Table 8: Comparison of simulated SO₂ concentrations mean values in $\mu\text{g.m}^{-3}$ (no assimilation) at observation location considering different Quality Control over August 2023.

The range of SO₂ concentration in the runs with no assimilation in Figure 54 is wide. DEHM and CHIMERE are the models that underestimate the most SO₂ over Europe. MINNI-OI and SILAM have a negative bias on average. EURAD-IM and GEM-AQ are the closest models to observations. Concentrations of GEM-AQ increase from August 14th most likely due to overestimation of Etna volcano emissions.

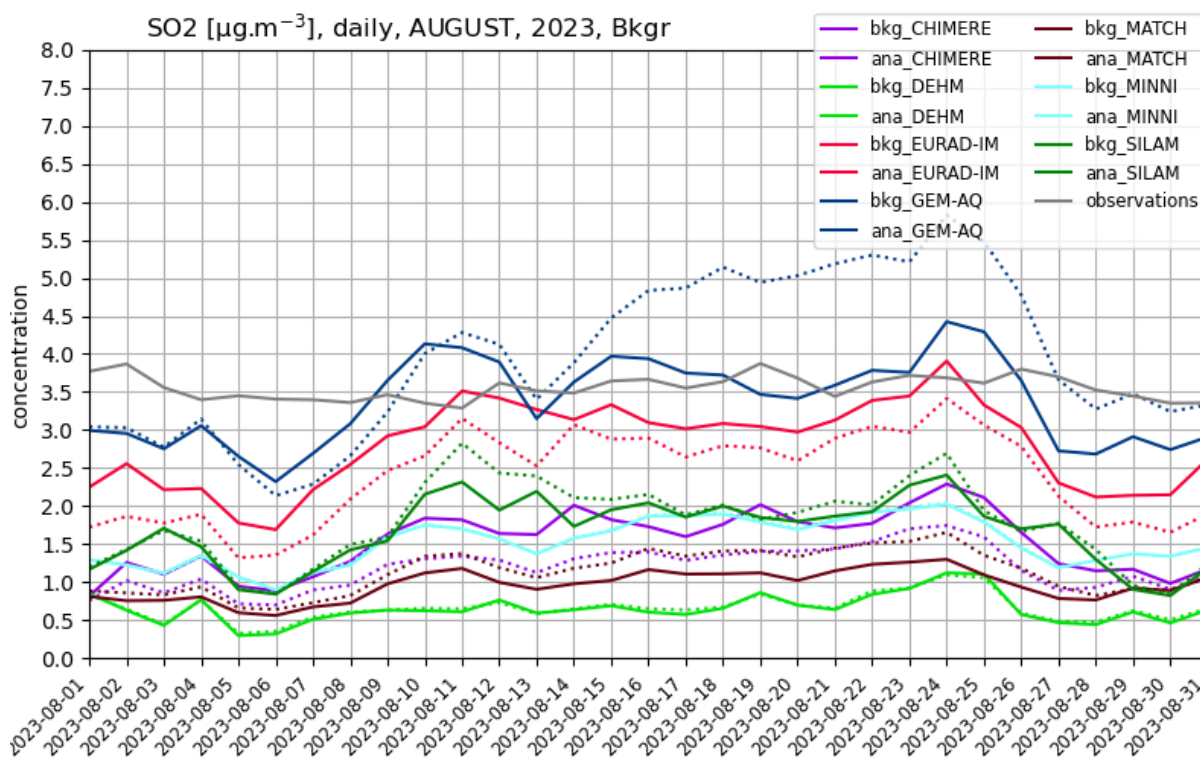


Figure 54: Intercomparison of time series over August 2023 of the mean observed surface SO₂ concentration in grey with the mean of simulated interpolated values at observation locations with assimilation (solid lines) and without assimilation (dashed lines).

Table 9 presents the statistical results evaluated for SO₂ daily mean over August 2023 in Europe. Data assimilation significantly reduces the bias of CHIMERE and EURAD-IM. The bias of GEM-AQ is the smallest, while there are no clear benefits of the assimilation found for DEHM and MINNI-OI. The negative bias of SILAM slightly increases. Considering 14 % of the highest observations overpassing 6 $\mu\text{g.m}^{-3}$ in Figure 55, the bias is reduced for CHIMERE and EURAD-IM, while the bias increases for GEM-AQ. The bias does not change much for DEHM, MINNI-OI and MATCH, and no clear tendency for SILAM is noticed.

CAMEO

The RMSE, presented in Table 9, is reduced for SILAM and CHIMERE (slightly), while no significant change is noticed for the other models. Figure 56 shows that RMSE of SILAM is decreasing for the highest observations that overpass 15 $\mu\text{g.m}^{-3}$ (2.1 %).

SO ₂	Concentration ($\mu\text{g.m}^{-3}$)	BIAS ($\mu\text{g.m}^{-3}$)	RMSE ($\mu\text{g.m}^{-3}$)	R
CHIMERE				
No assimilation	1.303	-2.366	5.640	0.052
Assimilation	1.610	-2.032	5.499	0.074
DEHM				
No assimilation	0.775	-2.894	6.322	0.002
Assimilation	0.762	-2.907	6.388	-0.002
EURAD-IM				
No assimilation	2.525	-1.144	4.574	0.390
Assimilation	2.921	-0.748	4.512	0.382
GEM-AQ				
No assimilation	4.089	0.420	4.894	0.317
Assimilation	3.507	-0.162	4.857	0.241
MATCH				
No assimilation	1.246	-2.423	5.215	0.163
Assimilation	1.068	-2.601	5.320	0.140
MINNI-OI				
No assimilation	1.646	-2.023	5.145	0.126
Assimilation	1.636	-2.033	5.151	0.125
SILAM				
No assimilation	1.897	-1.772	7.897	0.075
Assimilation	1.786	-1.883	7.340	0.091

Table 9: Intercomparison of statistical results based on daily mean of SO₂ surface concentration.

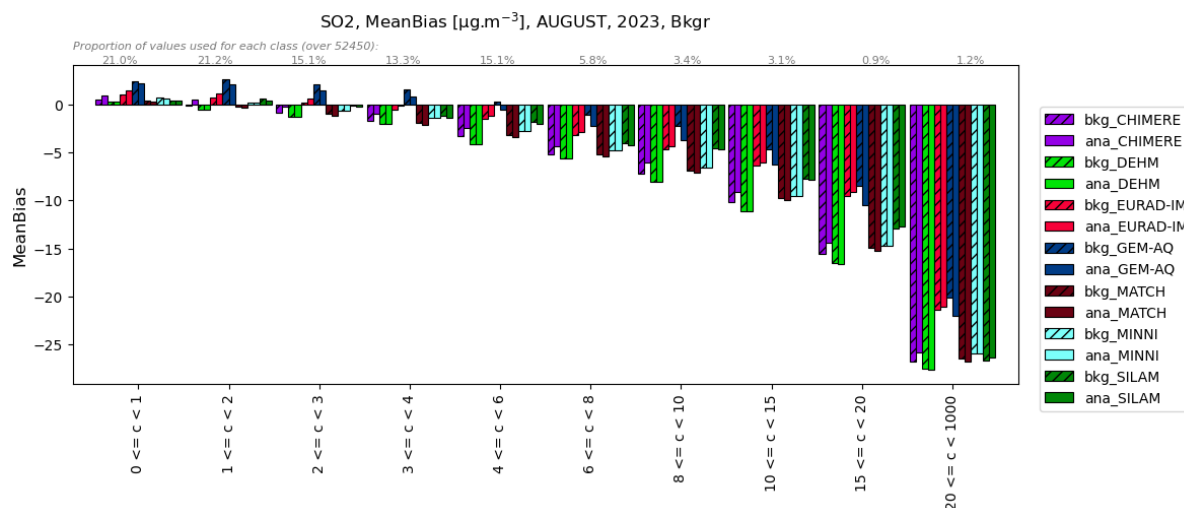


Figure 55: Intercomparison of frequency of bias by classes of SO₂ surface concentration over August 2023 (solid colors) and without assimilation (hashed colors).

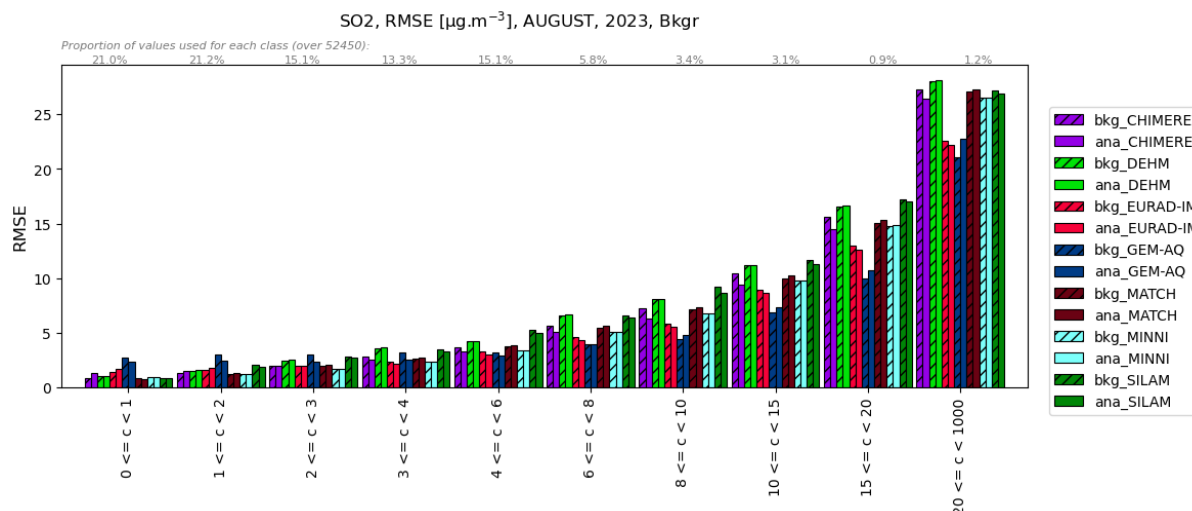


Figure 56: Intercomparison of frequency of RMSE by classes of SO₂ surface concentration over August 2023 (solid colors) and without assimilation (hashed colors).

Finally, no clear benefit in correlation between modelled and observed surface concentrations are found in Table 9. It could be expected that surface SO₂ concentration of DEHM and ERAD-IM will not be changed as the VCD SO₂ correlation haven't significantly changed as shown in Table 5. EURAD-IM has the best correlation in SO₂ surface correlation before and after assimilation while the correlation is slightly degraded for GEM-AQ from 0.32 to 0.24. In addition, section 4.3.1 shows that MINNI-OI has low surface increment even if large impact of data assimilation is shown on SO₂ VCDs. MINNI-OI has larger sensitivity than other models in the atmospheric layers above PBL, which considerably reduce impact at ground level. CHIMERE and SILAM, which used ensemble method, have SO₂ surface concentration correlation lower than 0.1 before and after assimilation. The uncertainties associated with these low scores require us to remain cautious in drawing conclusions. Even if section 4.3.1 shows that increment can be large close to the surface of hotspots such Sabac in Serbia, their number remain small to change the score consequently the score over Europe.

CAMEO

The hourly RMSE, BIAS, and correlation (R) scores presented in Table 10, lead to similar conclusions than for daily mean SO₂ concentration presented Table 9. It can be noticed the really poor hourly correlation for most of the model except for EURAD-IM and GEM-AQ.

SO ₂	Concentration (µg.m ⁻³)	BIAS (µg.m ⁻³)	RMSE (µg.m ⁻³)	R
CHIMERE				
No assimilation	1.367	-2.316	7.395	0.031
Assimilation	1.626	-1.856	7.294	0.065
DEHM				
No assimilation	0.844	-2.839	8.160	0.000
Assimilation	0.831	-2.852	8.209	-0.002
EURAD-IM				
No assimilation	2.634	-1.049	7.148	0.187
Assimilation	3.030	-0.653	7.155	0.181
GEM-AQ				
No assimilation	4.136	0.453	6.998	0.207
Assimilation	3.567	-0.116	6.997	0.142
MATCH				
No assimilation	1.314	-2.369	7.086	0.089
Assimilation	1.146	-2.537	7.167	0.070
MINNI-OI				
No assimilation	1.724	-1.959	7.044	0.071
Assimilation	1.714	-1.969	7.048	0.070
SILAM				
No assimilation	1.901	-1.782	9.3702	0.049
Assimilation	1.792	-1.891	8.992	0.058

Table 10: Intercomparison of hourly statistical of SO₂ surface concentration.

4.4 Conclusions

Seven teams perform Sentinel 5P SO₂ VCD data assimilation at regional scale over August 2023. Therefore, most of the modellers increase the vertical grid resolution of their operational configuration with a top level over 200 hPa, in order to have consistent modelling of the SO₂ total columns. The SO₂-COBRA VCD dataset, which has become the operational product since November 2024, is used in this study. All partners apply quality control and super-observation averaging the VCD, their related errors and meta-data, except MINNI-OI which uses the raw data. After creating super-observations, partners keep only SO₂ VCD positive values for data assimilation, except SILAM.

Data assimilation systems, such as 3D-Var (DEHM, EURAD-IM, MATCH) and OI (MINNI), use predefined statistics based on the NMC method to define the background error covariance error (B), while the ensemble methods of SILAM (ENKF), CHIMERE (EAKF) and MINNI (EAKF), estimate B from the perturbed ensemble members. Volcanic emissions are taken into account in SILAM and GEM-AQ. SILAM (ENKF) includes constant volcanic emissions while GEM-AQ includes a unique strong emission on August 14th according to the largest eruption in the period.

In Europe and over August 2023, the assimilation of SO₂ VCD, mainly leads to an increase of SO₂ VCD for EURAD-IM, CHIMERE, DEHM and SILAM, while it induces a decrease of VCD for GEM-AQ. In the southeast part of the domain (in Syria and Iraq), all models except DEHM, agree to decrease the SO₂ VCDs. The intercomparison of the simulation results, without (base run), and with data assimilation shows a general reduction of the VCD bias for all models, which however vary from slight to large bias changes. GEM-AQ is almost not biased after data assimilation. The RMSE largely decreases for GEM-AQ and MINNI-OI. It slightly decreases for CHIMERE, EURAD-IM and SILAM (neutral for DEHM). The results are also analysed at two hotspot locations of Etna in Italy and Sabac in Serbia. Statistics show a large reduction of bias at Sabac for all the models and a large reduction of RMSE for CHIMERE, DEHM, GEM-AQ and MINNI-OI. The analysis increments in SO₂ concentration varies according to the systems and models used. DEHM-3DVAR and MINNI-OI have likely larger increment in the highest layer of atmosphere and lower increment within the planetary boundary layer than other DA-systems

Finally, data assimilation results are evaluated for the seven air quality models by comparing the simulations with SO₂ surface concentration observations (from EEA service). The bias is reduced for SO₂ surface concentrations for CHIMERE, EURAD-IM and GEM-AQ. Large increments are possible and are shown for those models within the planetary boundary layer. Moreover, data assimilation does not have a significant effect on the bias for MINNI-OI and DEHM likely due to higher sensitivity in the highest model layers. No large benefits are found for the RMSE. CHIMERE and SILAM have a decrease of RMSE for August 2023 but the full year performed by SILAM doesn't confirm such improvement. No significant benefits are found for the correlation for all models.

5 Data Assimilation of other Sentinel 5P L2 products

5.1 Introduction

Partners had the opportunity to assess the feasibility and added value of assimilating HCHO, CO, or O₃ TROPOMI total columns coming from Sentinel 5P. Some highlights related to the Algorithm Theoretical Baseline Document (ATBD) of each product are described in Table 11. It can be noticed that the HCHO L2 product (De Smedt I et al., 2024) has 34 vertical levels while the CO product (Landgraf et al., 2024) has 50 vertical levels. Both retrievals have a pixel resolution of 5.5 x 3.5 km². A significant artificial striping pattern in the flight direction of the satellite for the original data retrieved for CO from the SWIR measurements of TROPOMI exists. The corrected total column of CO is also available and used in the following experiments. Considering O₃, total columns and profiles are available at lower resolution. While the total column has 15 vertical levels and a pixel resolution of 5.5 x 3.5 km², O₃ profile has 33 vertical levels for a pixel resolution of 28 x 28 km².

S5P L2 Products	HCHO	CO	O ₃ total column	O ₃ profile
Spectral range (nm)	328.5 – 359 (UV)	2324 – 2338 (SWIR)	267 – 300 and 300 – 332 (UV)	267 – 300 and 300 – 332 (UV)
Number of vertical layers	34	50	15	33
Horizontal resolution	5.5 x 3.5 km ²	5.5 x 3.5 km ²	5.5 x 3.5 km ²	28 x 28 km ²

Table 11: Description of Sentinel 5P L2 products.

5.2 Assimilation of HCHO in CHIMERE

The same configuration of the Ensemble Adjusted Kalman Filter is applied for the period of August 2023 to assimilate only total columns of HCHO. First, a quality control is applied to filter the observations with a quality flag above 0.8, solar zenith angle lower than 60°, and cloud fraction lower than 0.3. Second, super-observation is used to average the data and the associated error at the CHIMERE mesh grid resolution of 0.2 degree. Finally, only positive values are assimilated over August 2023.

The comparison of HCHO VCD with S5P observation presented in Figure 57, shows that the HCHO underestimation in the base case (no assimilation) is reduced in the run with assimilation. Most of the increase of HCHO VCD occurs mostly in the west part of the domain and in the south below 42° north latitude. The highest increases take place in areas such as west of Turkey, Greece and Georgia, while HCHO VCD decreases in countries such as Poland, Ukraine, Belarus, Estonia, Lithuania and Latvia.

Overall, Figure 58 shows that the VCD bias is reduced on average for most of the satellite orbit time in the run with assimilation of the timeseries. Both VCD bias and VCD RMSE are reduced by a factor slightly above 30 % over August 2023: Bias lows down from -5.72×10^{-4} mol.m⁻² to -3.86×10^{-4} mol.m⁻² while RMSE is reduced from 5.73×10^{-4} mol.m⁻² to 4.1×10^{-4} mol.m⁻². The PDF scores of biases and RMSE are presented Figure 59

CAMEO

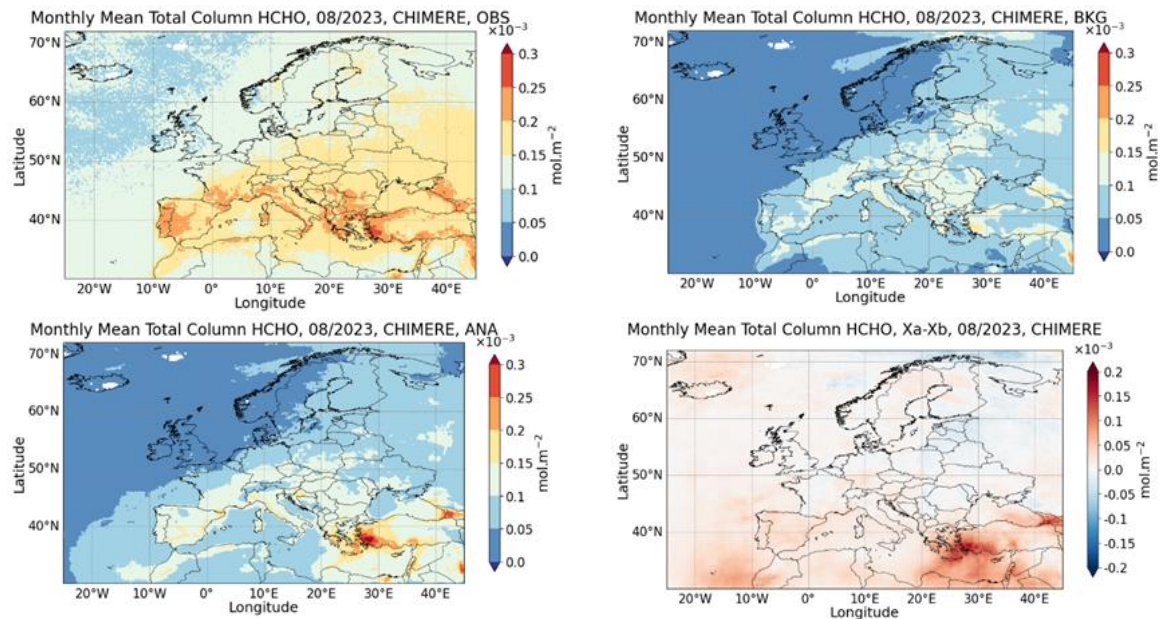


Figure 57: HCHO total columns mean over August 2023 of the S5P satellite observations on the top left, of CHIMERE mean no assimilation run on the top right, of CHIMERE mean with assimilation on the bottom left and the difference CHIMERE mean assimilation-no assimilation on the bottom right.

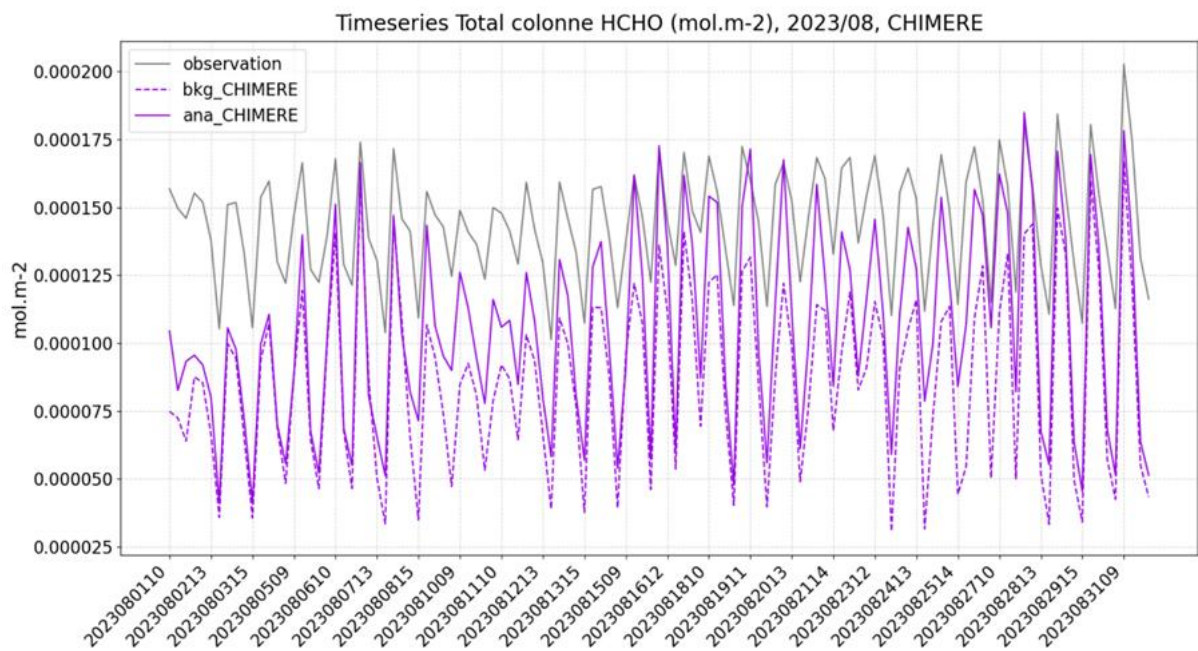


Figure 58: CHIMERE Time series of HCHO total column over August 2023 spatially averaged at orbit time.

CAMEO

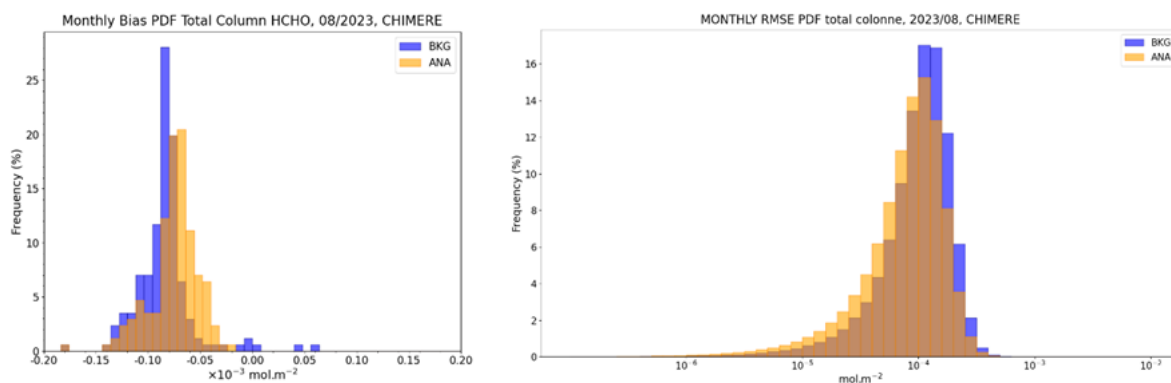


Figure 59: CHIMERE HCHO PDF score of bias on the left and PDF score of RMSE on the right

Finally, the HCHO differences in concentration at the surface, between the run with assimilation and no assimilation, are shown in Figure 60. The largest positive and negative differences are in the same areas as described for VCD (Figure 57). They are larger in Turkey. However, direct comparison of HCHO concentration with measurements is difficult because they are sparse in time and in space. A first evaluation is made analysing the results for ozone, as formaldehyde is also one of the precursors for ozone production.

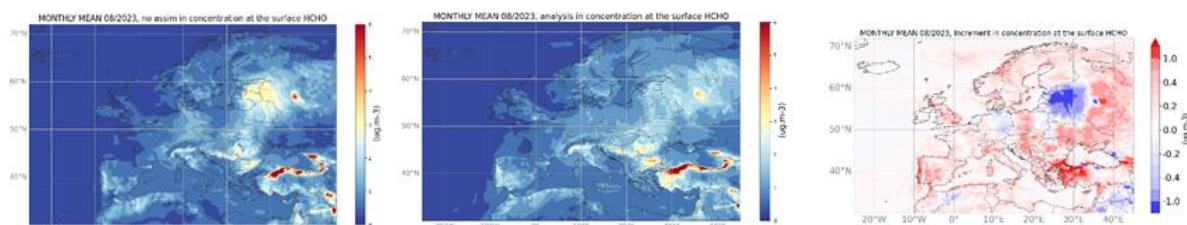


Figure 60: CHIMERE HCHO mean surface concentration over August 2023 on the left (no assimilation), on the middle (assimilation), and the difference of CHIMERE mean assimilation with no assimilation on the right.

When runs are compared to the O₃ concentration of Air Quality Reporting surface station, the assimilation of HCHO is leading on average to a slight increase of ozone concentrations. Figure 61 shows that bias is slightly negative in the base run and becomes slightly positive in the run with assimilation. RMSE slightly increases. The pre-processing of VCD observations, which is prone to have positive bias analysis when keeping only positive values, may have an impact. Results are not discussed in more detail because of their uncertainties. No obvious and general gain is shown by assimilating HCHO in this first approach other than a better fitting to HCHO total column. S5p/HCHO product has a low signal-to-noise ratio and temporal average of the product over one week have been applied, as well as, bias correction, for inversion modelling (Oomen et al., 2024). However, monitoring the differences of S5P VCD and VCD of CHIMERE evaluated on average over a period, should help to improve the modelling. It could help to look for sensibility for biogenic emissions according to inputs and to optimize parameters such as emission factor and ozone deposition.

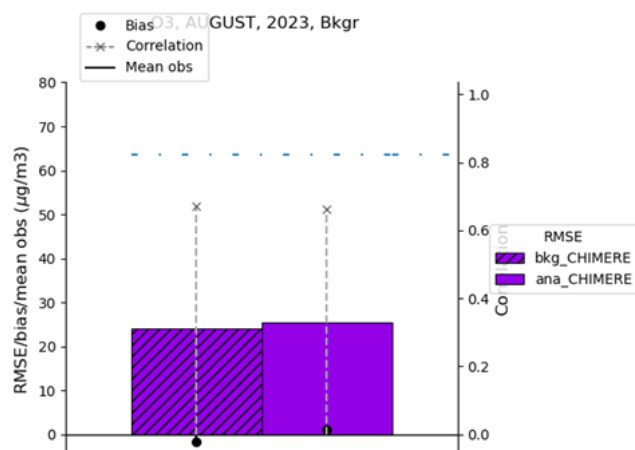


Figure 61: O₃ Barplot summary represents RMSE (columns), Bias (dots) and correlation (cross) calculated by hour. Hashed color represents CHIMERE base case (no assimilation) and solid color represent CHIMERE with assimilation

5.3 Assimilation of HCHO and CO in GEM-AQ

5.3.1 HCHO - August 2023

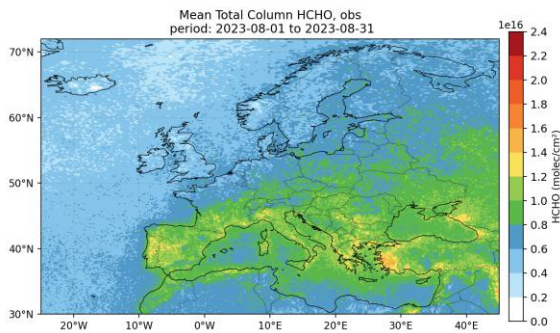
In the following section, the August 2023 results for formaldehyde (HCHO) assimilation in GEM-AQ are presented. The analysis is based on (i) total column comparisons with S5P retrievals, (ii) vertical distributions of HCHO and their associated impacts on ozone profiles, and (iii) surface concentrations and temporal variability in selected regions. Results are shown as monthly averages for August 2023 and as time series sampled at 12:00 UTC, consistent with the satellite overpass.

5.3.1.1 Impact of assimilation on the tropospheric column

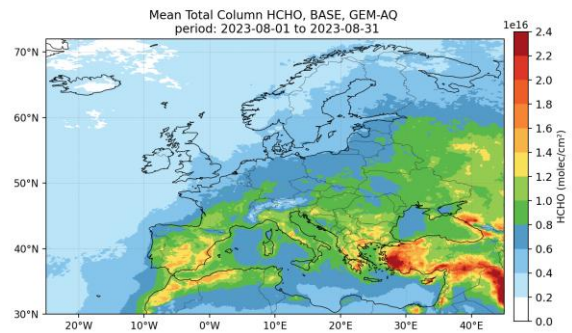
S5P observations show the expected summer pattern of HCHO over Europe in Figure 62, with higher columns over the Mediterranean Basin, the Balkans, and Turkey, and lower values over northwestern Europe and the Atlantic Ocean. In the BASE run, GEM-AQ overestimates HCHO over the eastern and southern Mediterranean (including Turkey) and parts of North Africa, while underestimating the land–sea contrast. After assimilation (ASSIM), both the magnitude and spatial patterns align better with the S5P observations. The increment (ASSIM – BASE) map shows widespread negative differences (reductions of approximately $0.2\text{--}1.0 \times 10^{16}$ molecules cm^{-2}) across the Mediterranean, the Balkans, and Turkey, effectively correcting the positive bias in BASE and enhancing spatial consistency with satellite data. Small, localized positive increments appear in the western part of the domain, but are much weaker than the negative corrections. Data gaps at high latitudes mainly reflect limited satellite sampling due to cloud cover and viewing geometry.

CAMEO

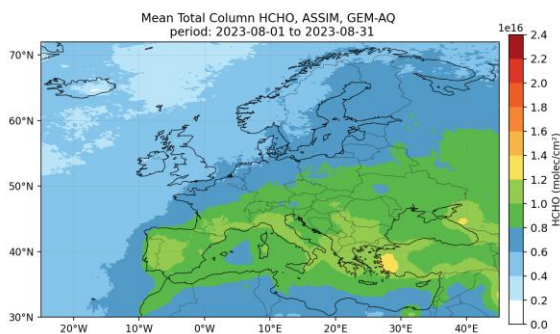
(a) S5P (observations)



(b) BASE (no assimilation)



(c) ASSIM (with HCHO assimilation)



(d) Increment (ASSIM – BASE)

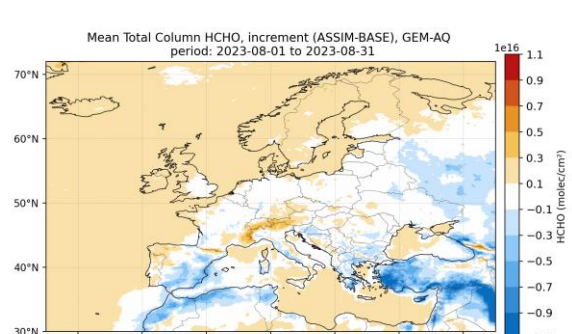


Figure 62: HCHO total column (monthly mean for August 2023). Panels: (a) S5P observations; (b) GEM-AQ BASE (no assimilation); (c) GEM-AQ ASSIM (with HCHO assimilation); (d) Increment (ASSIM – BASE). The increment shows broad reductions over the Mediterranean basin, Balkans and Turkey, leading to better spatial alignment with S5P.

Time series of tropospheric column (Figure 63)

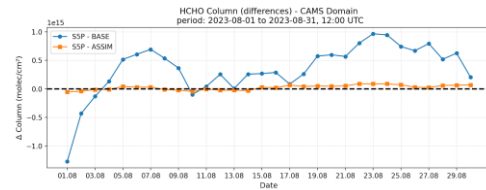
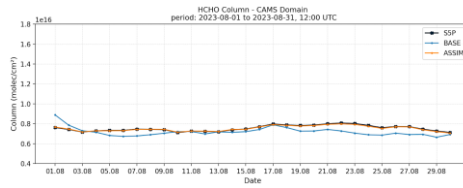
Across the CAMS domain, assimilation consistently reduces the model's departure from S5P: ASSIM follows the observations more closely than BASE, and the differences between S5P and ASSIM are smaller and less variable than between S5P and BASE. In the Mediterranean regions (Etna/R1, Italy/R2, Spain/R3), the positive bias in BASE is significantly diminished peaks and troughs align better with S5P, and mean errors decrease, as shown by the orange difference curves approaching zero. Over Central and Northern Europe (Poland/R4, Netherlands/R5), improvements are more moderate but systematic, with a narrower spread of S5P–ASSIM differences and only minor residual deviations. Overall, assimilation reduces both the systematic bias and the daily error variability compared to S5P, with the most notable improvements over the Mediterranean, where HCHO columns reach their highest levels

CAMEO

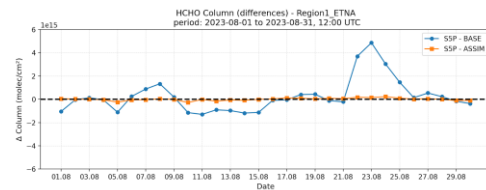
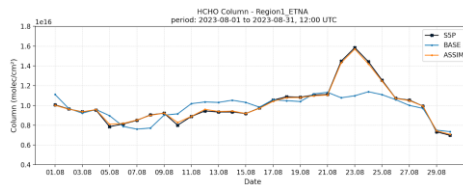
Time series of the tropospheric column

Difference of the tropospheric column

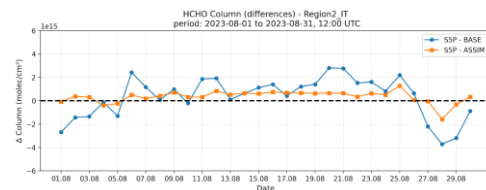
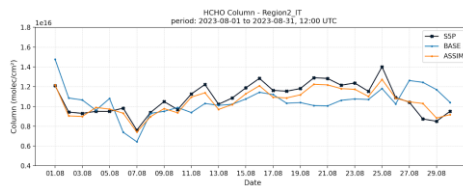
CAMS



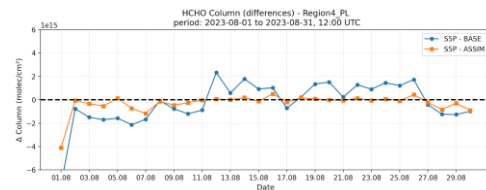
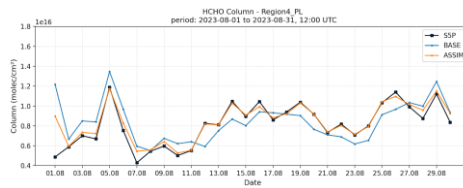
Etna



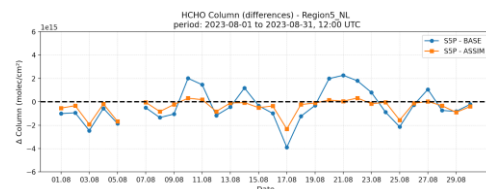
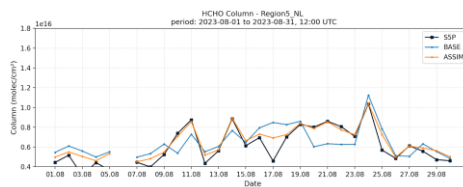
Italy



Poland



The Netherlands



Spain

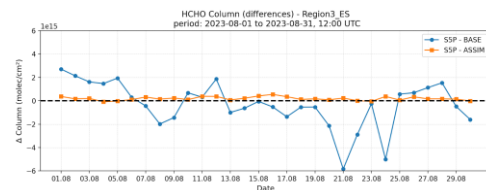
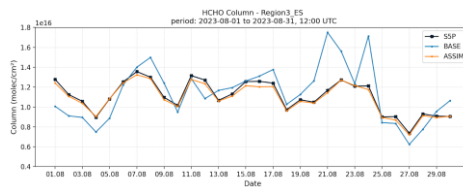


Figure 63: HCHO total-column time series for August 2023, sampled at 12:00 UTC (approx. S5P overpass). Left column: absolute columns from S5P (black), GEM-AQ BASE (blue), and GEM-AQ ASSIM (orange). Right column: differences to S5P (S5P-BASE and S5P-ASSIM). Rows (top to bottom): CAMS domain mean, Etna (R1), Italy (R2), Poland (R4), Netherlands (R5), Spain (R3). Units: molec/cm² (for both columns and differences). Note: positive differences indicate S5P is larger than the model; reduced amplitude of S5P-ASSIM relative to S5P-BASE indicates improved agreement after assimilation.

5.3.1.2 Vertical profile

The O₃ profiles in Figure 64 from the two scenarios—BASEv2 and ASSIM-HCHO—are nearly identical throughout the column, with differences generally within 1–3 ppbv. A pronounced land–sea contrast is evident: over land, O₃ concentrations are about 5–10 ppbv higher than over adjacent water surfaces from the near-surface level (≈ 0.99 hybrid) up to ~ 0.65 hybrid. The lack of a systematic offset between the scenarios indicates that HCHO assimilation has only a minor co-impact on the monthly mean O₃ vertical structure, which remains mainly controlled by photochemical processes and the land–sea contrast.

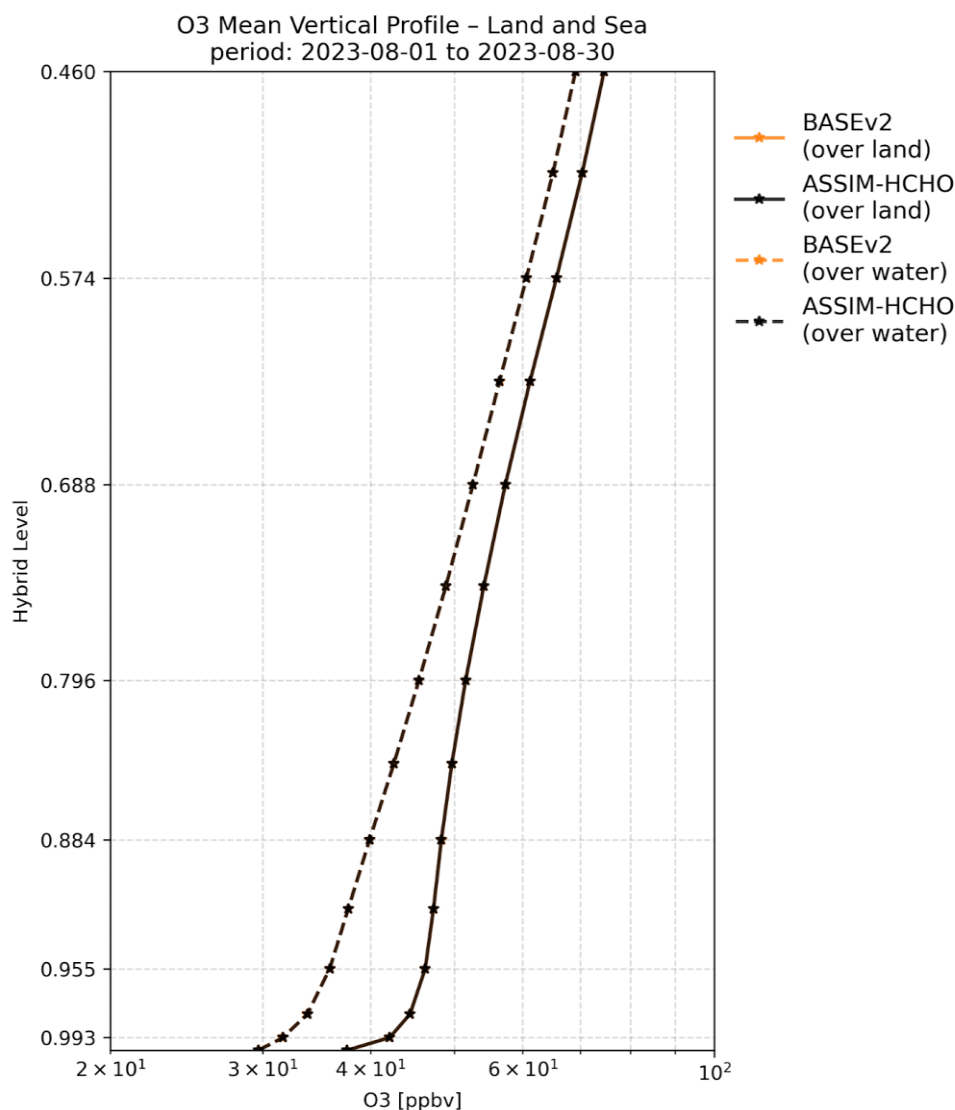


Figure 64: O₃ mean vertical profiles over the CAMS domain for August 2023 (monthly mean). Solid lines: over land; dashed lines: over water. Colours: BASEv2 (orange) and ASSIM-HCHO (black). The hybrid level increases downward (lower troposphere at higher values). Units: ppbv. Differences between BASE and ASSIM are minor throughout the column, indicating a limited co-impact of HCHO assimilation on the monthly-mean O₃ vertical profile; profiles over land are slightly higher than over water.

5.3.1.2 HCHO surface concentrations

Monthly mean HCHO concentrations at the lowest hybrid level in Figure 65 show characteristic summertime peaks along the Mediterranean rim (Iberia, Po Valley, Balkans, Turkey, and the North African coast) and lower values throughout northern and northwestern Europe. The BASE–ASSIM panel indicates that changes are generally modest, typically within ± 0.3 – 0.8 ppbv, and locally up to ~ 1 ppbv. Negative differences over the central and eastern Mediterranean, the Balkans, and Turkey suggest slightly higher values in ASSIM compared to BASE (i.e., small increases after assimilation). In contrast, positive differences over parts of western and northern Europe reflect minor decreases. Overall, assimilation mainly adjusts surface HCHO in areas of high photochemical activity, improving spatial consistency with column patterns while keeping surface impacts limited.

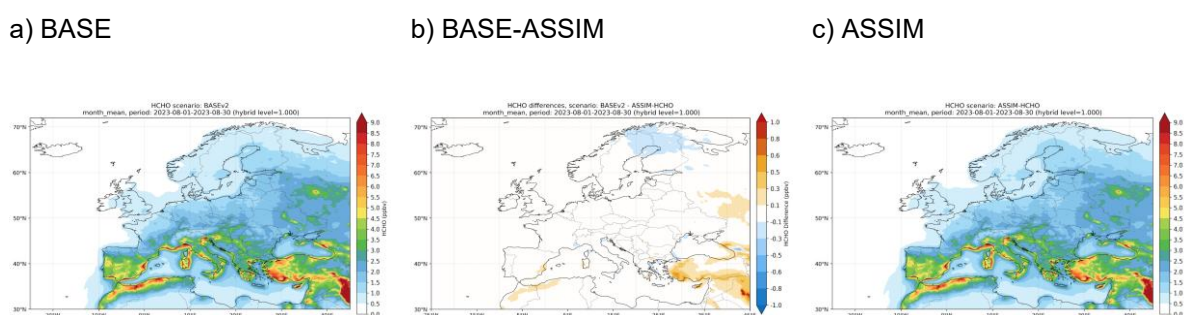


Figure 65: HCHO surface concentrations (hybrid level 1.000), monthly average for August 2023 over the CAMS domain. Panels: (a) GEM-AQ BASE, (b) BASE – ASSIM (difference), (c) GEM-AQ ASSIM (with assimilation of S5P HCHO columns). Units: ppbv. In panel (b), positive values indicate BASE > ASSIM (decrease after assimilation), while negative values indicate ASSIM > BASE.

5.3.2 CO - August 2023

This subsection presents the August 2023 assessment of carbon monoxide (CO) assimilation in GEM-AQ using S5P column retrievals. The analysis includes (a) maps of total column CO and their alignment with S5P, (b) regional time series and model–observation differences at 12:00 UTC (corresponding to the satellite overpass time), and (c) the co-impact on the vertical ozone profile along with surface CO fields. Unless otherwise noted, all diagnostics are based on monthly averages for August 2023 and time series sampled at 12:00 UTC.

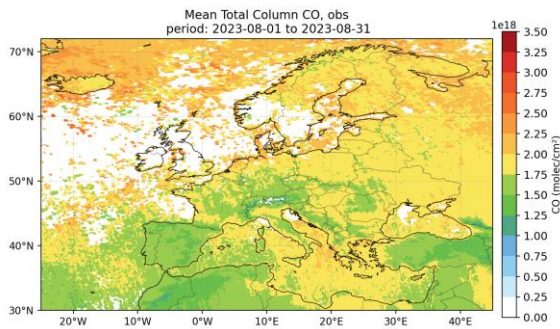
5.3.2.1 Impact of assimilation on the tropospheric column

S5P observations show the expected south–north gradient in CO columns, with higher values over southern Europe and the eastern Mediterranean, and lower values over northern Europe. Data gaps mainly result from cloud screening in Figure 66.

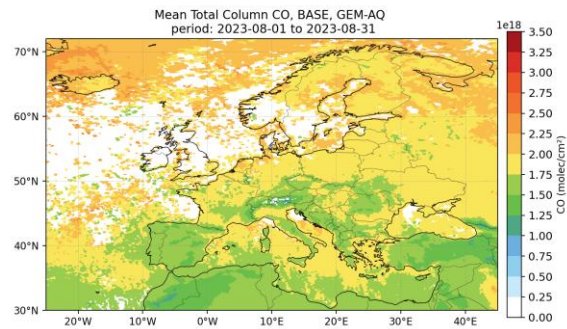
The BASE simulation broadly captures this pattern but exhibits an excess over western and northwestern Europe and underestimates over the eastern Mediterranean, the Balkans, and Turkey. After assimilation (ASSIM), the large-scale gradient is adjusted: the increment (ASSIM–BASE) is mainly negative over western and northwestern Europe and positive over the eastern Mediterranean, Balkans, and Turkey (locally reaching approximately 3×10^{17} molecules cm^{-2} , bringing model columns into closer agreement with S5P and reducing regional biases.

CAMEO

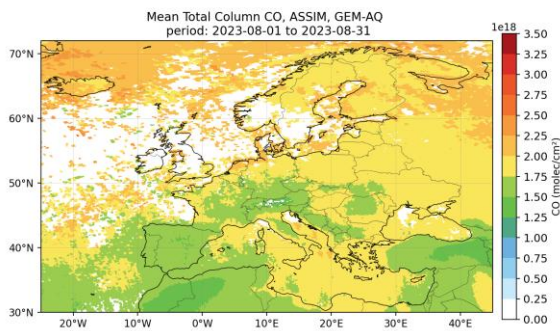
(a) S5P (observations)



(b) BASE (no assimilation)



(c) ASSIM (with CO assimilation)



(d) Increment (ASSIM – BASE)

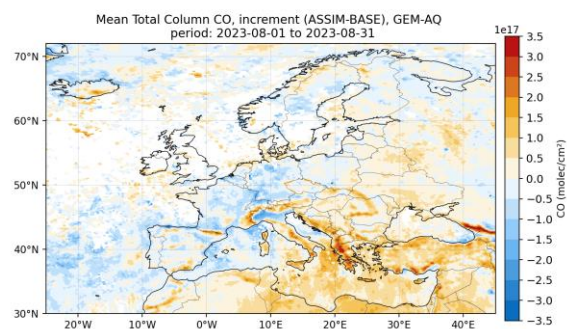


Figure 66: CO total column (monthly mean, August 2023). Panels: (a) S5P observations; (b) GEM-AQ BASE (no assimilation); (c) GEM-AQ ASSIM (with CO assimilation); (d) Increment (ASSIM – BASE). Units: molec cm⁻². The increment shows decreases over western/north-western Europe and increases over the eastern Mediterranean, Balkans and Turkey, which adjusts the large-scale gradient and brings model columns into closer agreement with S5P.

Time series of tropospheric column

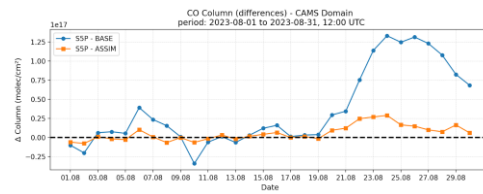
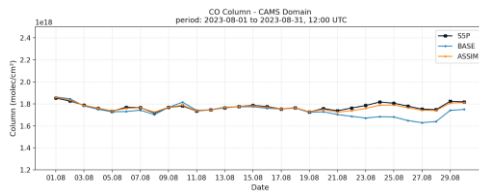
Across all regions, the assimilation run (ASSIM) aligns more closely with the S5P time series than the non-assimilating baseline (BASE) in Figure 67. This improvement is most noticeable in the right-hand panels, where the S5P–ASSIM residuals are consistently smaller and fluctuate closer to zero compared to S5P–BASE. On the CAMS domain scale, a positive drift seen in late August in S5P–BASE is mostly eliminated, mainly by assimilation, indicating a domain-wide reduction in bias. Over Mt. Etna (R1), the event around 23–25 August generates large positive S5P–BASE departures that are significantly reduced in ASSIM, resulting in a closer match to both the timing and magnitude of the observed peak. Italy and Spain (R2, R3) show moderate yet consistent improvements, with a noticeable decrease in day-to-day residual variability. In Poland and the Netherlands (R4, R5), the absolute corrections are smaller—reflecting lower variability—but the residuals are more tightly clustered around zero after assimilation. Overall, assimilation reduces both high and low model biases while preserving the observed temporal variability.

CAMEO

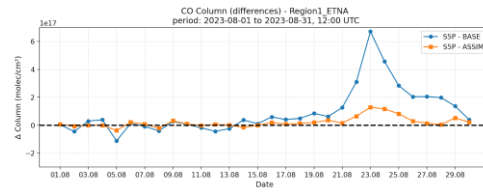
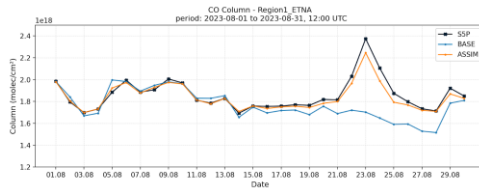
Time series of the tropospheric column

Difference of the tropospheric column

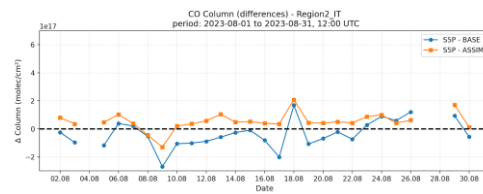
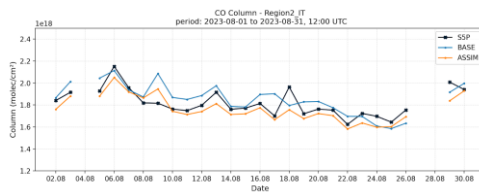
CAMS



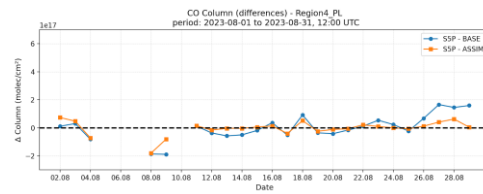
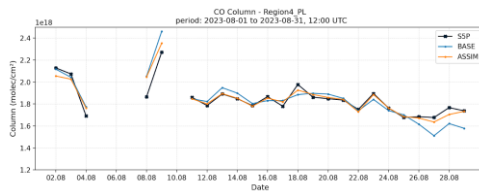
Etna



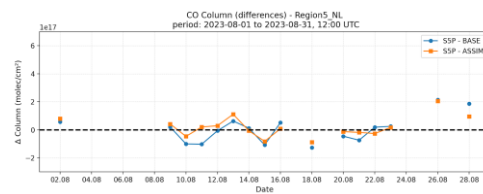
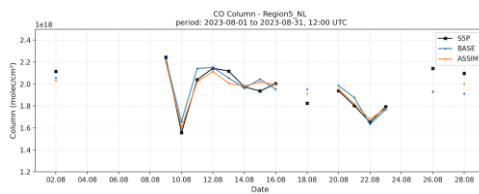
Italy



Poland



The Netherlands



Spain

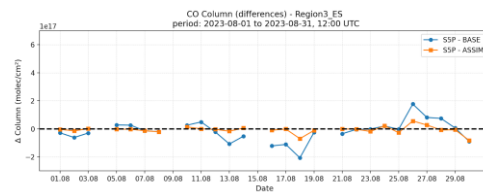
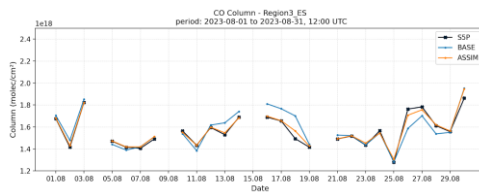


Figure 67: CO total-column time series and S5P–model differences for August 2023 (sampling at 12:00 UTC). Rows (top to bottom): CAMS domain mean, R1 Etna, R2 Italy, R3 Spain, R4 Poland, R5 Netherlands. Left panels: absolute columns for S5P (black), GEM-AQ BASE (blue), and GEM-AQ ASSIM (orange). Right panels: corresponding differences S5P–BASE (blue) and S5P–ASSIM (orange), in molec/cm². Overall, assimilation makes the model align more closely with S5P—most noticeable during the late-August CAMS-mean drift and the Etna episode (\approx 23–25 Aug), where large positive S5P–BASE residuals are significantly reduced in ASSIM; other regions exhibit smaller but consistent bias reductions.

5.3.1.2 Vertical profile

The O₃ profiles from the BASE and ASSIM-CO experiments in Figure 68 are virtually identical throughout the column, both over land (solid) and over water (dashed). This indicates that CO assimilation has only a secondary and indirect effect on ozone in the monthly mean, with no clear increase or decrease at any hybrid level. The consistent land–sea contrast remains, with slightly higher O₃ levels over land than over marine areas in the lower and middle troposphere, implying that boundary-layer photochemistry and surface precursor emissions mainly control ozone levels, with little influence from CO assimilation.

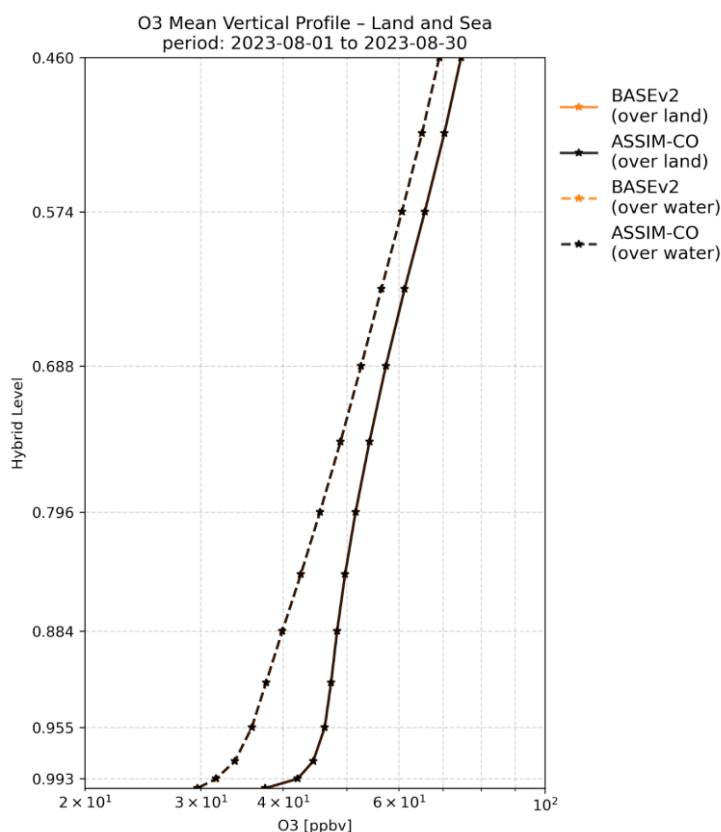


Figure 68: O₃ mean vertical profiles over the CAMS domain for August 2023 (monthly average). Solid lines: over land; dashed lines: over water. Colours: BASEv2 (orange) and ASSIM-CO (black). The hybrid level increases downward (larger values represent the lower troposphere). Units: ppbv. Differences between BASE and ASSIM are very small throughout the column, indicating only a minor co-impact of CO assimilation on the monthly-mean O₃ vertical profile; profiles over land remain slightly higher than over water.

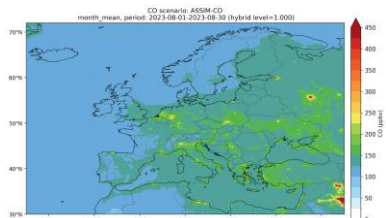
5.3.1.3 CO surface concentrations

The monthly average CO concentrations at the surface in Figure 69 show the expected north–south gradient, with higher values over southern Europe and the eastern Mediterranean, and lower values over the North Atlantic and northern Europe. The difference map (BASE – ASSIM) shows that assimilation generally reduces CO levels over the Mediterranean Basin, the Balkans, and Turkey (negative differences), while causing smaller increases over parts of western and northwestern Europe and the nearby North Atlantic (positive differences). These adjustments are spatially consistent but moderate in magnitude, preserving the main hotspot patterns linked to urban, industrial, and fire-affected regions. Overall, the assimilation shifts

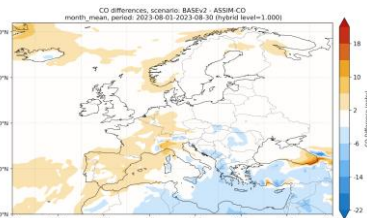
CAMEO

the model forecast toward a distribution more aligned with the satellite-constrained large-scale gradient.

a) BASE



b) BASE-ASSIM



c) ASSIM

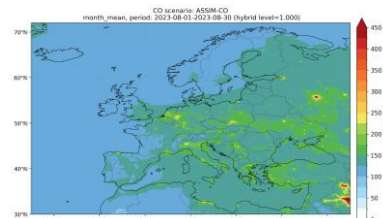


Figure 69: CO surface concentrations (hybrid level = 1.000), monthly mean for August 2023 over the CAMS domain. Panels: (a) GEM-AQ BASE, (b) BASE – ASSIM (difference), (c) GEM-AQ ASSIM (with assimilation of S5P CO columns). Units: ppbv. In panel (b), positive values indicate that BASE exceeds ASSIM (a decrease after assimilation), while negative values indicate that ASSIM exceeds BASE (an increase after assimilation); the largest negative differences are observed over the Mediterranean and Turkey, with weaker positive differences over parts of northern Europe and the North Atlantic.

5.4 Assimilation of HCHO in DEHM

The assimilation of S5P HCHO total columns is conducted with DEHM for August 2023. HCHO total columns in the S5P products in Figure 70 (left) show higher values over southern Europe, the Mediterranean region, and parts of eastern Europe, reflecting biogenic and anthropogenic emissions during summer. The DEHM prior (center) shows a systematic underestimation of HCHO total columns but captures a few hotspots in eastern Europe. The DEHM posterior exhibits predominantly positive adjustments (right), and the enhanced HCHO levels over southern and central Europe better align with the satellite observations, but also exhibits overestimations over hotspots.

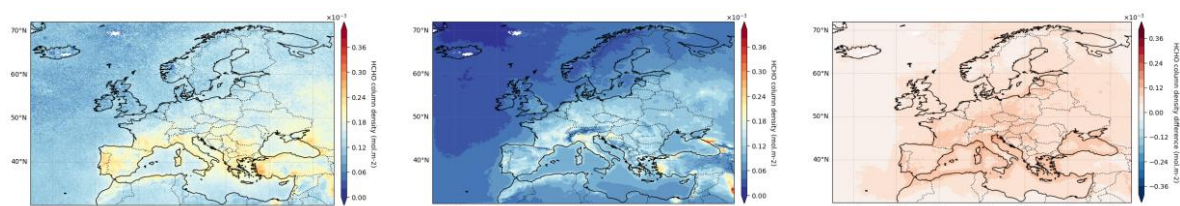


Figure 70: HCHO total columns mean over August 2023 of the S5P satellites observations on the left, of DEHM mean on the center (no assimilation), and the difference DEHM mean assimilation-no assimilation on the right

Overall, the simulation of HCHO total column is improved after data assimilation, with a RMSE reduced from 6.11×10^{-5} (prior) to 4.06×10^{-5} (posterior). The pdf plots of bias and root square error (RSE) are both closer to 0 as shown in Figure 71. Time series Figure 72 of daily mean total column density (on all available orbit hours) also show improved simulations throughout the period.

CAMEO

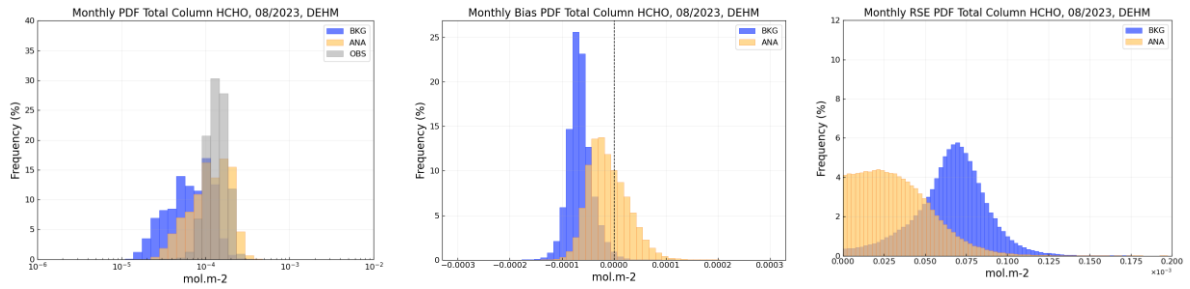


Figure 71: PDFs of the total column HCHO on the left, the bias of DEHM simulations compared with S5P on the center, and the root squared error on the right.

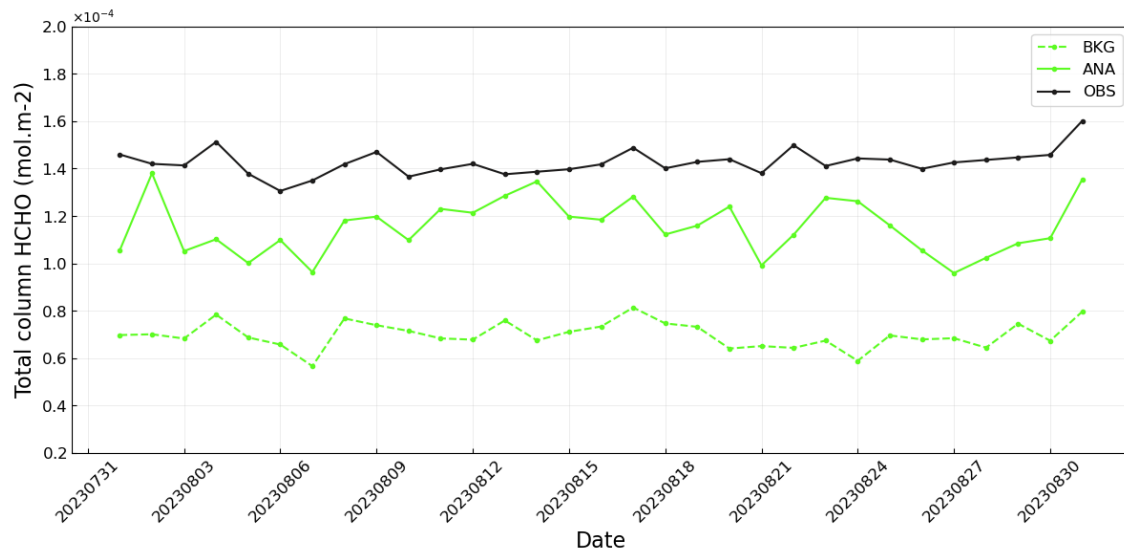


Figure 72: Times series of daily HCHO total columns over August 2023 for DEHM simulations

5.5 Assimilation of HCHO, CO and O₃ in MINNI-OI

MINNI-OI assimilation scheme described in 4.3.1.6 was applied to HCHO, CO and O₃ satellite data from Sentinel 5P for August 2023. The satellite retrievals with qa_value higher than 0.75 were considered. Figure 73 shows that the assimilation of satellite retrievals decreases the HCHO total column content in Central and Southern Europe and increases it in Western and Northern parts.

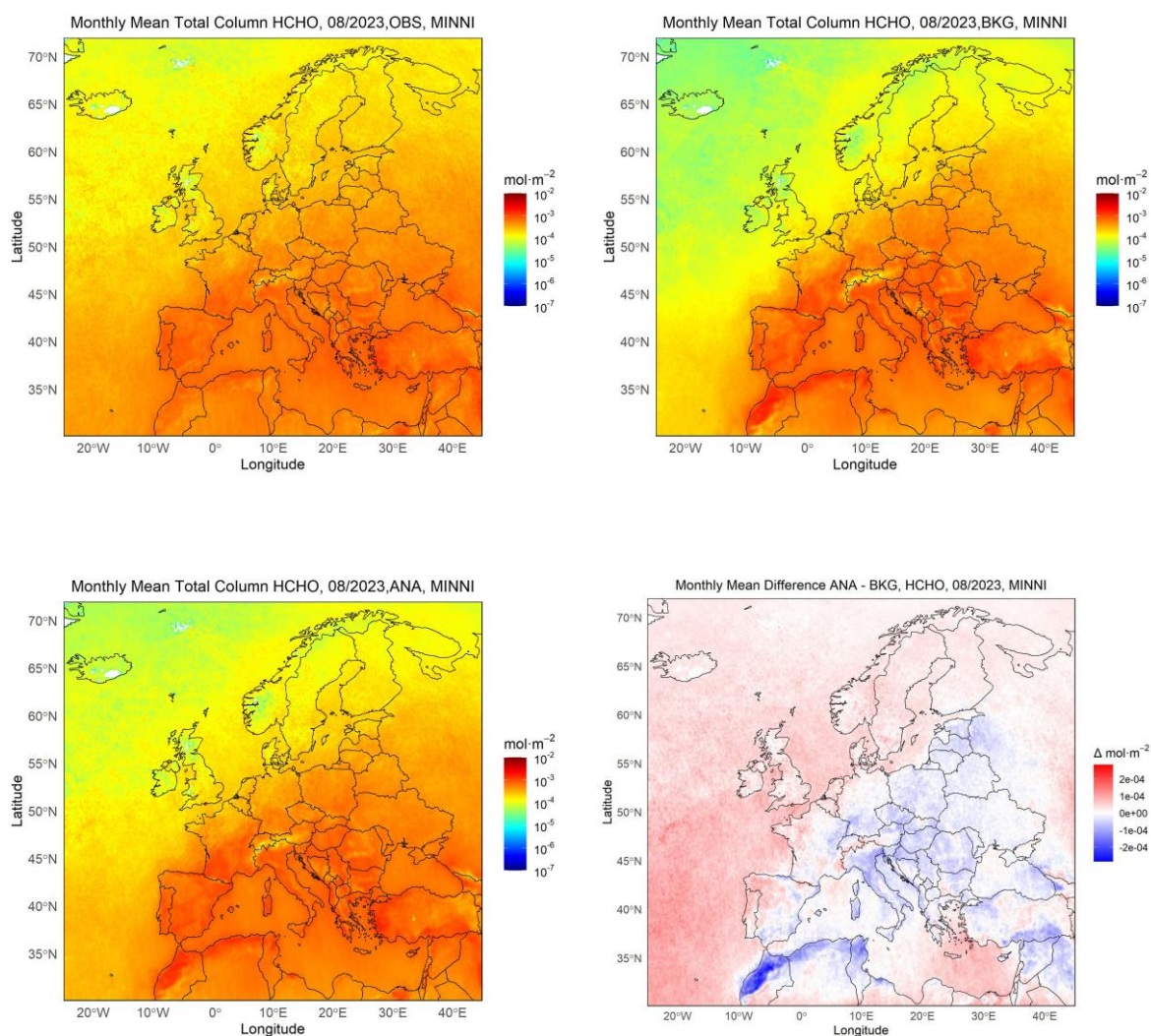


Figure 73 : HCHO total column mean over August 2023 of the S5P satellites observations on the top left, of MINNI-OI mean on the top right (no assimilation), of MINNI-OI mean with assimilation on the bottom left and the difference MINNI-OI mean assimilation-no assimilation on the bottom right

Figure 74 shows that MINNI-OI assimilation led to an overall increase of HCHO total column in the domain: the distribution after assimilation (ANA) is shifted to higher values on both axis with respect to the simulation without assimilation (BKG).

CAMEO

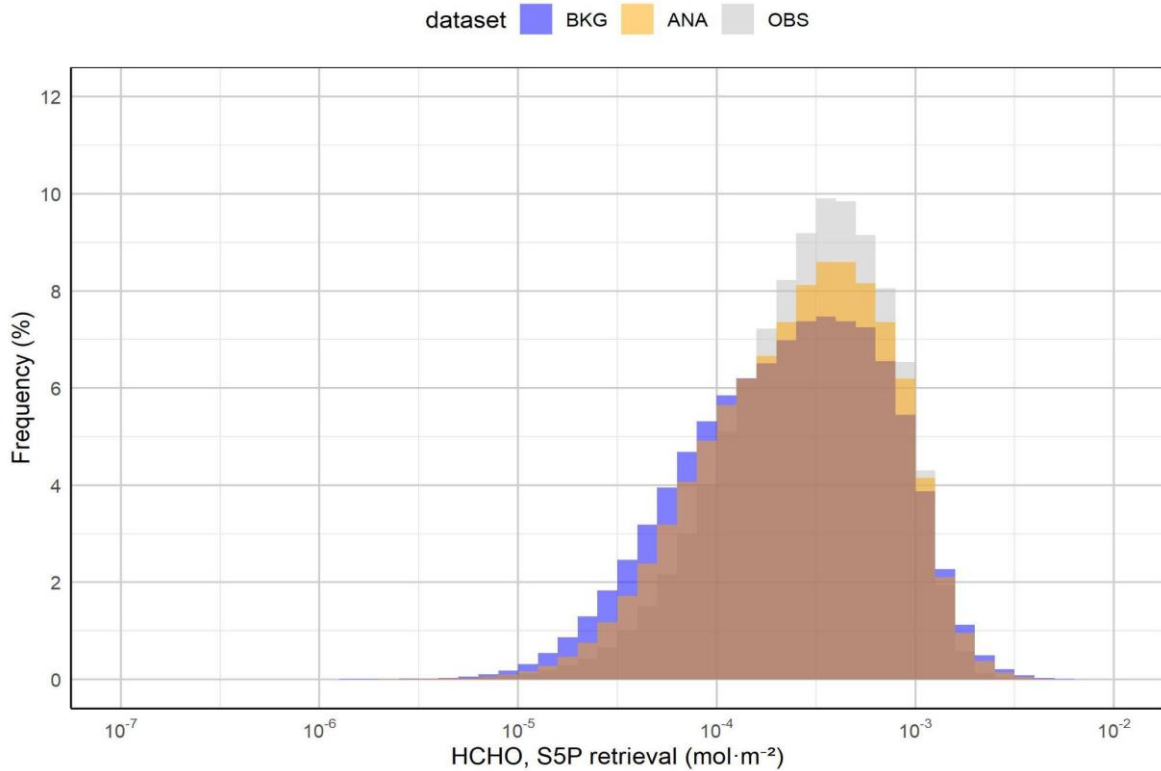


Figure 74: PDFs of the SENTINEL 5P HCHO total columns, simulated MINNI total columns (bkg) and simulated MINNI-OI total columns (ana).

Figure 75 shows that the MINNI-OI assimilation increases the simulated HCHO total columns (ana) with respect to simulations without assimilation (bkg) in correspondence of very few peaks.

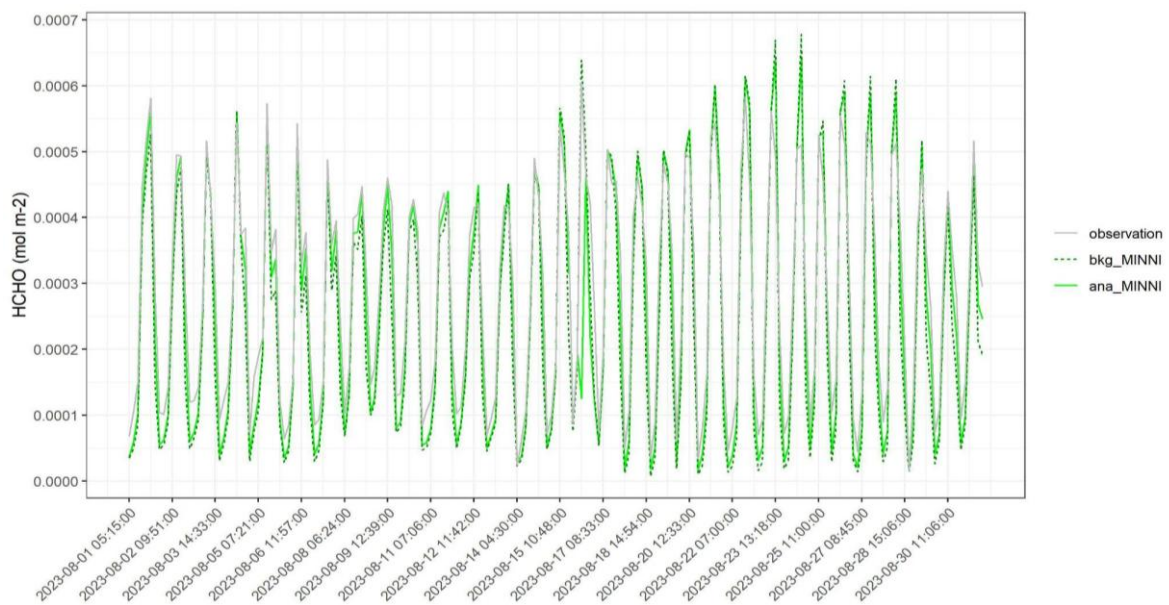


Figure 75: Times series of HCHO total column over August 2023

The assimilation experiments with MINNI-OI for CO and O3 with present modelling setup and satellite retrievals showed no significant impact both on total columns and surface concentrations.

5.6 Assimilation of HCHO in SILAM

TROPOMI HCHO assimilation was performed for August 2023. The output of the simulation was selected to be surface fields only (due to storage constraints). The assimilation setup was similar to that of the SO₂ concentration assimilation. The impact of the assimilation on the average model HCHO columns is shown in Figure 76. Overall, the assimilation reduced the domain average HCHO column from 0.083 mmol/m² to 0.066 mmol/m², whereas the general pattern of the distribution remained quite similar, although the columns over eastern Europe were reduced more strongly than those over western Europe. The resulting decrease of the average HCHO column contrasts somewhat against the behaviour of the assimilation of HCHO in other models, especially as the SILAM a priori columns were not especially high compared to the others. This is again very likely the result of SILAM assimilating also negative TROPOMI retrievals.

Due to the lack of HCHO observations, the impact of the assimilation was evaluated against surface measurement stations of O₃ and CO. At O₃ measurement stations (all EEA stations used for the CAMS validated reanalysis 2023), the model average value decreased from 65.6 ug/m³ to 64.6 ug/m³, while the average observed value was 64.4 ug/m³. The hourly RMSE stayed constant at 19.9 ug/m³ and the hourly correlation dropped from 0.756 to 0.753. When limited to operational evaluation stations, the average model value dropped from 64.5 ug/m³ to 63.5 ug/m³, the RMSE increased from 17.9 ug/m³ to 18.0 ug/m³ and the correlation decreased from 0.768 to 0.764. For CO at all stations, the average model value decreased from 167 ug/m³ to 164 ug/m³, the RMSE increased from 225 ug/m³ to 227 ug/m³, and the correlation decreased from 0.283 to 0.276. Thus, the assimilation of HCHO had only very minor impacts on the model, at least at the surface, but the effects were still slightly detrimental to the performance.

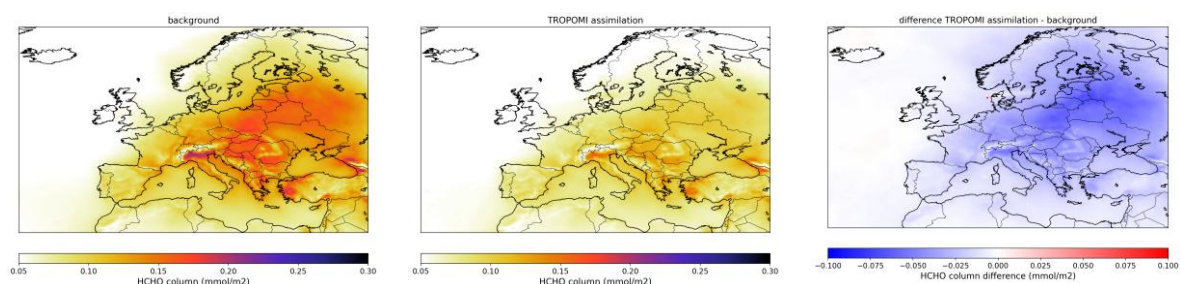


Figure 76: Average SILAM a priori HCHO total columns for August 2023 (left), average assimilated total columns for August 2023 (middle), and their difference (right)

5.7 Conclusions

HCHO experiments are performed by 4 teams over August 2023. Data assimilation improves spatial consistency with column patterns for all the models by reducing their bias. HCHO VCD decrease on average for SILAM and VCD increase for CHIMERE, DEHM. GEM-AQ and MINNI have positive and negative analysis increments over land on average. A smaller effect can be noticed in the north part of the domain, most likely due to clouds and availability of the retrieval to assimilate. GEM-AQ shows that assimilation mainly adjusts surface HCHO in areas of high photochemical activity, keeping HCHO impacts limited. Attention should be paid in areas, such as Atlantic Ocean and mediterranean sea, with low HCHO total columns. Analysis might be positively biased when only positive values are kept for assimilation.

Due to the lack of HCHO observations, CHIMERE and SILAM evaluate the impact of the assimilation against O₃ surface measurement stations (Air Quality Reporting observation used in CAMS regional). Moreover, no improvements or slight degradation over August 2023 are found on average.

S5p/HCHO product has a low signal-to-noise ratio and bias correction has not been considered in the first approach. However, monitoring the differences of S5P VCD with simulated VCD evaluated in average over a period, should help to improve the modelling. It could help to look for sensibility for biogenic emission according to inputs and to optimize parameters such as emission factor and ozone deposition. Emission inversion has not been tested in this work package.

Finally, GEM-AQ shows results of CO data assimilation generally reduces CO levels over the Mediterranean Basin, the Balkans, and Turkey (negative differences), while causing smaller increases over parts of western and northwestern Europe and the nearby North Atlantic (positive differences). No comparison is performed with surface observations, but data assimilation leads to moderate analysis increment that preserves the main hotspot patterns linked to urban, industrial, and fire-affected regions in monthly average.

6 Conclusion

The work achieved in this task allowed a step change in the ability of seven of the eleven CAMS Regional Models to assimilate TROPOMI retrievals of SO₂, HCHO, CO and Ozone.

First, all seven teams have assimilated SO₂-COBRA total columns over the same period August 2023. Processing of the observations, model background and data assimilation systems are different and provide common and various tendencies in the results. In addition, the quality control, the pre-processing such as super-observation led to the assimilation of slightly different data. In addition, all teams except SILAM assimilate only positive values while they represent around half of the data. This pre-processing, which may induce analysis positively biased, can be justified considering the uncertainties of data and when models underestimate total columns. The highest total columns have most likely the highest signal to noise ratio. All the models underestimate the SO₂ total column except GEM-AQ. The assimilation allows reducing the bias in total columns for all models and RMSE for some models. The analysis increment shows various impacts in concentration according to the systems and models used DEHM-3DVAR and MINNI-OI have more likely larger increment in the highest layer of atmosphere and lower increment within the planetary boundary layer than other DA-systems. In addition, it has been shown that assimilation at hotspot locations such as the Mt Etna or industrial site in Serbia, can have a strong effect on local SO₂ concentration which is encouraging. GEM-AQ, SILAM, MATCH and CHIMERE start testing introducing elevated volcanic emissions in the model in the regional model and effort should continue to improve SO₂ plumes modelling in operational forecast. Overall, regional models fit better SENTINEL 5P SO₂ columns but no clear improvement in the results is shown when comparing with EEA surface concentrations.

Second, five teams performed data assimilation of S5P HCHO products. CHIMERE and DEHM underestimate total columns on average while SILAM overestimates. GEM-AQ and MINNI show higher and lower total columns in different areas in Europe. Data assimilation reduces bias of all the models. Results in the north domain and over sea need to be carefully analysed because of the uncertainties in the data and their processing when only positive values are assimilated. Analysis can be positively biased. In addition, SILAM and CHIMERE performed O₃ concentration comparisons with ground-based surface stations which slightly degrade the results. HCHO

Third, GEM-AQ assimilates S5P/CO data assimilation leads to moderate analysis increment that preserves the main hotspot patterns linked to urban, industrial, and fire-affected regions in monthly average. No comparison was made with surface observations.

Finally, it remains a challenge for regional models to improve hourly or daily concentrations results at the surface, assimilating only S5P products. Even though they can have low signal to noise ratio, they provide useful information on average. Some additional work, such as on background error covariance, in the data assimilation regional systems should help to improve the results. The forthcoming availability of hourly data provided by Sentinel 4 will also allow further investigation. DA techniques should help to reduce the noise. The issue of the observation bias correction at regional scale should be addressed.

7 References

Adani, M.; Uboldi, F. Data assimilation experiments over Europe with the Chemical Transport Model FARM. *Atmos. Environ.* 2023, 306, 119806 DOI: 10.1016/j.atmosenv.2023.119806

Anderson Jeffrey L 2001. An Ensemble Adjustment Kalman Filter for Data Assimilation... *Monthly Weather Review*. Page(s): 2884–2903, DOI: [https://doi.org/10.1175/1520-0493\(2001\)129<2884:AEAKFF>2.0.CO;2](https://doi.org/10.1175/1520-0493(2001)129<2884:AEAKFF>2.0.CO;2)

Anderson, Jeffrey L. (2022). A Quantile-Conserving Ensemble Filter Framework. Part I: Updating an Observed Variable. *Monthly Weather Review*, 150(5), doi: 10.1175/MWR-D-21-0229.1.

Colette, A., Collin, G., Besson, F., Blot, E., Guidard, V., Meleux, F., Royer, A., Petiot, V., Miller, C., Fermond, O., Jeant, A., Adani, M., Arteta, J., Benedictow, A., Bergström, R., Bowdalo, D., Brandt, J., Briganti, G., Carvalho, A. C., Christensen, J. H., Couvidat, F., D'Elia, I., D'Isidoro, M., Denier van der Gon, H., Descombes, G., Di Tomaso, E., Douros, J., Escribano, J., Eskes, H., Fagerli, H., Fatahi, Y., Flemming, J., Friese, E., Frohn, L., Gauss, M., Geels, C., Guarnieri, G., Guevara, M., Guion, A., Guth, J., Hänninen, R., Hansen, K., Im, U., Janssen, R., Jeoffrion, M., Joly, M., Jones, L., Jorba, O., Kadantsev, E., Kahnert, M., Kaminski, J. W., Kouznetsov, R., Kranenburg, R., Kuenen, J., Lange, A. C., Langner, J., Lannuque, V., Macchia, F., Manders, A., Mircea, M., Nyiri, A., Olid, M., Pérez García-Pando, C., Palamarchuk, Y., Piersanti, A., Raux, B., Razinger, M., Robertson, L., Segers, A., Schaap, M., Siljamo, P., Simpson, D., Sofiev, M., Stangel, A., Struzewska, J., Tena, C., Timmermans, R., Tsikerdekis, T., Tsyro, S., Tyuryakov, S., Ung, A., Uppstu, A., Valdebenito, A., van Velthoven, P., Vitali, L., Ye, Z., Peuch, V.-H., and Rouïl, L.: Copernicus Atmosphere Monitoring Service – Regional Air Quality Production System v1.0, *Geosci. Model Dev.*, 18, 6835–6883, <https://doi.org/10.5194/gmd-18-6835-2025>, 2025.

De Smedt I., Theys N., Vlietinck J., Yu H., Danckaert T., Lerot C., Van Roozendael M.: S5P/TROPOMI HCHO ATBD BIRA-IASB institute, document number: S5P- BIRA-L2-400F-ATBD, CI-400F-ATBD, 2024.

Elbern, H., Strunk, A., Schmidt, H., and Talagrand, O.: Emission rate and chemical state estimation by 4-dimensional variational inversion, *Atmos. Chem. Phys.*, 7, 3749–3769, <https://doi.org/10.5194/acp-7-3749-2007>, 2007.

Gaspari, Gregory, and Stephen E. Cohn. (1999). Construction of correlation functions in two and three dimensions. *Quarterly Journal of the Royal Meteorological Society*, 125(554), doi: 10.1256/smsqj.55416.

Kahnert, M. (2008). Variational data analysis of aerosol species in a regional CTM: background error covariance constraint and aerosol optical observation operators. *Tellus B*, 60(5), 753–770. <https://doi.org/10.1111/j.1600-0889.2008.00377.x>

Landgraf J., Brugh J., Scheepmaker R. A., Borsdorff T., Houweling S., Hasekamp O. P. Algorithm Theoretical Baseline Document for Sentinel-5 Precursor Carbon Monoxide Total Column Retrieval, Netherlands Institute for Space Research SRON. Document number: SRON-S5P-LEV2-RP-002, CI-7430-ATBD, 2024.

Oomen G. , Jean-François Müller, Trissevgeni Stavrakou, Isabelle De Smedt, Thomas Blumenstock, Rigel Kivi, Maria Makarova, Mathias Palm, Amelie Röhlings, Yao Té, Corinne Vigouroux, Martina M. Friedrich, Udo Frieß, François Hendrick, Alexis Merlaud, Ankie Piters, Andreas Richter, Michel Van Roozendael, and Thomas Wagner. Weekly derived top-down

CAMEO

volatile-organic-compound fluxes over Europe from TROPOMI HCHO data from 2018 to 2021. *Atmospheric Chemistry and Physics*, 2024. <https://doi.org/10.5194/acp-24-449-2024>

Parrish, D. F. and Derber, J. C.: The National Meteorological Center's spectral statistical-interpolation analysis system, *Monthly Weather Review*, 120, 1747-1763, 1992. [https://doi.org/10.1175/1520-0493\(1992\)120%3C1747:TNMCSS%3E2.0.CO;2](https://doi.org/10.1175/1520-0493(1992)120%3C1747:TNMCSS%3E2.0.CO;2)

Silver, J. D., Christensen, J. H., Kahnert, M., Robertson, L., Rayner, P. J., & Brandt, J. (2016). Multi-species chemical data assimilation with the Danish Eulerian hemispheric model: system description and verification. *Journal of Atmospheric Chemistry*, 73(3), 261–302. <https://doi.org/10.1007/s10874-015-9326-0>

Theys, N., Vitali Fioletov, Can Li, Isabelle De Smedt, Christophe Lerot, Chris McLinden, Nickolay Krotkov, Debora Griffin, Lieven Clarisse, Pascal Hedelt, Diego Loyola, Thomas Wagner, Vinod Kumar, Antje Innes, Roberto Ribas, François Hendrick, Jonas Vlietinck, Hugues Brenot, and Michel Van Roozendae, A sulfur dioxide Covariance-Based Retrieval Algorithm (COBRA): application to TROPOMI reveals new emission sources. *Atmos. Chem. Phys.*, 21, 16727–16744, 2021. <https://doi.org/10.5194/acp-21-16727-2021>

Weaver, A. and P. Courtier, Correlation modelling on the sphere using a generalized diffusion equation, *Q. J. Royal Meteorol. Soc.*, 127, 1815–1846, 2001. <https://doi.org/10.1002/qj.49712757518>

Robertson, L., Langner, J., and Engardt, M.: An Eulerian limited-area atmospheric transport model. *J. Appl. Meteor.* 38, 190-210, 1999.

Spurr R., Loyola D., Heue K-P., Van Roozendaal M., Lerot C., Royal Netherlands Meteorological Institute Ministry of Infrastructure and Water Management. KNMI S5P/TROPOMI Total Ozone ATBD, document number: S5P-L2-DLR-ATBD-400A, CI-400A-ATBD, 2022.

Sasaki Y., 1969: Proposed Inclusion of Time, Variation Terms, Observational and Theoretical, in Numerical Variational Objective Analysis. *J. Met. Soc. Jpn.*, 47(2): 115 – 124.

Targa J. (4sfera Innova), Maria Colina (4sfera Innova), Lorena Banyuls (4sfera Innova), Alberto González Ortiz (EEA), Joana Soares (NILU), April 2025. [ETC HE Report 2025/2: Status report of air quality in Europe for year 2023, using validated data.](#)

Veefkind P., Keppens A., Haan J. TROPOMI ATBD Ozone Profile, DLR institute, document number S5P-KNMI-L2-0004-RP, CI-7340-ATBD, 2021.

Document History

Version	Author(s)	Date	Changes
0.1	Gael Descombes	October 2025	Initial version
0.2	Gael Descombes	October 2025	Second Version
0.3	Gael Descombes	November 2025	Third version
1.0	Gael Descombes	November 2025	Issued after internal reviews and updates

Internal Review History

Internal Reviewers	Date	Comments
Vincent Guidard (MF), Augustin Colette (INERIS)	Oct 2025	Reviewed within WP
Johannes Flemming (ECMWF), Katerina Sindelarova (CU)	Nov 2025	Project internal review comments

This publication reflects the views only of the author, and the Commission cannot be held responsible for any use which may be made of the information contained therein.